Dynamic Wind Speed in Dynamic Inflow Models

M.Sc. Thesis W.E. van der Deijl

TU Delft

Dynamic Wind Speed

In Dynamic Inflow Models

by

W.E. van der Deijl

to obtain the degree of Master of Science
at the Delft University of Technology,
to be defended publicly on 11th of July at 14:00.

Student number:	1516426	
Project duration:	Oct 1, 2017 – July 11, 2018	
Thesis committee:	Dr. ir. C. J. Simão Ferreira,	TU Delft, supervisor
	Dr. ir. A.H.. van Zuijlen,	TU Delft
	Dr. ir. M.B. Zaaijer,	TU Delft
	Ir. T. Berdowski,	TU Delft

This thesis is confidential and cannot be made public until 11th of July, 2018.

TU Delft

Preface

W.E. van der Deijl
Delft, June 2018

About 12 months ago I started the orientation of doing my thesis on the topic of rotor aerodynamics models, and specifically vortex models. As dry as it may sound, it was exactly what I was looking for. A year later with this finished thesis I can proudly say that my time as a M.Sc. student at the TU Delft has come to an end. I have taken the time to learn it all about wind energy and the beautiful peculiarities of aerodynamics. Not only have I learned about wakes, boundary layers and turbulence, I can also say that I learned about myself and why I do what I do. I am glad that I have been granted that opportunity.

Having said that, the past eight months of actual thesis work have been the smoothest months of my studies. For this I owe my thanks to Carlos Simão Ferreira and Tom Berdowski. They have given me a lot of freedom and flexibility in finishing this project, and I can only hope that it was as pleasant to them as it was to me. I wish that I had claimed more of Carlos his precious time though. Every meeting was enlightening, however short they may have been sometimes. It is admirable how quick Carlos identifies an issue and the explanation or solution for that issue. Thanks Carlos for making it all happen, from start to finish.

And thanks Tom for always being willing to listen and for helping me navigate doing the thesis work. Maybe I was not always clear in what I was trying to say, but sparring made it at least clear for myself. Also, I may not always have followed Tom his tips, but at least I can say that I knowingly fell for the pitfalls Tom warned me about.

Furthermore, I am glad to have Alexander van Zuijlen and Michiel Zaaijer in my the thesis committee during these busy months before the summer breaks.

I also wish to thank Gerard Schepers and Koen Boorsma from ECN for having me over and for the time to discuss. It was good to hear the practical considerations and questions about the project.

This preface would not be complete without acknowledging my family and my friends. The past year has been a great lesson that one does not need to face everything alone. Finally, I am extremely grateful for the unwavering support of my parents.

Contents

Abbreviations and Definitions

Symbols

A	=	Rotor area [m^2]
a	=	Induction factor [-]
c_d	=	Drag coefficient [-]
c_l	=	Lift coefficient [-]
C_p	=	Power coefficient [-]
C_t	=	Thrust coefficient [-]
F_{ax}	=	Thrust force in axial direction [N]
k	=	Reduced frequency $k = \frac{\omega R}{U_0}$ [-]
P	=	Power [W]
r	=	Radial coordinate [m]
R	=	Rotor radius [m]
T	=	Thrust [N]
u_{ind}	=	Induced velocity at the rotor [ms^{-1}]
U_0	=	Incoming wind speed [ms^{-1}]
δ	=	Viscous cut-off radius vortex element [-]
γ	=	Vorticity density in the wake [ms^{-1}]
Γ	=	Circulation at the rotor [m^2s^{-1}]
Φ_d	=	Response function at the disc [-]
ρ	=	Density [kgm^{-3}]
τ	=	$\tau = \frac{tU_0}{R}$ Non-dimensional time [-]
Ω	=	Rotational speed [rad/s]

Abbreviations

BEM	=	Blade Element-Momentum theory
ECN	=	Energy Research Centre of the Netherlands
FWVR	=	Free Wake Vortex Ring Model
VTM	=	Vortex Tube Model

Subscripts

d	=	Z-location at the disc
i	=	Time step index
k	=	Radial index
t	=	Thrust

List of Figures

Figures Part I

Figures Part II

List of Tables

Tables Part I

Tables Part II

Abstract

The objectives of this thesis were three-fold:

1. To investigate the difference in dynamic inflow between a varying incoming wind speed and a varying thrust at the rotor. The first effect corresponds to a constant bound circulation but a varying wake vorticity strength, while the second effect corresponds to a non-constant bound circulation and therefore also a varying wake vorticity.

2. To determine whether this difference was captured by the engineering models.

3. And if it is not, to improve the model by Yu to include the effect of dynamic wind speed by fitting Yu's model to the FWVR model responses.

To answer these questions the induced velocity response of an actuator disc was modelled through a free wake vortex ring model. The free wake model was able to capture the response in the wake, which was necessary to view the behaviour in the wake to a changing incoming wind speed.

The conclusions from the first objective are that there is a clear difference in dynamic inflow response between 'dynamic wind' and 'dynamic thrust'. This difference in response corresponds to the difference between bound circulation change and wake vorticity strength change. Or, in other words, the induced velocity response is a combination of the strength of the shed vorticity, and the density of the vorticity. A free-wake-vortex-ring model was able to show both effects clearly. It can also be concluded that dynamic inflow in general is the summation of two effects. Dynamic thrust shows both the first order effect of the change of thrust at the rotor and the slower second order effect of the wake. Dynamic wind only exhibits the second order effect of the wake change as the strength of the shed vorticity does not change, but the density does.

And even though dynamic wind does not show as drastic as a response as dynamic thrust, the scale of the induced velocity change is on the same order as in the dynamic thrust case. Also, the lag between induced velocity and thrust coefficient change is larger because of the slower response. Finally, it is clear that there is an induced velocity response, contrary to what is currently assumed in research.

It has to be noted that dynamic wind and dynamic thrust in reality are coupled. A change in wind speed will result in a change in axial force. The distinction is therefore rather hypothetical and may be hard to observe in practice. Nevertheless this distinction tells us how dynamic inflow should be modelled in general.

These conclusions could be carried through towards the engineering models of dynamic inflow. It can be concluded that dynamic inflow engineering models only capture the first order effect, and that the time constants used in the models appear to be off. Øye's model has two different time scales though, and may represent the two effects better than the model by Pitt-Peters or ECN. Because they do not take into account the slower effect of wake adjustment, the engineering models are not very adequate at predicting the dynamic inflow effects of dynamic wind. On top of that, as was also found in previous research, the engineering models ultimately underestimate the effect of dynamic inflow in general.

The Duhamel's integral model by Wei Yu performs better in the dynamic thrust case, which is to be expected as it was fitted to that response. However, the model is currently unable to capture the difference between dynamic wind and dynamic thrust as previously described. Although the model output reflects the two time scales that are present, the input and fit of the model are limited to the dynamic thrust case.

In order to be able to make this distinction, the Duhamel's integral is extended to capture the response to a changing wind speed. Just like the dynamic thrust case, dynamic wind could be expressed as a summation of two exponentials, and the fitted functions to radius and thrust coefficient are good. The model therefore performs well in the dynamic wind case, and is also able to capture a mix of thrust and wind speed changes.

1 Introduction

The European Union has committed itself to 80-90% decarbonisation in 2050 with respect to 1990 levels. It is currently en route to achieve halfe of that. To realise the other half, the European Commission (EC) sees a large role for renewable energy sources. It expects at least 55%, but perhaps even 97%, of electricity to be produced by renewables in 2050 [EC, 2012].

This commitment inevitably leads to a large increase in wind energy, both onshore and offshore. This large increase in wind energy is accompanied by a general trend of ever increasing rotor diameters, especially for offshore wind turbines. This means that unsteady effects on the rotor scale are increasing, and the importance of accurate aero-elastic models increases. One of these unsteady effects is called dynamic inflow. It is defined as the delay between a change in rotor loading and the induced velocity response.

The problem is that the most popular method of modelling the aerodynamics of a wind turbine, Blade Element-Momentum theory (BEM), assumes steady conditions. Luckily additions that remedy this assumption exist, but the question of the accuracy of these dynamic inflow models remains. Recently Yu et al. [80], [81], [83], raised some doubts about the application of these engineering models. Hence, to improve the modelling of dynamic inflow Yu proposed a new model in [79].

Additionally, rotor loading is defined by the thrust coefficient C_t, and it can be changed by changing the rotor forces (e.g. pitching a blade) or by changing the incoming wind speed. However, all engineering models are applied to unsteady rotor forces. It is assumed that unsteady incoming wind speed has a negligible effect on dynamic inflow, but the research into this assumption is limited to the Joule project, Snel and Schepers et al. [60]. A new model was developed by Hammam [18] though, which distinguishes between the effect of dynamic wind speed and dynamic thrust. Nevertheless, whether unsteady wind is different from unsteady thrust still needs to be ruled out.

1.1. Aim and Hypothesis

The aim is therefore to understand the effects of dynamic wind speed by comparing the response to dynamic wind speed to the response of dynamic thrust. The effects on the wake will require special attention, as this is where differences are most likely to exist. It is also where an explanation for the differences at the rotor can be found. Therefore a free wake vortex ring (FVWR) model will be used, as it can adequately model the dynamics in the wake.

The main hypothesis can be formulated as follows:

> *The effect of dynamic wind speed on the actuator disc and the wake is different from the effect of dynamic thrust, and it therefore needs to be included in current engineering models.*

It is also implied that the scale of the response is significant enough to warrant the inclusion in engineering models. It could be that there is an effect, yet the effects are small.

But if this hypothesis is found to be true, the next points of attention will be the engineering models, to see how the differences between these two inputs are modelled. If the engineering models fail to properly account for these differences an adjustment will need to be made.

Finally, the new engineering model by Yu will require special attention, as it improved upon the older engineering models. If an adjustment is found to be necessary, it will therefore be made to this model.

To summarise, the objectives of these thesis are three-fold:

1. To investigate the difference in dynamic inflow between a varying incoming wind speed and a varying thrust at the rotor. The first effect corresponds to a constant bound circulation but a varying wake vorticity strength, while the second effect corresponds to a non-constant bound circulation and therefore also a varying wake vorticity.
2. To determine whether this difference was captured by the engineering models.
3. And if it is not, to improve the model by Yu to include the effect of dynamic wind speed by fitting Yu's model to the FWVR model responses.

1.2. Research Questions

These objectives correspond to the following research questions:

1. What is the physical difference between dynamic wind speed and dynamic thrust?
   (a) What is the effect of either dynamic on the actuator disc, and on the induced velocity response?
   (b) What is the effect of either dynamic on the wake?
2. What is the scale of the dynamic wind speed effect on dynamic inflow, and most importantly: is it necessary to take it into account?
3. To what extent do engineering models already cover the resulting effects?
4. If current engineering models do not include the effect of dynamic wind speed, to what extent can the model by Yu be modified to include it?

So, the focus throughout this work lies on the difference between the two drivers of unsteady thrust. What is the result of varying incoming wind speed on the induced velocity response?

Structure of the Report

The structure of this report is split in two. The answers to the hypothesis and results of the main objectives can be found in the first part I. It is structured as a research paper and functions as a standalone document. It can therefore be read as such. The second part shows the chapters that give a more in-depth explanation of current literature, a description of the used models and the verification of the new model. Note that figures, tables and equations are often shown in both the first and second part of the report. So the second part consists of the literature review in chapter 2. The free wake vortex ring model is described in chapter 3. The performance of the engineering models is also shown in the research paper, but a more extensive investigation is shown in chapter 4. The extension to Yu's model, the fitted coefficients and the accuracy of the fit is shown in chapter 5. After this the extended model is verified in chapter 6. This thesis report finishes with the conclusions and recommendations in chapter 7 and the bibliography in page 97.

Research Paper

Dynamic Wind Speed in Dynamic Inflow Models

W.E. van der Deijl
Delft University of Technology

Supervisor: Dr. ir. C. J. Simão Ferreira
Delft University of Technology

Second supervisor: Ir. T. Berdowski
Delft University of Technology

In the case of unsteady loading conditions at a rotor, the induced velocity response lags the thrust coefficient at the rotor. The two parameters that are responsible for unsteady loading conditions are rotor thrust (due to blade pitch, or rotational speed) and incoming wind speed. The induced velocity response to these two sources of unsteadiness have been compared in a free wake vortex ring model. It was found that a varying wind speed has a non-negligible dynamic inflow effect, and the effect is different from varying rotor thrust. Additionally, current engineering models are incapable of capturing this difference. Recently a new engineering model was proposed by Yu [1], and this model is extended such that it is able to distinguish between the response to dynamic wind and to dynamic thrust.

Nomenclature

A	=	Rotor area $[m^2]$
a	=	Induction factor [-]
k	=	Reduced frequency $k = \frac{\omega R}{U_0}$ [-]
C_t	=	Thrust coefficient [-]
F_{ax}	=	Thrust force in axial direction $[N]$
r	=	Radial coordinate $[m]$
R	=	Rotor radius $[m]$
u_{ind}	=	Induced velocity at the rotor $[ms^{-1}]$
U_0	=	Incoming wind speed $[ms^{-1}]$
δ	=	Viscous cut-off radius vortex element [-]
γ	=	Vorticity density in the wake $[ms^{-1}]$
Γ	=	Circulation at the rotor $[m^2 s^{-1}]$
ρ	=	Density $[kgm^{-3}]$
τ	=	$\tau = \frac{tU_0}{R}$ Non-dimensional time [-]
BEM	=	Blade Element-Momentum theory
ECN	=	Energy Research Centre of the Netherlands

FWVR = Free Wake Vortex Ring Model

Subscripts

i = Time step index

k = Radial index

d = Z-location at the disc

I. Introduction

The strength of Blade-Element Momentum (BEM) theory is its simplicity while still providing relatively accurate solutions to the rotor aerodynamics of wind turbines. One only needs accurate airfoil polars for BEM to be accurate, as pointed out by Hansen et al. [2]. To achieve this simplicity a couple of assumptions are made; one of them being the assumption of steady conditions. Because of this assumption BEM predicts an instant relation between induced velocity at the rotor and loading conditions. In reality the induced velocity will lag the thrust coefficient considerably because the air around the rotor has to be accelerated. This lagging effect is called Dynamic Inflow. Besides the acceleration of air explanation, another reason can be found in the wake: the wake has to adapt to the new conditions and it takes time before new shed vorticity convects downstream and replaces the old vorticity, which was also discussed by Sanders [3].

The effect of dynamic inflow scales with rotor diameter. Since rotors are ever increasing in size, taking the lagging effect of dynamic inflow becomes ever more important in aero-elastic calculations as discussed by Van Engelen and Van der Hooft [4] and Odgaaard et al. [5]. Including a correct response to unsteadiness into BEM is therefore imperative.

Different additions to BEM have been made to model the transient response to unsteady loading. The first of these additions was made for helicopters by Pitt and Peters [6], based on the work by Carpenter and Fridovich [7]. Next to this model, both Øye [8] and Snel and Schepers [9] developed a dynamic inflow model specifically for wind turbines. Schepers [10] provides an overview of these three models. These dynamic inflow models have been compared against experiments on two occasions. The Joule 1 project, see Snel and Schepers [11], and the project by NREL, see Fingersh and Hand et al. [12][13], are two benchmark studies for unsteady rotor aerodynamics. In these studies it was found that the dynamic inflow models generally provide good results. However, more recently Yu et al. [14] [15], compared the models against a free wake vortex model and against experiments. They concluded that the engineering models underestimate the dynamic inflow effect. Yu [1] therefore proposed a different approach to model dynamic in order to overcome the inaccuracies.

Additionally, current approaches to dynamic inflow have always focused on a dynamically changing thrust as the driver of unsteady loading conditions. Despite the name 'dynamic inflow', a varying wind speed has been assumed to result in negligible dynamic inflow effects. The reason was that a changing wind speed would not result in a large absolute wind speed difference at the rotor, although it would change the induction factor, as concluded by Schepers [10]. To investigate this notion, the topic and hypothesis in this work will be that dynamic wind speed

will result in dynamic inflow effects:

> The effect of dynamic wind speed on the actuator disc and the wake is different from the effect of dynamic loading, and it therefore needs to be included in current engineering models.

Which will be investigated by using a free wake vortex model and comparing the response to thrust and wind speed change. If the hypothesis is found to be true, the second objective will be to find out whether the current engineering models correctly distinguish between a dynamically varying thrust and wind speed. And if they do not, whether the effect can be included.

The following section II will discuss the terminology, approach and methodology. The differences between dynamic wind and dynamic thrust will be shown in section III. The predicted response by the current engineering models is shown in section IV. The performance of the alternative model by Yu is discussed in section V. Section VI proposes a modification to Yu's model, which will be validated in section VII. The conclusions are discussed in the final section VIII.

II. Approach

This section will show the different test cases and their terminology, and it will briefly describe the model that has been used throughout this work. The assumption of dynamic wind is is also shown, and the effects of this assumption.

A. Terminology of Dynamic Inflow

First of all the different terms that are being used in literature, and throughout this work, need to be clarified and defined. **Dynamic Inflow** is the general name used in literature to describe the lag between induction at the rotor and the thrust coefficient C_t. Despite the name 'inflow', a dynamic incoming wind speed is usually not considered, and only the thrust is dynamic. Other names commonly used for the same effect are **Dynamic Wake** or **Dynamic Induction**. More specifically, throughout this work two other names will be used to describe the two different sources of unsteady conditions. The first of these is **Dynamic Thrust**, which describes an unsteady C_t due to varying axial thrust at the rotor.

$$C_t(t) = \frac{F_{ax}(t)}{0.5\rho A U_0^2} = f(F_{ax}(t)) \tag{1}$$

This can be regarded as a blade pitch change. A rotational speed change, as studied in the Mexico project by Schepers et al. [16], also results in an angle of attack change and therefore a thrust change.

The second source of unsteady conditions is wind speed: **Dynamic Wind**. This describes an unsteady C_t due to varying incoming wind speed. In this case the axial thrust is assumed constant, and only the wind speed is dynamic.

$$C_t(t) = \frac{F_{ax}}{0.5\rho A U_0^2(t)} = f\left(\frac{1}{U_0^2(t)}\right) \tag{2}$$

B. Methodology

The methodology and flow of the work is quite straightforward. A vortex model was constructed, which functions as higher fidelity method as compared to BEM. In this vortex model dynamic wind and dynamic thrust are compared against each other in a couple of test cases. After this current engineering models added to BEM are compared against these results, in a similar fashion as done by Yu [1]. Finally a new model is constructed by fitting it over a wide range of thrust coefficients to the vortex model response to dynamic wind.

Vortex Model To evaluate dynamic inflow a free wake vortex ring model is chosen here. The reason is because a vortex model is reasonably flexible in evaluating different cases, and a good compromise between accuracy and speed. In this work the focus lies on an actuator disc without distinct lifting bodies. And if no wake rotation is assumed, then all vorticity is concentrated in rings that are continually being shed by the actuator disc, and thus form a sheet behind the disc. This is the simplest description available, and already posed by Joukowsky, see Okulov et al. [17]. Yoon and Heister [18] have derived analytical solutions for an infinitely thin vortex ring. This vorticity sheet and the discretisation into rings is shown in figure 1.

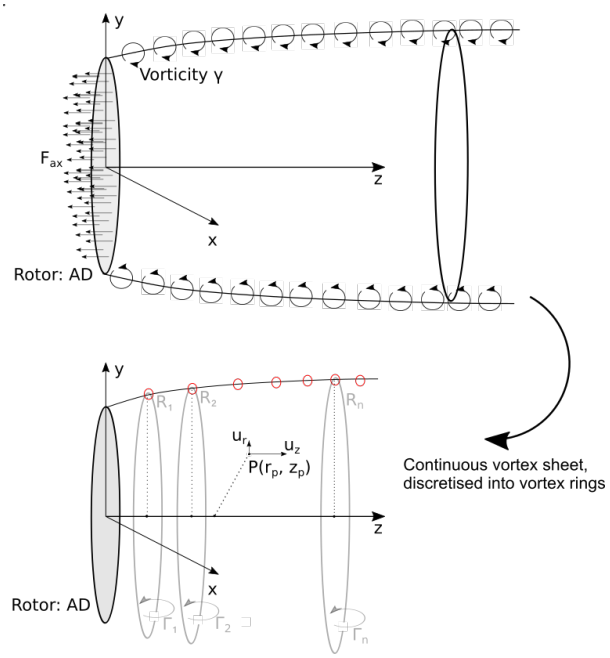

Figure 1 Wake vorticity behind actuator disc (top). Vortex ring model (bottom).

Because investigating dynamic inflow effects requires a dynamically changing wake, a prescribed wake vortex ring model will not suffice. A free wake vortex ring (FWVR) model is better at capturing the velocity response in the dynamic inflow case than a prescribed wake model because it allows the wake to have a transient response to a change. This can be seen in the study conducted by Yu et al. [19]. Van Kuik and Lignarolo [20] showed that a vortex ring model is very useful to validate certain assumptions of BEM, and that its results can give good insight in the physics of rotor aerodynamics.

The FWVR that will be discussed in this section is based on the model outlined by Baldacchino and van Bussel

[21]. The same approach is also used by Van Kuik and Lignarolo [20], Øye [22] and Yu et al. [15]. It consists of a free wake part, and a part where the wake is fully expanded which is regarded as a semi-infinite tube.

Model Limitations In this FWVR model there are three parameters that govern the accuracy and speed: the time step Δt, the vortex cut-off radius (viscous core) δ, and the point at which the free wake ends and the vortex tube starts. Yu et al. [15] and Van Kuik and Lignarolo [20] all found convergence values for these parameters. This FWVR model has been validated against experiments by Yu et al. [15], and was cross-verified by Van Kuik and Lignarolo [20]. The model parameters that have been used here are shown in table 1. The same model parameters

Table 1 Limiting parameters used in the FWVR model.

Parameter	Value	From Yu et al. [15]
Vortex cut-off δ	10^{-5}	10^{-5}
Time Step $\Delta\tau$	0.02	0.02
Extension of vortex rings	11R	11R

have been chosen as the FWVR model by Yu et al., who estimated the modelling error with these parameters. It was shown that by using these values the influence of the time step, cut-off radius and number of vortex rings is very small.

Test Cases Initialy, the following test cases have been evaluated:

Step Change $C_t = 7/9$**:** $\Delta C_t = \pm 1/9$.

Step Change $C_t = 6/9$**:** $\Delta C_t = 1/9$.

Harmonic Change $C_t = 7/9$**:** $\Delta C_t = 1/9$. The reduced frequencies tested here are $k = 0.2, 0.5, 1$.

These cases have been chosen because they can easily be compared against the results by Yu. The test cases in the experiments by Hong [23] and Kaur [24] have also been evaluated as verification and baseline.

Time and frequency are non dimensionalised through:

$$\tau = \frac{tU_0}{R}$$
$$k = \frac{\omega R}{U_0}$$

C. Effect of Dynamic Wind Assumption

Before looking at the differences between dynamic wind and dynamic thrust, the implementation of dynamic wind must be evaluated. It is expected that the way the gust convects influences the way the wake responds, and therefore the response at the rotor. The three different implementations are described in the following section.

Modelling Dynamic Wind How a wind speed change is implemented will determine how a change is perceived at the rotor and how the vortex rings convect downstream. Three different options are considered.

1. **Wave-front:** $U_0 = f(z, a)$ The first option is to change the wind in the domain in a wave-like way. The wind speed is not constant at every z but a function of z. If the wave speed is the absolute wind speed: $U_0(1 - a)$ the 'gust' convects at the same speed as the vortex rings. The wind speed at $t = i$ can then be implemented as an inherent property of the i-th vortex ring.
2. **Wave-front:** $U_0 = f(z)$ The second option is again a wave, but now the wave-front speed is constant and the same as the wind speed: the 'gust' convects faster or slower than the vortex rings.
3. **Uniform change:** $U_0 = f(t)$ The third and final option is a uniform change across the spatial domain. The wind changes everywhere at the same time. This is the least 'physical' description of a wind gust.

Differences between Approaches The resulting differences of the three cases previously described are shown in figure 2. For comparison the dynamic thrust case is also shown.

From these graphs two conclusions can be drawn:

A uniform change results in a different response than a wave-front response. The response of a uniform change is faster than a wave-front. Which is expected, as a wave should result in a gradual change in the wake, while a uniform change would impose a more sudden change on the wake. The similarity to dynamic thrust in the case of a uniform change is surprisingly striking however: apparently a local change in load (and thus circulation) starting from the actuator disc, has a similar exponential effect as changing the velocity in the entire wake.

The exact value of the wave-front velocity does not have a large influence. The difference between the first and second approach of modelling the wave-front is small. The exact velocity at which the wave front travels through the wake can thus be neglected.

In the following analysis the wave-front approach with a convection speed of $U_0(1 - a)$ will be used, such that the wave convects at the same speed as the vortex rings. The reason for this is two-fold, first because a uniform change is not very realistic, and second because the wind velocity becomes an inherent property of a vortex ring. This is similar to the dynamic thrust approach, where the C_t, and thus circulation strength are inherent properties of the shed vortex rings. It would be interesting to see the difference between the two properties that define the C_t.

III. Response to Dynamic Wind as compared to Dynamic Thrust

In this section both dynamic inflow drivers will be compared against each other in the FWVR model. The dynamic thrust case is the baseline, and the following sections will show in which ways dynamic wind deviate from the dynamic thrust response.

A. Dynamic Wind Effects on Wake

The wake probably explains the differences between dynamic thrust and dynamic wind best. Because there are two things to note when looking at the wake behind the rotor:

The expansion of the wake does not differ between dynamic thrust and dynamic wind, see figure 3a. This

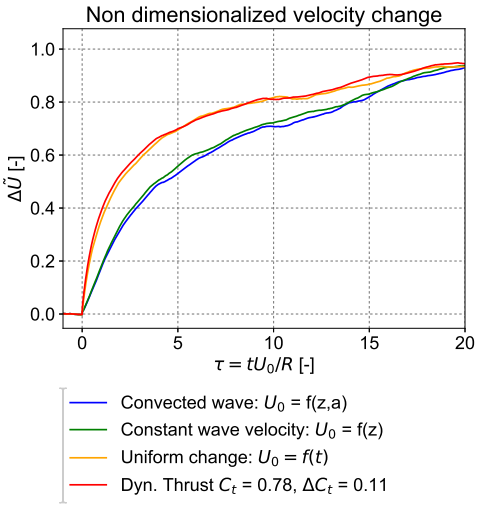

(a) Non dimensionalised change in induced velocity U_{ind} vs τ.

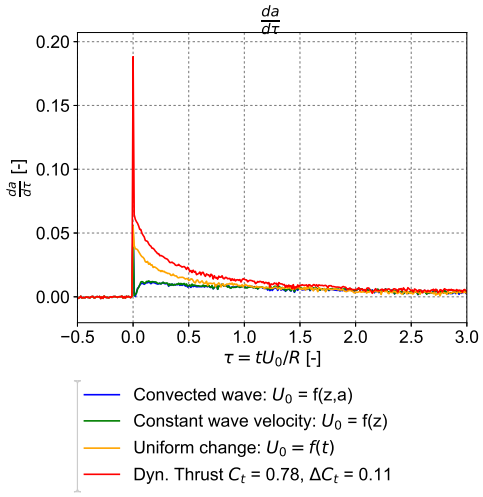

(b) Change in induction factor per unit of time.

Figure 2 Different implementations of a change in velocity throughout the domain and wake. $C_t = 7/9$**,** $\Delta C_t = 1/9$**.**

makes sense, because the thrust coefficient alone defines the expansion of the wake. The cases reach the equilibrium differently though.

The wake is 'stretched' or 'compressed' in the dynamic wind case as compared to dynamic thrust. The vortex rings are closer together or further apart, depending on an increase or decrease of C_t. This can be seen in figure 3b: where the wake is convected further or less far as compared to dynamic thrust. This is due to a different absolute value of velocity in the wake. As a result of this, the strength of the vorticity Γ/dz changes, even though the circulation Γ remains constant in the dynamic wind case.

The second notion is important, as it touches the core of the difference. In the dynamic thrust case the induction changes are driven by the change in shed vorticity, while in the dynamic wind case the induction changes are a resultant of changes in the wake.

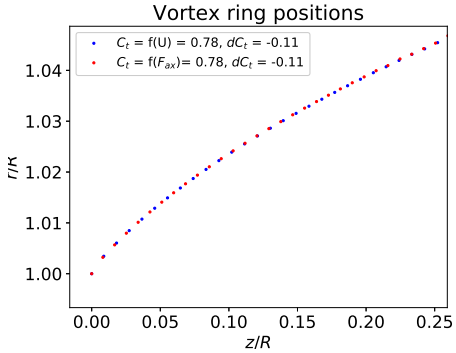

(a) Position of vortex rings, $C_t = 7/9$, $\Delta C_t = 1/9$.

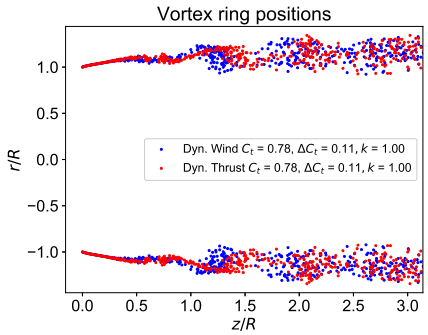

(b) Position of vortex rings, $C_t = 7/9$, $\Delta C_t = 1/9$, $k = 1$.

Figure 3 Vortex ring positions for different cases compared.

B. Relevancy and Scale of Dynamic Wind

The previous section discussed the effects on the wake. This section will show the scale of the dynamic wind response and its relevancy as compared to dynamic thrust.

The change of induced velocity is smaller in the dynamic wind case. When looking at figures 4a, 4b and 4d, it can be concluded that the induced velocity change is smaller. However, because the induction factor is also a function of the velocity, the induction factor matches the induction factor of the dynamic thrust case very closely. So induced velocities are different, but induction factors are similar.

The instantaneous induction factors are only similar for small and slow changes in C_t. When the thrust coefficient changes rapidly (i.e. harmonically at a high frequency $k = 1$), the induction factors are no longer similar. See figure 5a. This is because the induced velocity does not respond as quickly in the dynamic wind case as in the dynamic thrust case, as shown in figure 5b. When the changes are less rapid ($k = 0.2$), the induction factors follow a similar pattern again, as can be seen in figures 6a and 6b. This effect can also be seen in figures 10a and 10b. The amplitude of the induced velocity is smaller in the case of dynamic wind for $k = 0.2$, resulting in a larger amplitude of induction factors as compared to dynamic thrust.

To conclude, the induced velocities are different, and so is the induction factor if the changes are rapid. If the rate of change is slower, the induction factors correspond to the induction factors of dynamic thrust. Either way, the induced velocity and induction factor change are on the same order of magnitude, albeit smaller, and therefore just as relevant as in the dynamic thrust case.

C. Rate of Change and Transient Response

A few differences were already discussed in the previous sections, and this section will combine the previous conclusions into a fundamental notion about the response to a dynamic wind speed change.

The rate of change in the dynamic wind case is smaller and different. The rate of change of induced velocity at the rotor can be seen in figures 7a and 7b. In the dynamic thrust case the induction factor adjusts rapidly and the rate of change decreases exponentially. In the dynamic wind case the rate of change remains rather constant.

This difference may be explained by how the change originates at the rotor, and how the wake responds. This is shown in figure 8. In the dynamic thrust case the first order effect is due to the convection of changing vorticity strength because the circulation Γ changes. This effect is immediate and instantly results in changing induced velocities. The second slower effect is the result of the adaptation of the wake to the new conditions. In the dynamic wind case, the first order effect is because of the changing density of vorticity γ. The circulation Γ remains constant. This is because circulation is defined as:

$$\Gamma = \frac{C_t U_0^2 \Delta t}{\rho} \tag{3}$$

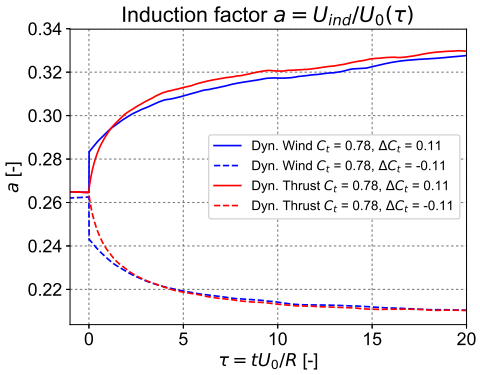

(a) a **[-] versus** τ **[-] for step change in** C_t**.**

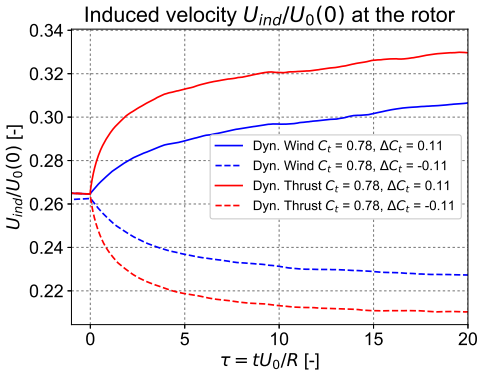

(b) U_{ind} **[m/s] versus** τ **[-].**

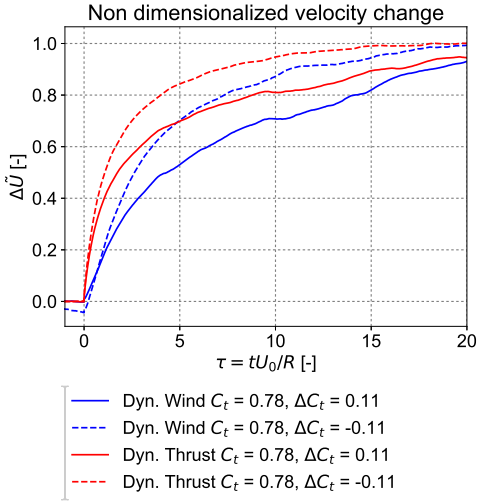

(c) Non dimensionalised change in induced velocity U_{ind} **versus** τ **[-].**

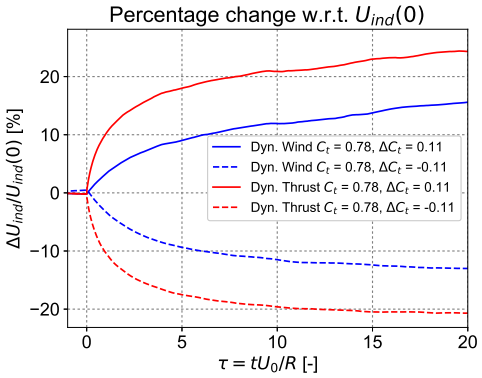

(d) Relative change in percentage of induced velocity at $tau = 0$ **versus** τ **[-].**

Figure 4 Induction factor and induced velocity for $C_t = 7/9$ **and** $\Delta C_t = \pm 1/9$**.**

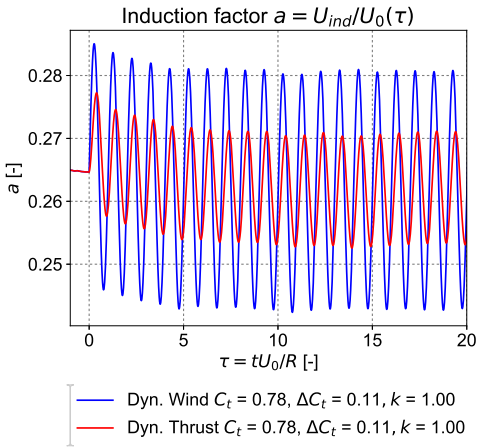

(a) a **[-] versus** τ **[-] at** $k = 1$

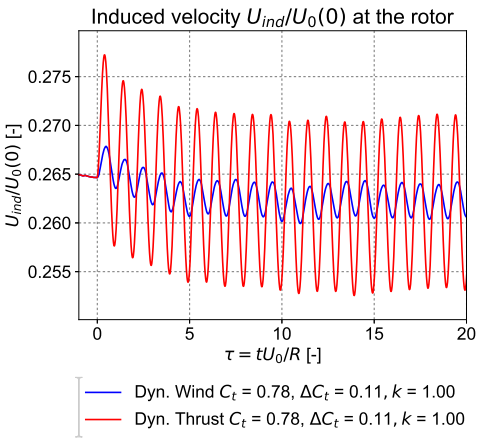

(b) U_{ind} **[m/s] versus** τ **[-] at** $k = 1$

Figure 5 Induction factor and induced velocity for $C_t = 7/9$ **and** $\Delta C_t = 1/9$ **at** $k = 1$**.**

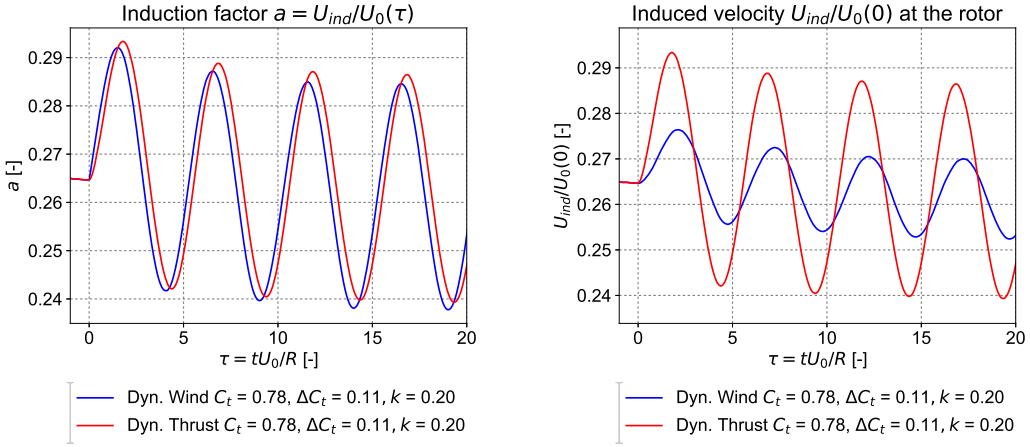

(a) a **[-] versus** τ **[-] at** $k = 0.2$ **(b)** U_{ind} **[m/s] versus** τ **[-] at** $k = 0.2$**.**

Figure 6 Induction factor and induced velocity for $C_t = 7/9$ **and** $\Delta C_t = 1/9$ **at** $k = 0.2$**.**

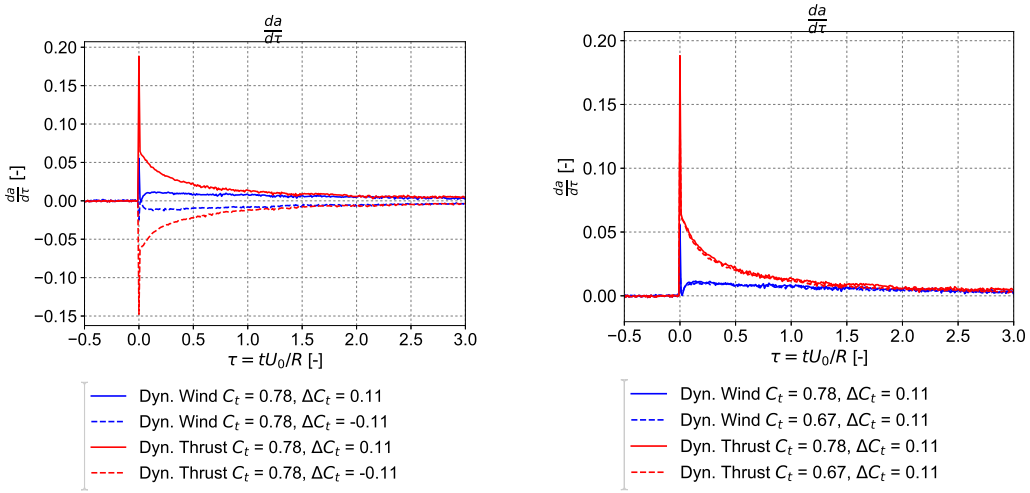

(a) Change in induction factor per unit of time, $\Delta C_t = \pm 1/9$**. (b) Change in induction factor over time,** $\Delta C_t = 1/9$**.**

Figure 7 Change in induction factor per unit of time for $C_t = 7/9$ **and** $C_t = 6/9$**.**

Vorticity does change, because vorticity is the density of the vortex rings:

$$\gamma = \frac{\Gamma}{\mathrm{d}z} \tag{4}$$

So the only change is the vorticity strength. However, this is a gradual change, and not as immediate as the change in shed vorticity strength. And because of this, the initial rate of change in the case of dynamic wind is slower. The second order effect is similar to the dynamic thrust case, and is due to the wake gradually changing to its new strength. Which brings the next conclusion:

The dynamic wind case matches the rate of change of the thrust case after a certain period of time. This could also be seen in figure 4a. The rate of change of induction factor initially is slower and after a while follows the thrust case. This makes the conclusion likely that dynamic thrust (and dynamic inflow in a general sense) is the summation of two effects: a first order quick response due to the change in shed vorticity strength, and a second order slower response due to the wake changing shape and density.

(Note that dynamic wind could also turn into a rapid change if it is regarded as a uniform change across the flow field, as discussed in section II.C. In that case the same peak and exponential decay can be observed.)

Slower rate of change is also present in the harmonic case, because the dynamic wind response is not as quick as in the dynamic thrust case. Figures 9a and 9b show the different harmonic responses. It was already observed that the induced velocity does not change as much, but there is also a phase difference: there is a phase lag of the dynamic wind cases as compared to dynamic thrust. The difference is also clear in figures 10a and 10b, in which the absolute velocity is plotted against the thrust coefficient. Different instantaneous thrust coefficients correspond to different velocities at the rotor for both cases.

The response is the same for different steady thrust coefficients , as can be seen in figure 7b . Both the $C_t = 7/9$ and $C_t = 6/9$ case follow the same response. This can be observed for both the wind and dynamic thrust case. Although there is no difference in this regard, it may be interesting as it implies that the time scales of dynamic inflow effects are relatively independent for small changes of steady thrust coefficients.

D. Conclusions

To summarise the results: two major differences can be observed. First of all the rate of change in the dynamic wind case is different. It is a gradual change, which can be explained in the way the vorticity is convected in the wake.

Second, as a result of this, the induced velocity response in the case of dynamic wind is not as large and quick as in the case of dynamic thrust. Therefore a different phase difference may be observed. Both of these notions are important in the implementation of dynamic inflow models.

Furthermore, a conclusion may be drawn that in general dynamic inflow can be modelled as a summation of two effects. First the transient response with a quick exponential decay, corresponding to the shedding of the vorticity. And second a slower rate of change corresponding to the wake changing density and shape. Dynamic

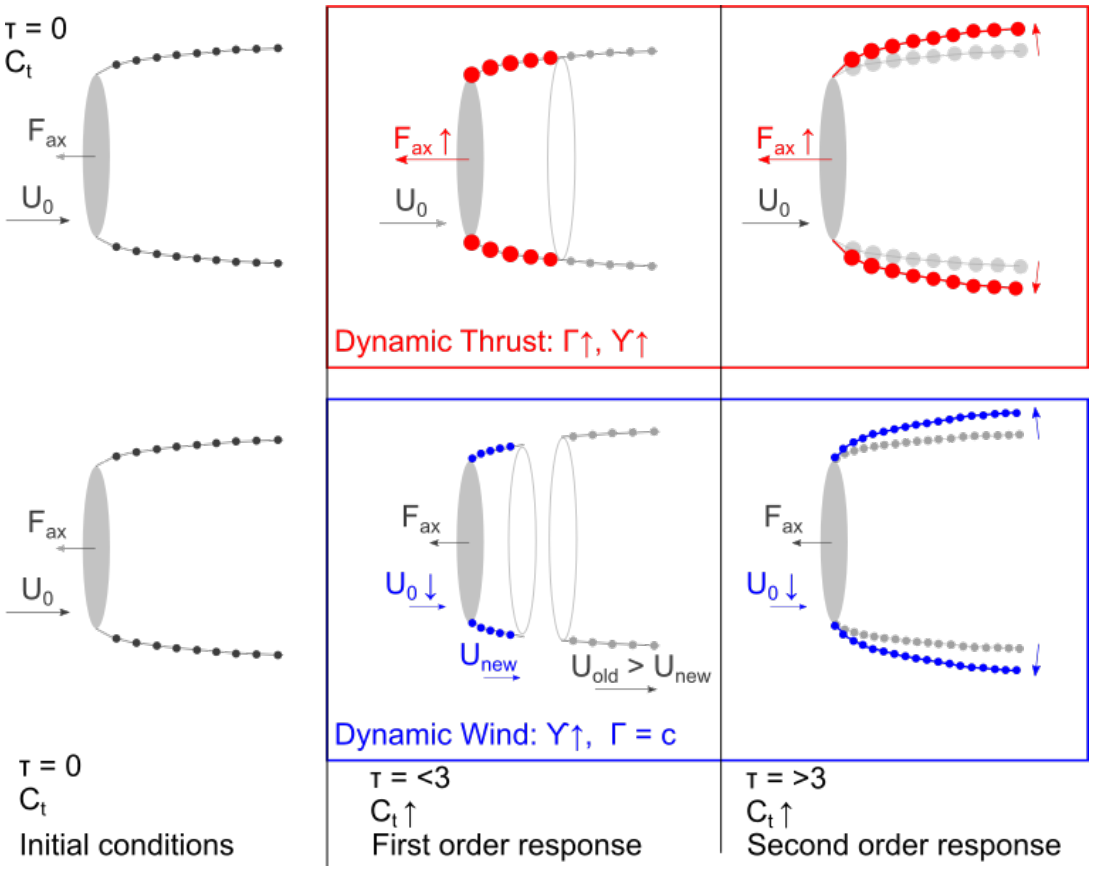

Figure 8 Rotor and wake representation. Left: initial conditions. Center: first order response. Right: second order response. Circles indicate vortex ring positions (density: vorticity γ) and vortex ring strength (circulation Γ).

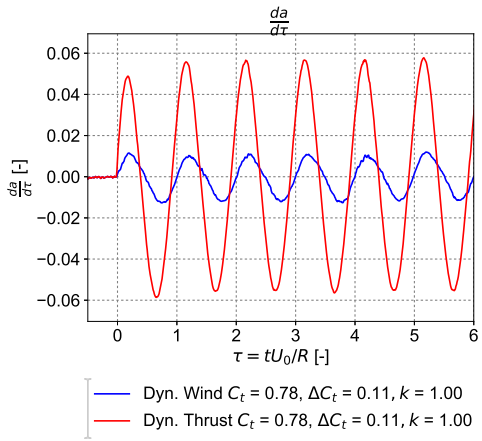

(a) Change in induction factor per unit of time, $k = 1$..

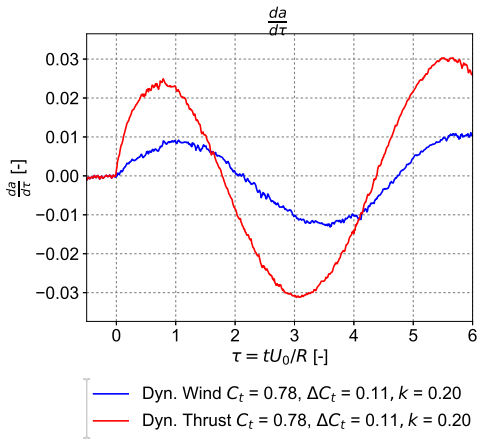

(b) Change in induction factor per unit of time, $k = 0.2$.

Figure 9 Induction factor change per unit of time, $C_t = 7/9$, $\Delta C_t = 1/9$, $k = 1$ and $k = 0.2$.

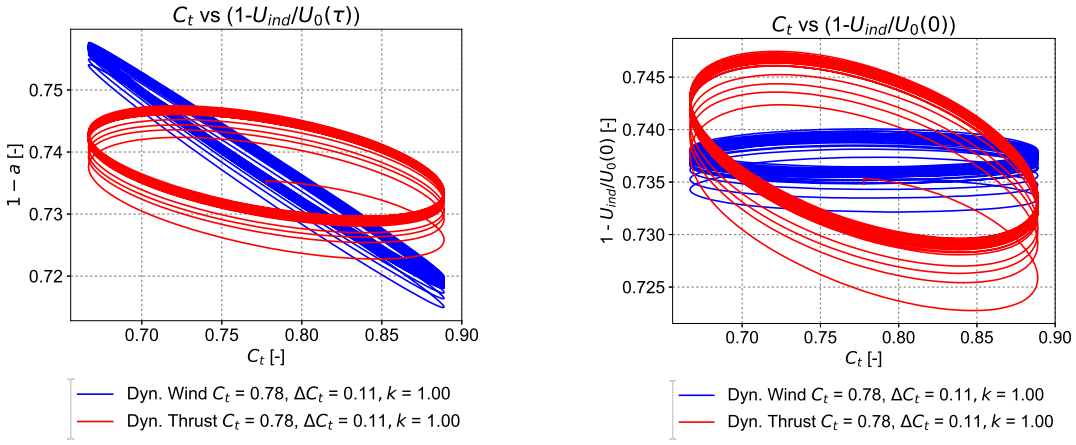

(a) C_t **vs** u_{ind}**, non dimensionalised by** $U_0(\tau)$**.** **(b)** C_t **vs** u_{ind}**, non dimensionalised by** $U_0(0)$**.**

Figure 10 Phase difference: instantaneous thrust coefficient versus induced velocity. $C_t = 7/9$**,** $\Delta C_t = 1/9$**,** $k = 1$ **and** $k = 1$**.**

wind only shows the second order effect.

Finally, it must be noted that the way the dynamic wind is modelled has an influence on the results. A wave-front or a uniform change across the domain will result in different responses.

IV. Performance of the Models by Øye, Pitt-Peters and ECN

The three most commonly used engineering models will be evaluated here, to see how they perform in dynamic inflow as compared to the FWVR model. Both the dynamic thrust cases as dynamic wind cases will be used in the evaluation.

The three models that will first be compared against the results from the FWVR model are 1.Øye's model, developed by Øye [22], 2. Pitt-Peter's model by Pitt and Peters [6] and 3. ECN's model by Snel and Schepers [11].

1. Øye Developed by Øye, [22], this model describes the induced velocity response over time by two first-order linear differential equations. It defines the quasi-steady state velocity V_{qs} as the velocity from momentum theory. And $\frac{dV_{qs}}{dt}$ as the steady state response to a change, which is immediate in the case of momentum theory. This is then inserted into the following two equations:

$$V_{int} + \tau_1 \frac{dV_{int}}{dt} = V_{qs} + \kappa\tau_1 \frac{dV_{qs}}{dt} \tag{5}$$

$$V + \tau_2 \frac{dV}{dt} = V_{int} \tag{6}$$

V_{int} is simply the intermediate velocity value. With the quasi-steady state input from BEM, this then results into the actual induced velocity response V. κ, τ_1 and τ_2 were found using Vortex Ring models with a prescribed wake [22].

The accuracy of Øye's model depends on the values found for the time constants. The original time constants

were found with a prescribed wake vortex method and through correlations with experimental data. But the question rises whether such a prescribed wake model is capable of capturing the transient wake response, and whether the experiments can be generalised towards all turbines.

2. Pitt-Peters Carpenter and Fridovich [7] did experimental research into unsteady loading. They developed the notion that the transient behaviour observed in unsteady conditions is due to the mass of air that requires time to settle to a new equilibrium. Pitt and Peters [6] developed a system of linear equations to account for this mass time dependence.

The Pitt-Peters model has been validated extensively for helicopters, and is convenient because it produces consistent results both in hover as in forward flight (axisymmetric and yawed flow).

In the axisymmetric case and translated to wind turbines it can be applied to BEM through, (see Snel et al. [11]):

$$T_k = \frac{8}{3\pi}\rho A_k r \frac{\mathrm{d}V_{i,k}}{\mathrm{d}t} + 2\rho A_k V_{i,k}\left(V_0 + V_{i,k}\right) \tag{7}$$

For every annular ring in k with area A_k, and at every time step i. T_k is the thrust in the annular ring, and $V_{i,k}$ is the induced velocity at time step i in annular ring k. The model by Pitt and Peters is used in most commercial software for BEM, such as GH Bladed.

3. ECN Snel and Schepers [11] also outline an additional dynamic inflow model, based on integral relations of a stream tube model (see [10] or [25] for an overview of a stream tube model).

$$4Rf_a \frac{\mathrm{d}}{\mathrm{d}t}\left(V_i\right) + 4V_i\left(V_0 - V_i\right) = \sigma V_{eff}^2 c_n \tag{8}$$

Equation 8 is a differential equation for the induced velocity V_i at each annulus in BEM. In this equation the time constant τ is the $\frac{R}{V_0} f_a$ portion. Finally, the dependency on r/R, which was lost in the derivation of equation 8, is reintroduced through f_a as:

$$f_a = 2\pi / \int_0^{2\pi} \frac{\left[1 - (r/R)\cos\phi_r\right]}{\left[1 + (r/R)^2 - 2\,(r/R)\cos\phi_r\right]^{3/2}} \mathrm{d}\phi_r \tag{9}$$

Analogous to equation 8 a similar equation can be derived for the tangential momentum balance.

A. Dynamic Thrust in Engineering Models

First the performance of the engineering models in the dynamic thrust case is evaluated. The results and test cases shown here are similar to Yu's verification study [15]. Figures 11 and 12 show the response to a step change of $\Delta C_t = 1/9$.

The FWVR model predicts a slower initial change and a much larger time scale of the effect afterwards. It can be concluded that the engineering models underestimate the effect of dynamic inflow. The explanation for

this underestimation is different for each model. Pitt-Peters does not consider the wake at all, and was made for helicopter thrust cases. The ECN model is similar in form to Pitt-Peters, but its time constants are based on a frozen cylindrical wake model and therefore very different. Øye's model is the only model that considers two different time scales and is therefore closest to the effects seen in the FWVR model. However, the time constants used in Øye's model seem to be incorrect. These time constants were derived from a wake model. However, the wake model used by Øye was a prescribed fixed wake model and the question is whether a fixed wake model is capable of properly capturing the dynamic inflow effects. The free wake vortex model used here shows that the wake requires a longer time to adjust than predicted by the engineering model of Øye.

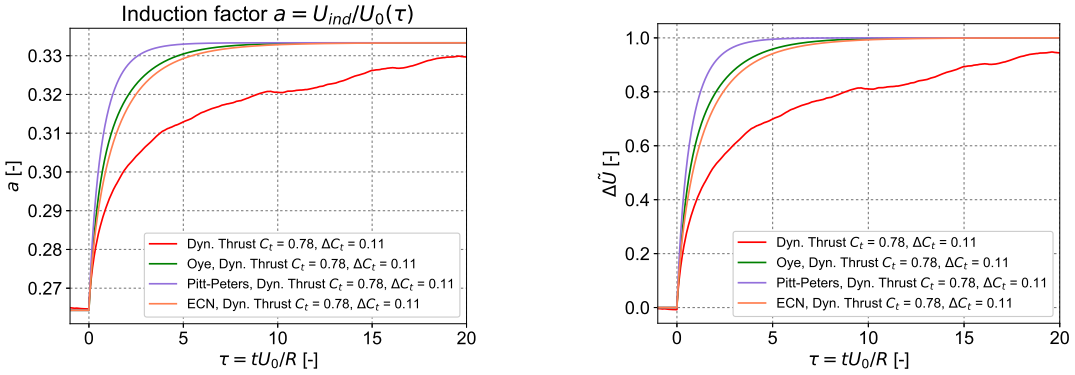

(a) Induction factor vs τ.

(b) Non dimensionalised change in induced velocity U_{ind} versus τ [-].

Figure 11 Comparison of the dynamic inflow effects of dynamic thrust between FWVR models and the engineering models, $C_t = 7/9$, $\Delta C_t = 1/9$.

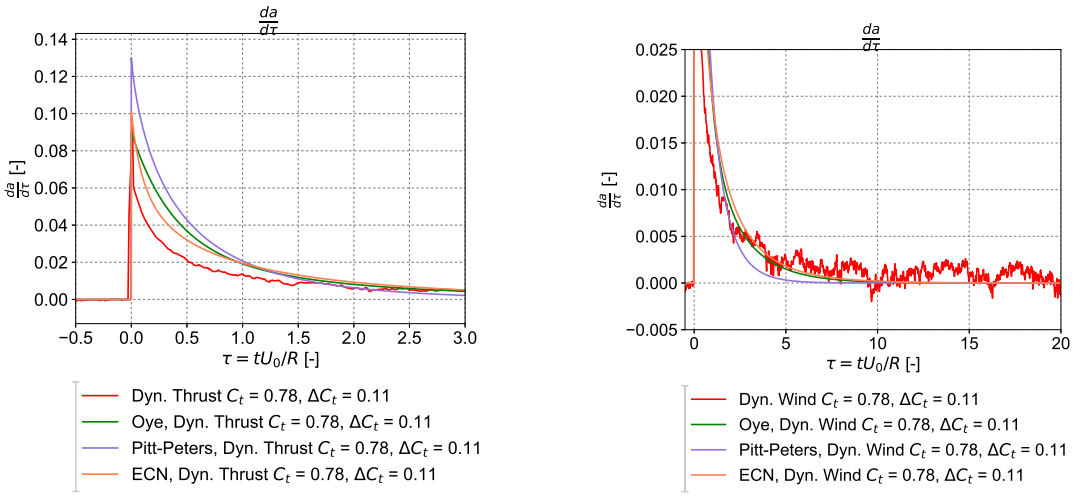

(a) Rate of change of induced velocity vs $\tau < 3$.

(b) Rate of change of induced velocity vs $\tau < 20$.

Figure 12 Comparison of the dynamic inflow effects of dynamic thrust between FWVR models and the engineering models, $C_t = 7/9$, $\Delta C_t = 1/9$.

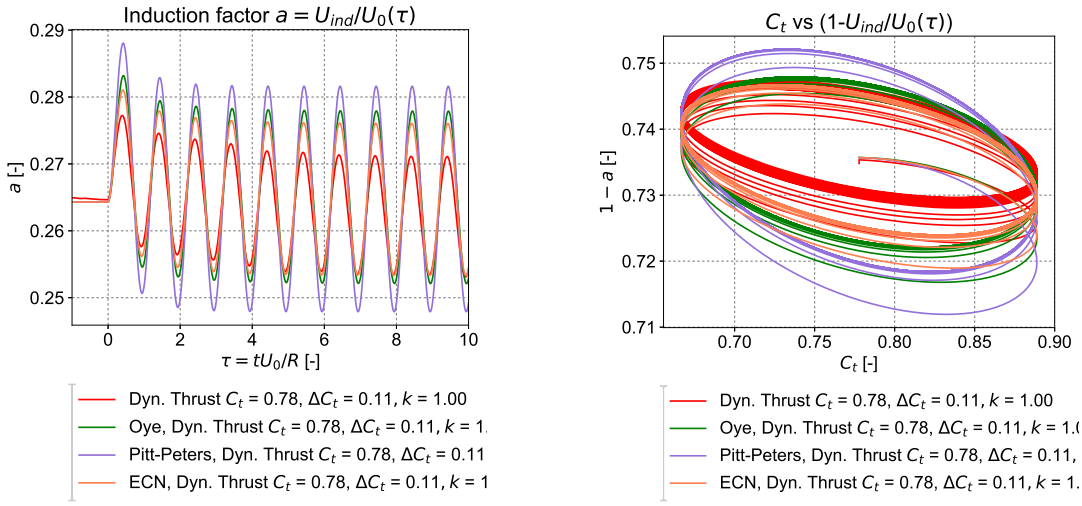

(a) Induction factor a vs τ. **(b) C_t vs u_{ind}, non dimensionalised by U_0 at τ.**

Figure 13 Comparison of the dynamic inflow effects of dynamic thrust between FWVR models and the engineering models, $C_t = 7/9$, $\Delta C_t = 1/9$, $k = 1$.

B. Dynamic Wind in Engineering Models

The previous section evaluated the engineering models in the case of a load change: $C_t = f(F_{ax})$. This section will put the engineering models through the case of a changing incoming wind: $C_t = f(U_0)$.

Modelling the transient response to a changing wind speed has never been the purpose of the engineering models, so it is not to be expected that the engineering models will be able to properly capture the transient in this case. Figures 14 and 15 will show the response to a step change of thrust coefficient of $\Delta C_t = 1/9$ due to a change in the incoming wind U_0. Figures 16 and 17 show a harmonically varying change in wind speed.

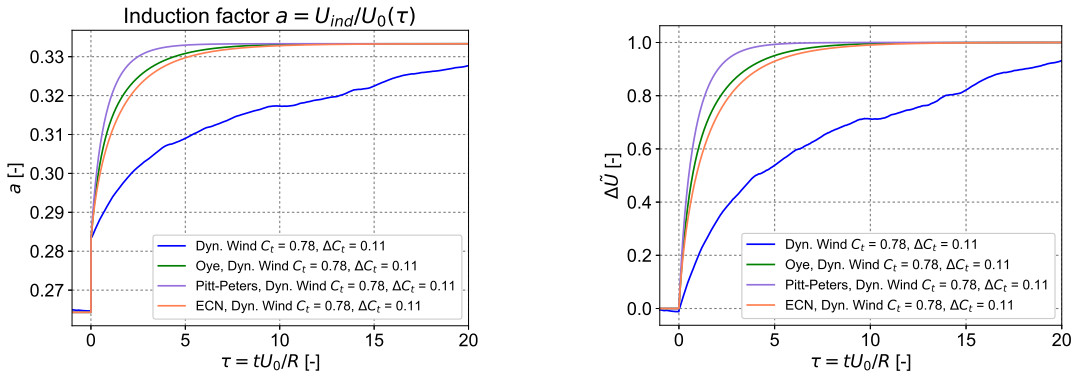

(a) Induction factor vs τ. **(b) Non dimensionalised change in induced velocity U_{ind} versus τ [-].**

Figure 14 Comparison of the dynamic inflow effects of dynamic wind between FWVR models, experimental results and the engineering models, $C_t = 7/9$, $\Delta C_t = 1/9$.

As can be seen from figures 14 to 17, the engineering models are fundamentally different from the expected dynamic wind effect. The predicted response is too fast for dynamic wind (even more than in the dynamic thrust case). This is because all dynamic inflow models are modelled with dynamic thrust in mind, and therefore follow the faster first order effect of dynamic thrust. The differential in the engineering model equations is a derivative of

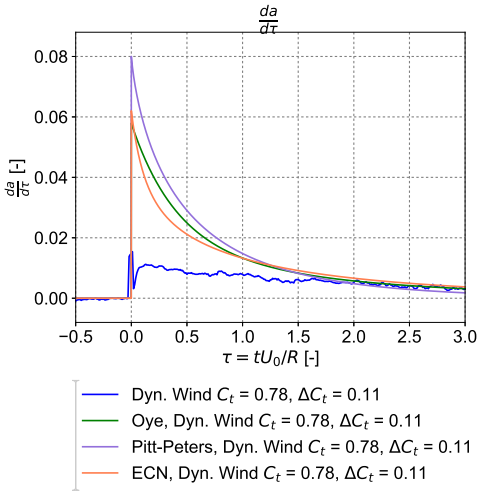

(a) Rate of change of induced velocity vs $\tau < 3$.

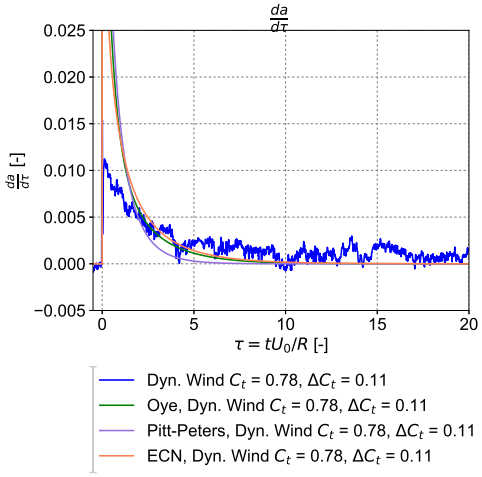

(b) Rate of change of induced velocity vs $\tau < 20$.

Figure 15 Comparison of the dynamic inflow effects of dynamic wind between FWVR models and the engineering models, $C_t = 7/9$, $\Delta C_t = 1/9$.

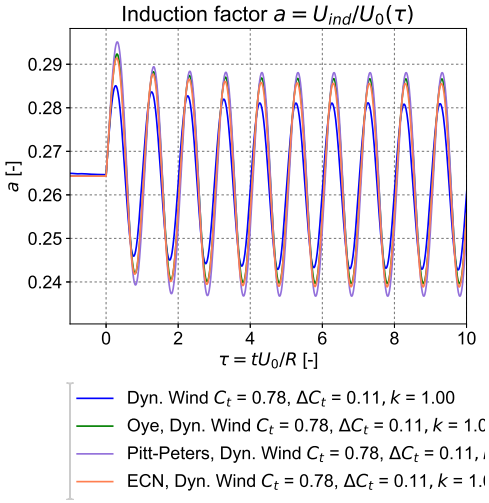

(a) Induction factor a vs τ.

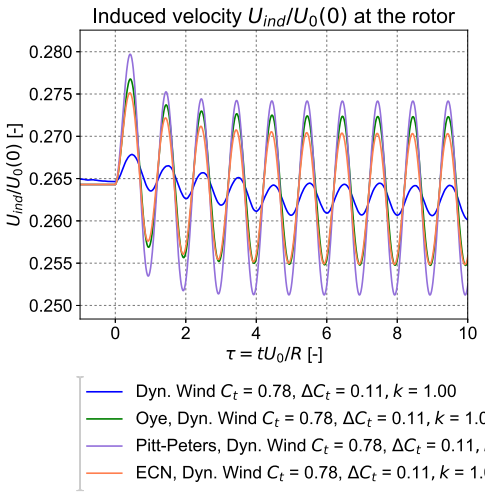

(b) Induced velocity a vs τ.

Figure 16 Comparison of the dynamic inflow effects of dynamic wind between the FWVR model and the engineering models, $C_t = 7/9$, $\Delta C_t = 1/9$, $k = 1$.

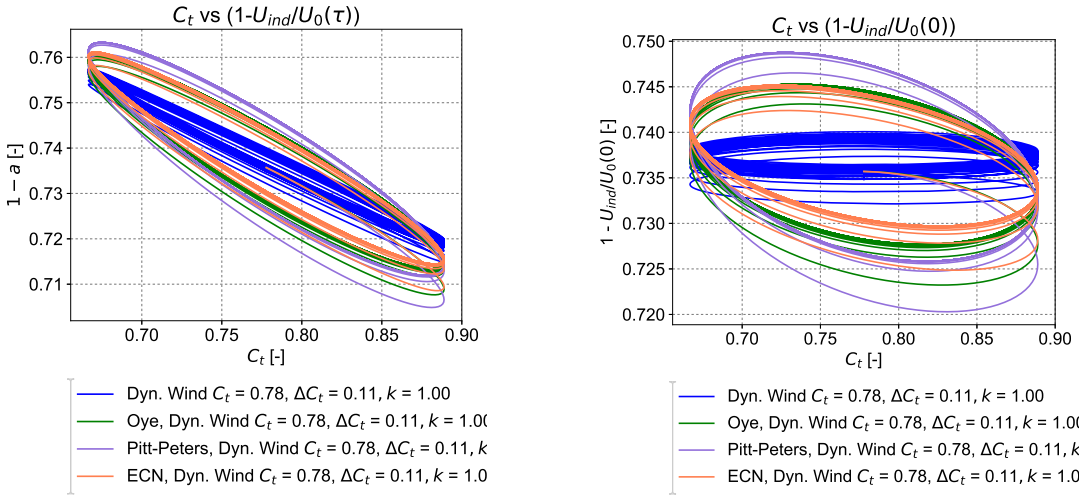

(a) C_t **vs** $u_z/U_{0,t}$**.** **(b)** C_t **vs** $u_z/U_{0,0}$**.**

Figure 17 Comparison of the dynamic inflow effects of dynamic wind between the FWVR model and the engineering models, $C_t = 7/9$**,** $\Delta C_t = 1/9$**,** $k = 1$**.**

a change in bound circulation at the rotor, and is therefore inadequate to model the slower second order effect of dynamic wind.

On the other hand, these two effects could be modelled as two time scales, and that is exactly what Øye's model does. The time scales used in the model are too small tough, and Øye's model over predicts the quickness of the response just like the other models.

V. New Approach by Yu

It has been established that the current and older engineering models underestimate the effect of dynamic inflow due to dynamic thrust, and that they do not distinguish between dynamic thrust and dynamic wind. Therefore three alternative models will be tested against the FWVR as well. The first model is a vortex tube model (VTM), analogous to ECN's approach. The second model is an integro differential model by Hammam [26] and the third model is Yu's model, as outlined in [1]. The focus will lie on this new model, as it was found to perform well in the dynamic thrust case.

A. Duhamel's Integral by Yu

Yu [1] proposes a different approach by using the general solution to the second order damping equation, which can often be found to be of the form of one or more exponentials. Yu uses a free wake vortex ring model to fit the damping coefficients and frequencies. This exponential function can then be inserted in Duhamel's integral to calculate the response.

The following form of the indicial response function was defined, which describes the induced velocity response due to a change in vorticity:

$$\Phi_d(r,t) = 1 - \beta e^{\omega^1 t} - (1-\beta)\, e^{\omega^2 t} \tag{10}$$

In this equation β, ω^1 and ω^2 are the coefficients used to make the fit. These coefficients are a function of radius and base thrust coefficient, and the radial dependency was created through a third order polynomial. See Yu [1] for a description of the coefficients. The coefficients are also described in the appendix at the end of this paper.

The Duhamel's integral describes the response x to an arbitrary excitation $F(\tau)$, and the response function $h(t-\tau)$ to that excitation at time τ:

$$x(t) = \int_0^t F(\tau)\, h(t-\tau)\, \mathrm{d}\tau \tag{11}$$

The induced velocity response is then written in terms of the Duhamel's integral as:

$$u_{ind}(r,t) = \gamma(0)\Phi_d(r,t) + \int_0^t \frac{\mathrm{d}\gamma}{\mathrm{d}\sigma}\Phi_d(r,t-\sigma)\mathrm{d}\sigma \tag{12}$$

Combining equations 10 and 12, and differentiating the Duhamel's integral, Yu finds the following expression for the induced velocity response at time step j in the form of a time marching scheme:

$$u_{ind}(r,t) = 0.5\left(\gamma(t) - c_j^1(t) - c_j^2(t)\right) \tag{13}$$

With c_j^1 and c_j^2 being intermediate differential functions:

$$\frac{\mathrm{d}c_j^1(t)}{\mathrm{d}t} - \omega_j^1 c_j^1(t) = \beta_j \frac{\mathrm{d}\gamma(t)}{\mathrm{d}t} \tag{14}$$

$$\frac{\mathrm{d}c_j^2(t)}{\mathrm{d}t} - \omega_j^2 c_j^2(t) = \left(1-\beta_j\right)\frac{\mathrm{d}\gamma(t)}{\mathrm{d}t} \tag{15}$$

Equation 13 can then be implemented into BEM through equations 14 and 15.

B. Dynamic Thrust in Alternative Models

The alternative models have been compared against the current engineering models and against the FWVR model. Both the dynamic wind case and dynamic thrust case have been tested here. Figures 18 and 19 show the response to a step change in $\Delta C_t = 1/9$ at $C_t = 7/9$.

Yu's model in the form of the Duhamel's integral performs better than all the other models in the case of dynamic thrust, and shows a comparable response as the FWVR model. This is expected, as Yu's model is fitted to the FWVR model. This can be seen in the response to dynamic thrust as shown in figures 18. The Duhamel's integral approach shows a slower initial response and a longer overall duration to reach the new equilibrium. This is comparable to the findings from the FWVR model: two different time scales for the effect of bound circulation change and wake vorticity change.

The vortex tube model is very similar to ECN's results, and therefore offers no improvement. Hammam's model seemed promising, but it has a few flaws that prohibit it from working properly.

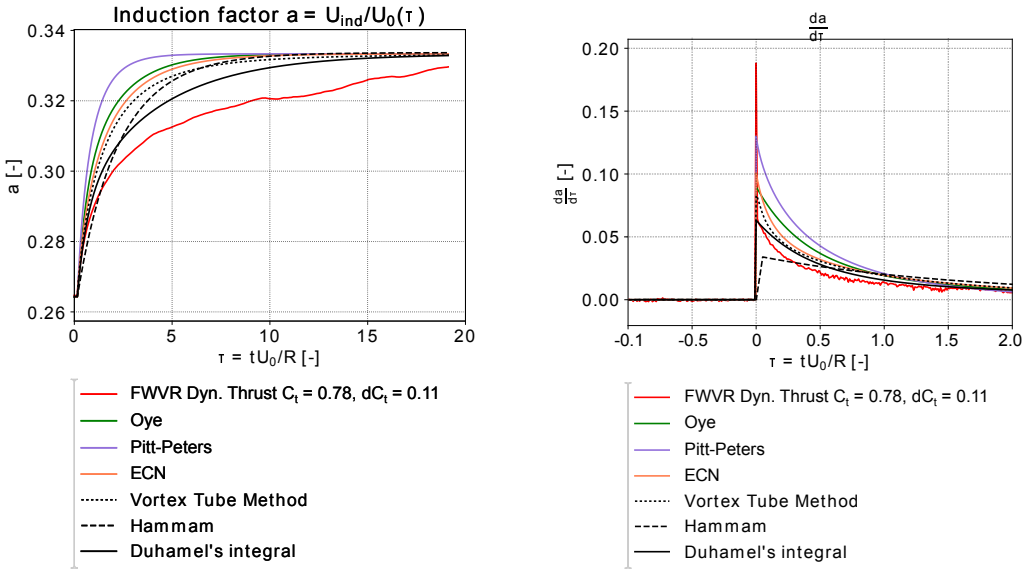

(a) Induction factor vs time. **(b) Induction factor change per unit of time.**

Figure 18 Alternative models vs FWVR and engineering models $C_t = 7/9$, $\Delta C_t = 1/9$, dynamic thrust case.

C. Dynamic Wind in Alternative Models

Although this Duhamel's integral model performs well in the case of dynamic thrust, it behaves the same as the other engineering models and offers only a minor improvement over current models. This is due to the usage of γ as a linear function of the instantaneous thrust coefficient:

$$\gamma(t) = U_0(t)\left(\sqrt{1 - C_t\,(t)} - 1\right) \tag{16}$$

As a result, $\gamma(t)$ has an instant quick response, instead of the slower adjustment of the wake. $\gamma(t)$ may in that regard replaced by the circulation at the rotor $\Gamma(t)$, which is only a function of the instantaneous thrust coefficient and wind speed.

This becomes more clear if one looks at $\mathrm{d}\gamma(t)/\mathrm{d}t$. The derivative of $\gamma(t)$ is zero everywhere in the case of a step change, except at $t = \tau$, when the step change happens. In the case of a step change, the Duhamel's integral is simply the response to a single excitation. And this is the same for both a change in wind speed as a change in load. However, in the dynamic wind case the density of vorticity γ does not change instantly as it is actually a function of induced velocity at the rotor. Therefore the model by Yu does not distinguish between dynamic thrust and dynamic wind in its input. To conclude, in order to distinguish between $\Gamma(t)$ and $\gamma(t)$ a new fit or amendment to Yu's model is necessary.

VI. Extension to Yu's Model

Three ways to amend Yu's model have been considered. The first method is to change the forcing function $\gamma(t)$ and make it a function of u_{ind} at the rotor. This would be the most physical representation of the effect of dynamic wind. This would however alter the way dynamic thrust is modelled, since dynamic thrust and dynamic

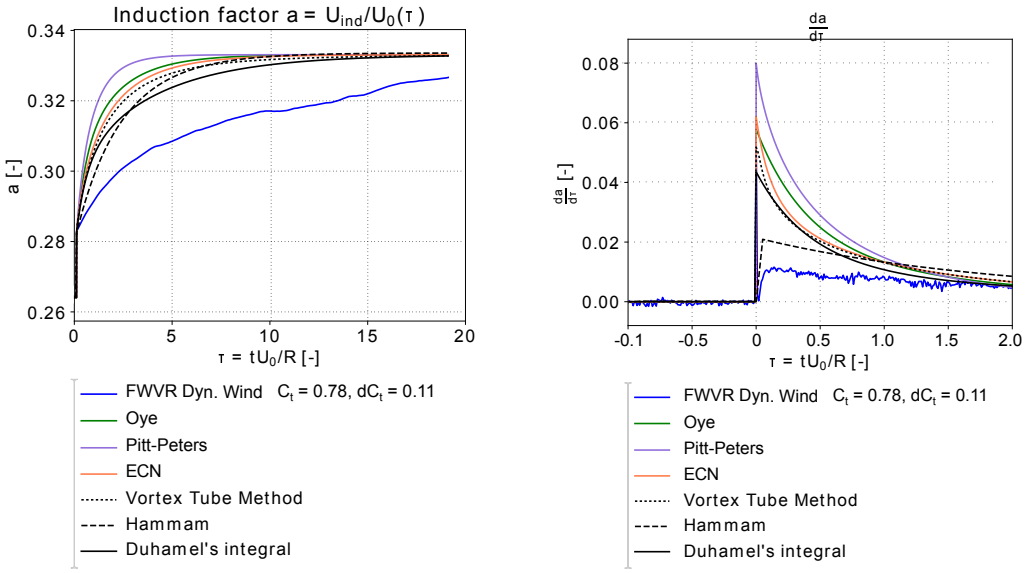

(a) Induction factor vs time. **(b) Induction factor change per unit of time.**

Figure 19 Alternative models vs FWVR and engineering models $C_t = 7/9$, $\Delta C_t = 1/9$, dynamic wind case.

wind have a different change of γ for the same change in C_t. The problem is therefore that $\Delta\gamma$ defines both the absolute change in induced velocity and defines the forcing function in the Duhamel's integral. Since both the forcing function and the absolute change are different for both effects, it becomes difficult to find an overarching way to model both way simultaneously.

The conclusions drawn from section III also suggest that the two effects may be modelled independently as a function of $\Gamma(t)$ and $\gamma(t)$. Dynamic wind would then be a function of γ, and dynamic thrust would be a summation of both changes. This would be the second way to model dynamic inflow in general. However, the same problem arises that it is difficult to combine the two models with the same integrals. Furthermore, the dynamic wind response would not fit to a single exponential, and therefore two exponentials would be needed again for each forcing function.

The third method would be the most simple way, and that is to keep Yu's model the same, but add a similar integral modelling the dynamic wind response. The two responses are then independent functions from each other:

$$u_{ind}(r,t) = 0.5\gamma(0) + (1-\kappa)\underbrace{\int_0^t \frac{\mathrm{d}\gamma}{\mathrm{d}\sigma}\Phi_{d,1}(r,t-\sigma)\mathrm{d}\sigma}_{\text{Fit to dynamic thrust}} + \kappa\underbrace{\int_0^t \frac{\mathrm{d}\gamma}{\mathrm{d}\sigma}\Phi_{d,2}(r,t-\sigma)\mathrm{d}\sigma}_{\text{Fit do dynamic wind}} \tag{17}$$

κ is a function of the change in wind speed and thrust coefficient, defining which fit is closer to the case at hand:

$$\kappa = \frac{C_t}{\Delta C_t}\left(\left(\frac{U_0}{U_0+\Delta U_0}\right)^2 - 1\right) \tag{18}$$

Which is 0 if $\Delta U_0 = 0$, and 1 if ΔU_0 is the only change. The dynamic wind response $\Phi_{d,2}$ is fitted in the same way as the dynamic thrust response as done by Yu [1]. The question is how this combination behaves in the general

dynamic inflow case with a combined thrust and wind speed change.

Here the third method is chosen because of its simplicity. This way the dynamic wind case can easily be modelled and it would be interesting to see the response to a combined thrust and wind speed change.

Analogous to the approach outlined by Yu, the response function $\Phi_{d,2}$ is a fit to two exponentials:

$$\Phi_{d,2}(r,t) = 1 - \beta_2 e^{\omega^3 t} - (1-\beta_2)\, e^{\omega^4 t} \tag{19}$$

β_2, ω^3 and ω^4 have different values as used by Yu, since the response is different for dynamic wind. The following polynomial fits have been found to give good results for the dynamic wind case:

$$\beta_2(r) = \frac{1}{a_3 r^3 + a_2 r^2 + a_1 r^1 + a_0 r^0} \tag{20}$$

$$\omega^3(r) = a_3 r^3 + a_2 r^2 + a_1 r^1 + a_0 r^0 \tag{21}$$

$$\omega^4(r) = \frac{1}{a_3 r^3 + a_2 r^2 + a_1 r^1 + a_0 r^0} \tag{22}$$

Which reintroduces the radial dependency. The following values for the coefficients a_n have been found:

Table 2 Polynomial parameters of the exponential coefficients β_2, ω^3 and ω^4 for the dynamic wind case, based on a free wake vortex ring method.

	β_2	ω^3	ω^4
a_3	$221C_t^2 - 297C_t - 101$	$-2.21C_t + 1.35$	$7.31C_t - 4.43$
a_2	$-262C_t^2 + 364C_t - 130$	$2.62C_t - 1.72$	$-6.30C_t + 6.02$
a_1	$-62.1C_t^2 + 70.0C_t - 17.7$	$-0.71C_t + 0.45$	$2.39C_t - 1.65$
a_0	$108C_t^2 - 147.7C_t + 53.2$	$0.01C_t - 0.05$	$-2.31C_t - 1.51$

The polynomial functions are therefore a function of C_t, and the response depends on the radial location and the thrust coefficient. Note that these values are different for the dynamic thrust coefficients, which have already been fitted by Yu, [1], they are also shown in the appendix to this paper.

VII. Verification

Now that a Yu's model is extended with different coefficients this new model is put to the test and the results are shown in this section. A pure dynamic wind case is first shown, and afterwards the performance in the case of a combined response of dynamic thrust and dynamic wind is presented.

A. Dynamic Wind Case

The new coefficients of the Duhamel's integral model have been tested against results from the free wake vortex ring model. The results are shown in figures 20 and 21 for a step change, and in figures 22, 23 for a harmonic variation. As can be seen in the step change, the fit is very good for low thrust coefficients ($C_t = 0.2$), but at higher

thrust coefficients $C_t = 0.8$ becomes less good. Nevertheless, the initial response has a similar slope, as can also be seen in the rate of change in figure 21b. This results in a good fit in the harmonic case, 22, since the initial response is most important there. The amplitude and phase difference are very close, as can also be seen in figure 23. Overall, the improvement over the coefficients which were fit to the dynamic thrust case is large, both for a step change, as well as for a harmonic change.

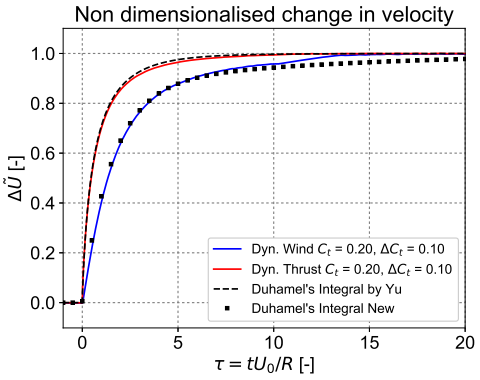

(a) Induced velocity U_{ind} vs τ.

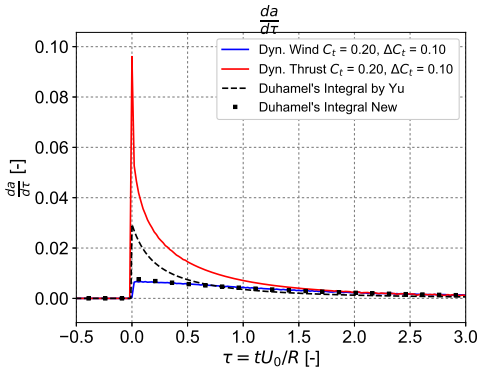

(b) Change in induction factor per unit of time.

Figure 20 Results of FWVR versus Duhamel's integral models, with different coefficients. $C_t = 0.2$, $\Delta C_t = 0.1$.

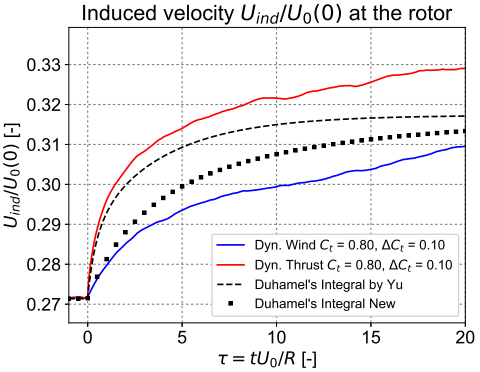

(a) Induced velocity U_{ind} vs τ.

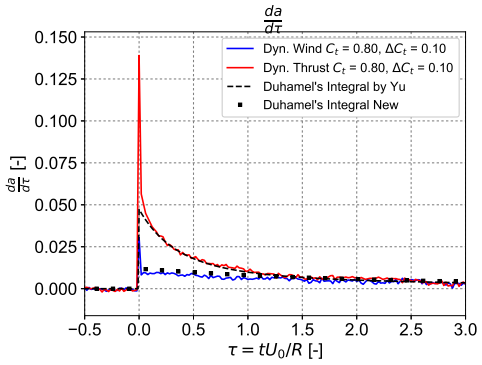

(b) Change in induction factor per unit of time.

Figure 21 Results of FWVR versus Duhamel's integral models, with different coefficients. $C_t = 0.8$, $\Delta C_t = 0.1$.

B. Combination Dynamic Wind and Thrust

The next step is to evaluate how the combination of Yu's coefficients work together with the new coefficients in the case of a combined change in dynamic inflow. Can the model still work if both the wind speed as the thrust are changed? Two cases are presented here, a total $\Delta C_t = 0.1$ at $C_t = 0.2$ and at $C_t = 0.8$. Half of the ΔC_t is due to a change of U_0, and the other half ΔC_t is due to a change in F_{ax}. The two response functions $\Phi_{d,1}$ and $\Phi_{d,2}$ then both cover half of the response as $\kappa = 0.5$ in equation 17. The results to this combined change is shown in figures 24 and 25.

The first thing that must be noted is that a combined response is relatively similar to the dynamic thrust response.

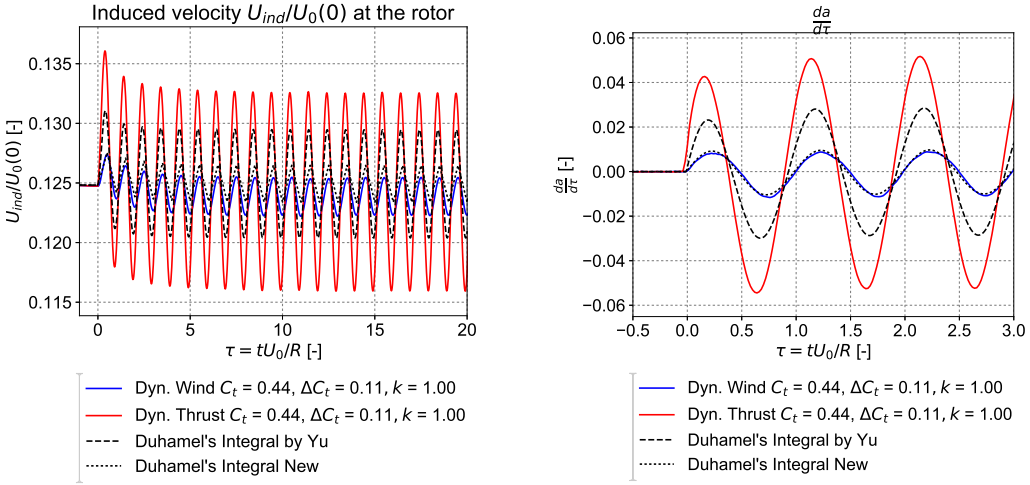

(a) Induced velocity U_{ind} vs τ. **(b) Change in induction factor per unit of time.**

Figure 22 Results of FWVR versus Duhamel's integral models, with different coefficients. $C_t = 4/9$, $\Delta C_t = 1/9$, $k = 1$.

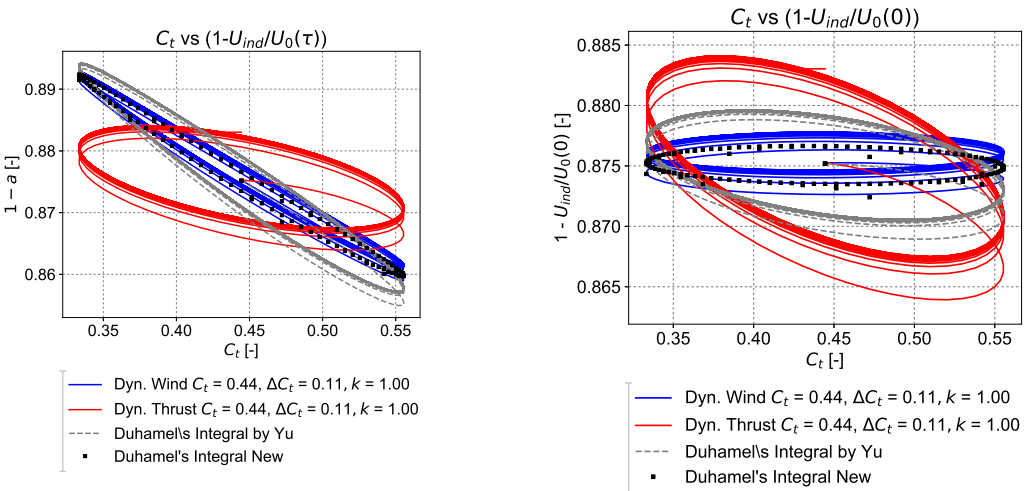

(a) C_t vs $u_z/U_{\infty,t}$ **(b) C_t vs $u_z/U_{\infty,0}$**

Figure 23 Results of FWVR versus Duhamel's integral models, with different coefficients. $C_t = 4/9$, $\Delta C_t = 1/9$, $k = 1$.

Even though $\Delta\Gamma$ is less than half of the dynamic thrust $\Delta\Gamma$, the change in shed vorticity strength is the largest contributor in the quick response.

This also means that the differences between the model fitted to dynamic thrust and the combined Duhamel's integral are small. Overall the combination of the two responses performs well and is able to predict the response of the combination. The question that remains however is whether the dynamic wind fit is really necessary in a combined response, since the response is similar to dynamic thrust.

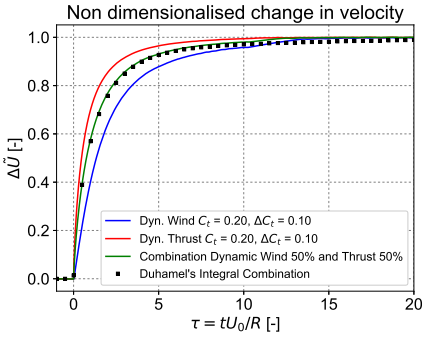

(a) Non dimensionalised change in induced velocity U_{ind} vs τ.

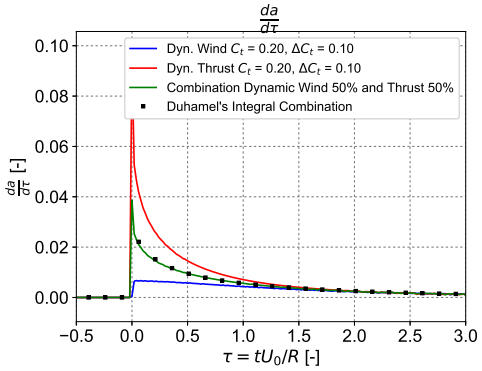

(b) Change in induction factor per unit of time.

Figure 24 Results of FWVR versus Duhamel's integral models, with different coefficients. $C_t = 0.2$, $\Delta C_t = 0.1$. Green line and Duhamel's Integral express a combination of dynamic wind (50%) and dynamic thrust (50%).

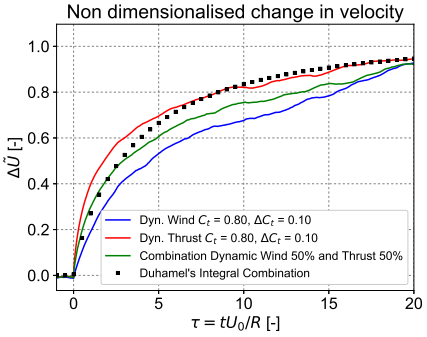

(a) Non dimensionalised change in induced velocity U_{ind} vs τ.

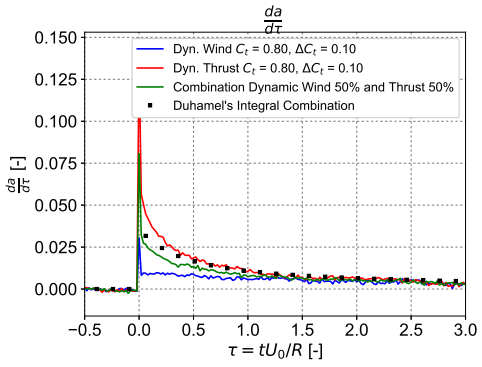

(b) Change in induction factor per unit of time.

Figure 25 Results of FWVR versus Duhamel's integral models, with different coefficients. $C_t = 0.8$, $\Delta C_t = 0.1$. Green line and Duhamel's Integral express a combination of dynamic wind (50%) and dynamic thrust (50%).

VIII. Conclusions

The focus of this work has been on two different drivers behind dynamic inflow effects: a changing thrust, and a changing incoming wind speed. Both parameters result in a changing thrust coefficient, and therefore a changing wake. In both cases dynamic inflow effects could be seen: the induced velocity at the rotor lags the thrust coefficient. The hypothesis posed in the introduction that dynamic wind speed also results in a transient response is thus found to be true. On top of that, the response is different from the dynamic thrust case. It is slower and it

is a more gradual change, as opposed to the exponentially decaying response of dynamic thrust. It can therefore be concluded that dynamic wind speed is fundamentally different from dynamic thrust. Furthermore, the dynamic thrust case and dynamic wind case converge to the same asymptote over time, which tells us how dynamic inflow in general behaves with regards to the wake. And how it should be modelled.

Because the transient response to dynamic wind is different from the dynamic thrust case, the engineering models fail to predict the dynamic wind response. This is not surprising, as dynamic thrust is the load case for which the engineering models were made. Moreover, the engineering models underpredict the effect of dynamic inflow in general, as the response is too fast, which was also concluded by Yu et al. [15], [1].

The Duhamel's integral model as proposed by Yu was found to perform well in the dynamic thrust case, and it was found to be an improvement over the existing engineering models. However, in the dynamic wind case the prediction is again off, since it is fitted to the rapid response of dynamic thrust. Therefore a proposal for an extension was made. The previous section showed that in the dynamic wind case the model predicts the response well, especially the initial response in the first few seconds, which are most important.

Finally, the Duhamel's integral was tested against a combined thrust and wind speed change. The model performed well and was able to predict the mixed response. It can be concluded that the Duhamel's integral model can be adjusted such that a dynamic wind speed is included.

Recommendations

In the free wake vortex ring model a clear difference between dynamic thrust and dynamic wind speed could be observed. Two comments have to be made here though:

- In the dynamic wind case it is assumed that the thrust remains constant. In reality the thrust will change with changing wind speed as well, and they can not be viewed independently. As a result it may be expected that a changing wind speed will also result in a thrust change, and may therefore result in a similar response as simply changing the thrust force directly. So the remaining question here is whether the effect can also be observed independently in reality. And following from this, whether the same scale of the effect is present in reality.
- In addition to this, dynamic wind speed has been modelled as a wave-front moving through the wake. Although a sudden uniform change throughout the domain does not resemble reality, the conclusions posed here rely on the wave-front assumption. A different representation of a wind speed change will have pro-found effects on the way the wake behaves. This gust wave-front therefore requires further verification.

References

[1] Yu, W., "The wake of an unsteady actuator disc," Phd., TU Delft, 2018.

[2] Hansen, M., Sørensen, J., Voutsinas, S., Sørensen, N., and Madsen, H., "State of the art in wind turbine aerodynamics and aeroelasticity," , 2006. doi:10.1016/j.paerosci.2006.10.002, URL http://ac.els-

cdn.com/S0376042106000649/1-s2.0-S0376042106000649-main.pdf?{_}tid=f2a3c098-60b2-11e7-a985-00000aab0f6c{&}acdnat=1499170915{_}7543c9a4cc3d4ee81f0b60bf3b384dc0.

[3] Sanderse, B., "Aerodynamics of wind turbine wakes: Literature review," Tech. rep., 2009. doi:10.1002/we, URL https://www.ecn.nl/docs/library/report/2009/e09016.pdf.

[4] van Engelen, T., and van der Hooft, E., "Dynamic inflow compensation for pitch controlled wind turbines," *Proceedings of EWEC*, London, 2004, pp. 22–25. URL ftp://ftp.ecn.nl/pub/www/library/report/2004/rx04129.pdf.

[5] Odgaaard, P., Knudsen, T., Overgaard, A., Steffensen, H., and Jørgensen, M., "Importance of Dynamic Inflow in Model Predictive Control of Wind Turbines," *IFAC-PapersOnLine*, Vol. 48, No. 30, 2015, pp. 90–95. doi:10.1016/j.ifacol.2015.12.359, URL www.sciencedirect.comhttp://linkinghub.elsevier.com/retrieve/pii/S2405896315030013.

[6] Pitt, M., and Peters, D., "Theoretical Prediction of Dynamic-Inflow Derivatives," *Sixth European Rotorcraft and Powered Lift Aircraft Forum*, Bristol, England, 1980. URL https://dspace-erf.nlr.nl/xmlui/bitstream/handle/20.500.11881/1796/ERF1980-47.pdf?sequence=1.

[7] Carpenter, P., and Fridovich, B., "Effect of a Rapid Blade-Pitch Increase on the Thrust and Induced-Velocity Response of a Full-Scale Helicopter Rotor," Tech. Rep. November, NACA, 1953. doi:10.1097/00152192-198911000-00004, URL https://ntrs.nasa.gov/archive/nasa/casi.ntrs.nasa.gov/19930083686.pdf.

[8] Øye, S., "Wind turbine: dynamic flow measurement," Tech. rep., Department of Fluid Mechanics, Technical University of Denmark, DTU, Copenhagen, 1992.

[9] Snel, H., and Schepers, J., "Engineering moles for dynamic inflow phenomena," *Journal of Wind Engineering and Industrial Aerodynamics*, Vol. 39, No. 1-3, 1992, pp. 267–281. doi:10.1016/0167-6105(92)90552-L, URL http://ac.els-cdn.com/016761059290552L/1-s2.0-016761059290552L-main.pdf?{_}tid=6e0261ba-7754-11e7-b786-00000aab0f26{&}acdnat=1501659201{_}625c6ee2f809b427400bd83d81ca687f.

[10] Schepers, J., "Engineering models in wind energy aerodynamics," Phd thesis, Delft University of Technology, 2012. URL http://repository.tudelft.nl/assets/uuid:92123c07-cc12-4945-973f-103bd744ec87/PhD{_}Schepers.pdf.

[11] Snel, H., and Schepers, J., "Joint investigation of dynamic inflow effects and implementation of an engineering method," Tech. rep., 1995. doi:ECN-C--94-107.

[12] Fingersh, L., Simms, D., Hand, M., Jager, D., Cotrell, J., Robinson, M., Schreck, S., and Larwood, S., "Wind Tunnel Testing of NREL's Unsteady Aerodynamics Experiment," *Proc. of the AIAA 39th Aerospace Sciences Meeting & Exhibit*, 2001. doi:doi:10.2514/6.2001-35, URL https://arc.aiaa.org/doi/pdfplus/10.2514/6.2001-35.

[13] Hand, M., Simms, D., Fingersh, L., Jager, D., Cotrell, J., Schreck, S., and Larwood, S., "Unsteady Aerodynamics Experiment Phase VI: Wind Tunnel Test Configurations and Available Data Campaigns," Tech. rep., 2001. doi:10.2172/15000240, URL https://www.nrel.gov/docs/fy02osti/29955.pdfhttp://www.osti.gov/servlets/purl/15000240-1FhaHo/native/.

[14] Yu, W., Simão Ferreira, C., and van Kuik, G., "Analytical actuator disc solution for unsteady load," *34th Wind Energy Symposium*, 2016. doi:10.2514/6.2016-0751, URL https://www.researchgate.net/profile/Wei{_}Yu18/publication/306356722{_}Analytical{_}actuator{_}disc{_}solution{_}for{_}unsteady{_}load/links/57bdaa4308aeaf647bcb51b8.pdfhttp://arc.aiaa.org/doi/10.2514/6.2016-0751.

[15] Yu, W., Simão Ferreira, C., van Kuik, G., and Baldacchino, D., "Verifying the Blade Element Momentum Method in unsteady, radially varied, axisymmetric loading using a vortex ring model," *Wind Energy*, Vol. 20, No. 2, 2017, pp. 269–288. doi:10.1002/we.2005, URL http://doi.wiley.com/10.1002/we.2005.

[16] Schepers, J., Boorsma, K., Cho, T., Gomez-Iradi, S., Schaffarczyk, P., Jeromin, A., Shen, W., Lutz, T., Meister, K., Stoevesandt, B., Schreck, S., Micallef, D., Pereira, R., Sant, T., Madsen, H., and S{\o}rensen, N., "Final report of IEA Task 29, Mexnext (Phase 1): Analysis of Mexico wind tunnel measurements," Tech. Rep. Phase 1, 2012. URL http://orbit.dtu.dk/files/56752175/ecn{_}e12004.pdf.

[17] Okulov, V., Sørensen, J., and Wood, D., "The rotor theories by Professor Joukowsky: Vortex theories," *Progress in Aerospace Sciences*, Vol. 73, 2015, pp. 19–46. doi:10.1016/j.paerosci.2014.10.002, URL https://ac.els-cdn.com/S0376042114000967/1-s2.0-S0376042114000967-main.pdf?{_}tid=d950f5fc-a4fa-11e7-a4f1-00000aab0f27{&}acdnat=1506678475{_}6e4a2cf79666a3985c6f95672a3f7553.

[18] Yoon, S., and Heister, S., "Analytical formulas for the velocity field induced by an infinitely thin vortex ring," *International Journal for Numerical Methods in Fluids*, Vol. 44, No. 6, 2004, pp. 665–672. doi:10.1002/fld.666, URL http://doi.wiley.com/10.1002/fld.666.

[19] Yu, W., Hong, V., Simão Ferreira, C., and van Kuik, G., "Validation of engineering dynamic inflow models by experimental and numerical approaches," *Journal of Physics: Conference Series*, Vol. 753, No. 2, 2016, p. 022024. doi:10.1088/1742-6596/753/2/022024, URL http://stacks.iop.org/1742-6596/753/i=2/a=022024?key=crossref.a5021875b25c355fb9838721e1c241a3.

[20] van Kuik, G., and Lignarolo, L., "Potential flow solutions for energy extracting actuator disc flows," *Wind Energy*, Vol. 19, No. 8, 2016, pp. 1391–1406. doi:10.1002/we.1902, URL http://doi.wiley.com/10.1002/we.1902.

[21] Baldacchino, D., and van Bussel, G., "Wind turbine wake stability investigations using a vortex ring modelling approach," *Journal of Physics: Conference Series*, Vol. 555, 2014, p. 012111. doi:10.1088/1742-6596/555/1/012111, URL http://stacks.iop.org/1742-6596/555/i=1/a=012111?key=crossref.50e47c89e158595612bdaac665081407.

[22] Øye, S., "A simple vortex model," *Proc. of the third IEA Symposium on the Aerodynamics of Wind Turbines, ETSU, Harwell*, 1990, pp. 1–4.

[23] Hong, V., "Analysis of an actuator disc under unsteady loading," Msc. thesis, TU Delft, 2015.

[24] Kaur, K., "Experimental Analysis of an Actuator Disk under cyclic unsteady loading," Msc. thesis, TU Delft, 2017.

[25] Hansen, M., *Aerodynamics of Wind Turbines*, 2nd ed., 2008. URL www.earthscan.co.uk.

[26] Hammam, M., "Analytical Unsteady Aerodynamic Models for Horizontal Axis Wind Turbines," Phd., University of Calgary, 2016. URL http://theses.ucalgary.ca/bitstream/11023/2863/1/ucalgary{_}2016{_}hammam{_}mohamed.pdf?cv=1{&}session-id=77fb13d02c792e5c800101830f7f4319.

Appendix: Coefficients Duhamel's Integral by Yu

In this appendix the proposal by Yu is summarised. See the research by Yu [1] for a complete overview of the basis and performance of this approach. The induced velocity at the rotor in the form of the Duhamel's Integral model is given by:

$$u_{ind}(r,t) = \gamma(0)\Phi_d(r,t) + \int_0^t \frac{\mathrm{d}\gamma}{\mathrm{d}\sigma}\Phi_d(r,t-\sigma)\mathrm{d}\sigma \tag{23}$$

Such that the induced velocity is a function of a change in γ times the response function Φ_d. The response function is approximated as:

$$\Phi_d(r,t) = 1 - \beta e^{\omega^1 t} - (1-\beta)\, e^{\omega^2 t} \tag{24}$$

In this equation β, ω^1 and ω^2 are the coefficients used to make the fit. These coefficients are a function of radius and base thrust coefficient, and the radial dependency was created through a third order polynomial:

$$\beta(r) = a_3 r^3 + a_2 r^2 + a_1 r^1 + a_0 r^0 \tag{25}$$

$$\omega^1(r) = a_3 r^3 + a_2 r^2 + a_1 r^1 + a_0 r^0 \tag{26}$$

$$\omega^2(r) = \frac{1}{a_3 r^3 + a_2 r^2 + a_1 r^1 + a_0 r^0} \tag{27}$$

These polynomial parameters were then fitted to the response calculated through a free wake vortex ring method, and they are shown in table 3. The accuracy of the fit through these parameters is shown by Yu in [1].

Table 3 Polynomial parameters of the exponential coefficients β, ω^1 and ω^2, based on a free wake vortex ring method.

	β	ω^1	ω^2
a_3	$0.98C_t - 1.09$	$3.45C_t^2 - 5.19C_t + 2.01$	$0.05C_t - 0.60$
a_2	$-2.01C_t + 1.99$	$-4.60C_t^2 + 7.01 - 2.81$	$-0.38C_t + 1.6$
a_1	$0.57C_t - 0.34$	$0.06C_t - 0.09$	$0.32C_t - 0.23$
a_0	$0.62C_t - 0.03$	$-0.07C_t - 0.12$	$-0.19C_t - 0.79$

Finally, the vorticity is defined as:

$$\gamma(t) = U_0(t)\left(\sqrt{1 - C_t\,(t)} - 1\right) \tag{28}$$

II

Supporting Chapters

2

Literature Review

This chapter will discuss the current state on unsteady rotor aerodynamic modelling. It starts with the basics behind blade-element-momentum theory and rotor unsteadiness in section 2.1. The additions to BEM, the engineering models, are shown in section 2.2. Even though the research into the difference between dynamic thrust and dynamic wind is scarce, the conclusions of this research are summarised in section 2.3. Afterwards other methods such as acceleration potential models, CFD or experiments are discussed in respectively sections 2.4, 2.5 and 2.6. The different methods are compared in section 2.7 and this chapter ends with a summary 2.8 and the conclusions of the literature review 2.9.

2.1. Blade-Element-Momentum Theory

There are several ways to model a rotor and its interaction with the flow. From a full representation of the rotor blades and flow discretisation to an actuator disc with a momentum source (helicopter) or sink (wind turbine). This section will discuss the most widely used method: Blade Element-Momentum Method, its flaws with respect to unsteady loading and wake aerodynamics and the methods that seek to remedy these flaws.

2.1.1. Actuator Discs

The most simple way to represent a rotor is as a disc in the flow. This disc is porous, and functions as a momentum source or sink. In its most basic form: a uniformly loaded actuator disc with axial forces only, has the following assumptions:

- Axial forces only: the wake is not rotated, and only slowed down. The 3 dimensionality is lost in this case.
- Uniform loading in azimuthal direction: no blades. This is equivalent to a rotor with an infinite number of blades.
- Uniform loading in radial direction: all vorticity is concentrated at the disc edge. This also means the velocity increase/decrease is uniform across the disc.

The forces of the actuator disc then need to be coupled to the flow dynamics. This can be done in several ways. Navier-Stokes solvers provide the most accurate solutions, but also the most computational expensive, for example the method used by Sørensen and Kock [61]. And on the other end of the spectrum a simple momentum, mass and energy balance can be used. Rankine [49] and Froude [16] were the first to come up with this approach. This momentum balance results in the following relation between power generation, rotor thrust and the flow:

$$C_P = \frac{P}{\frac{1}{2}\rho A V_\infty^3} = 4a(1-a)^2 \tag{2.1}$$

$$C_T = \frac{T}{\frac{1}{2}\rho A V_\infty^2} = 4a(1-a) \tag{2.2}$$

Where A is the rotor area, and a is the induction factor and defined as the velocity deficit at the rotor:

$$a = 1 - \frac{V_1}{V_\infty} \tag{2.3}$$

2.1.2. Blade Element-Momentum Method

The most commonly used engineering method to calculate rotor aerodynamcis is Blade Element-Momentum method (BEM). It uses the actuator disc with the momentum exchange as discussed previously, and couples it to local lift, drag and angle of attack at blade elements at varying radii. The blade element theory can be attributed to Drzewiecky [13] and it was Glauert who combined Momentum and Blade Element theory [17]. Although the name implies a disc, in BEM the disc is split in independent rings, and the equations are solved in each annular ring, see figure 2.1. As a result, the forces are not necessarily constant along the radius. This then gives all the necessary information to calculate the blade forces and power extraction at each ring:

$$\frac{a}{1-a} = \frac{\sigma_r \left(c_l \cos\phi + c_d \sin\phi\right)}{4\sin^2\phi} \tag{2.4}$$

In which σ_r is the local rotor solidity, and ϕ is the angle between the wind velocity at the rotor, and the relative velocity seen by a blade angle, see figure 2.2.

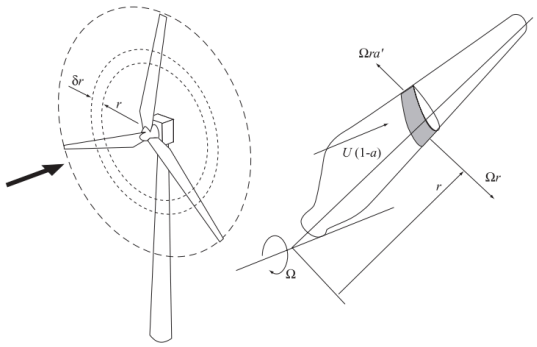

Figure 2.1: Annular ring of a wind turbine rotor, from [10]

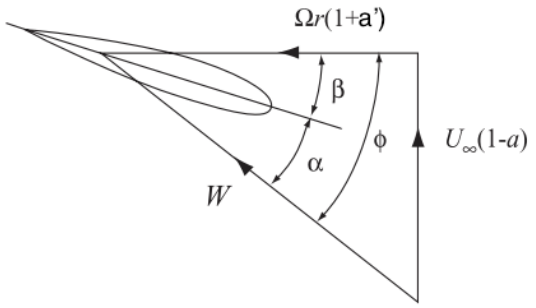

Figure 2.2: Velocity triangle at blade element, from [10].

The following assumptions apply to BEM, some of which follow from momentum theory, and some can be mended by additional equations or models, as discussed by Schepers [52].

Incompressible (inviscid) flow Generally compressibility effects are not an issue, as tip speeds stay below $M < 0.3$. Viscous effects are taken into account in the airfoil drag coefficient properties. The way the lift and drag polars are used determine the extent of which viscous (and even compressibility) effects are included.

No wake rotation This assumption is actually easily removed by adding a rotational momentum balance. In this balance an additional induction factor is introduced, linked to rotor torque. Forces and induction in azimuthal direction are thus introduced. See azimuthal induction a' in figure 2.2.

Uniform forces in azimuthal direction The actuator disc, or the annular rings, assume a constant force distribution in a ring. For a real rotor the number of blades or rotational speed is limited, and therefore this assumption does not hold. This is usually fixed by adding a tip-loss factor, which describes the relation between average induction in a ring and local induction at the blade.

The flow does not reverse From the momentum equations it follows that the velocity in the wake becomes zero if the induction $a \geq 0.5$. This assumption results in BEM breaking down if the induction factor is greater than $a \approx 0.4$. However, in reality a turbine will be able to have higher induction factors through the turbulent wake state. For highly loaded rotors an empirical correction was developed by Glauert [17].

Independent annular rings BEM assumes that each annular ring is independent. This does not hold if there is a large flow in radial direction: from one ring to another. This is especially the case at the blade root, in yawed flow, and in unsteady flow.

Steady flow The momentum equations assume that a change in flow or forces is instantaneous: the forces and wake adjust immediately to any change. This is not true, as there is both a lag in airfoil forces (unsteady airfoil aerodynamics) and a lag of the effect of the wake on the rotor (dynamic inflow). Therefore BEM only holds true in steady flow. The following sections will go into further detail of this assumption, its results and the methods that fix this.

2.1.3. Sources of Unsteady Loading

As mentioned before, BEM is only valid in steady flow. However, wind turbines operate in the boundary layer of the Earth, and therefore often in unstable turbulent flow. To summarise, the following inherent dynamics that result in unsteady conditions are present:

Turbulence In the boundary layer of the Earth (<100m), the wind is more turbulent than in higher layers [50]. Additionally, geographic features can increase or decrease turbulent levels. Onshore the turbulence is generally higher than offshore. Either way, a wind turbine always operates in turbulent conditions, and wind is therefore never steady. An extreme form of turbulence is a gust. Bierbooms [6] provides a description of gusts, and IEC standards [26] include requirements for the extreme loads due to gusts.

Turbine wake In addition to atmospheric turbulence, a turbine operating in the wake of another wind turbine will experience higher turbulence levels.

Wind shear Another effect of the boundary layer is the shearing of the wind: the wind velocity increases with height. A rotating blade will therefore experience different wind velocities during a cycle. This results in cyclic unsteady loading.

Tower shadow Wind shear is not the only phenomenon that results in cyclic loading. The wind is impaired by the tower, and a blade will therefore see a lower wind speed when it crosses the tower. Hence an unsteady cyclic loading of the blades.

Turbine operations Finally, the turbine itself can be the source of unsteady conditions. Obviously when it starts and stops, but also during operations when it changes the pitch angle of the blades. This could even develop further as smart rotor solutions are investigated (Berg et al. [5].), which continuously change loading of the blade during turbine operations.

These sources of unsteady loading are also shown in the diagram of figure 2.3.

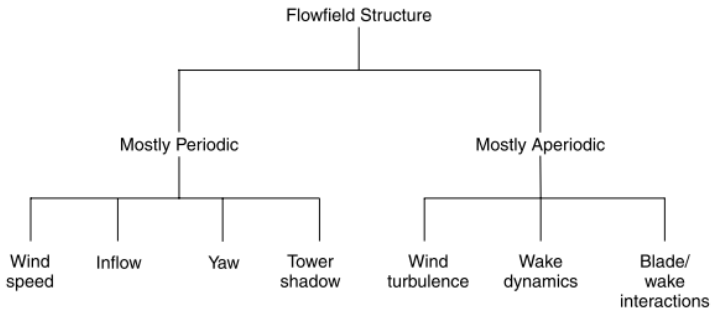

Figure 2.3: Break down of different sources of unsteadiness, from [31].

As a result of the unsteady loading, blade loads and the wake will never be steady. But an important distinction must be made between two different aerodynamic effects that result from the unsteady loading. These two effects are airfoil dynamics, which will be discussed in section 2.1.4, and dynamic inflow, section 2.1.5. Hammam [18] treats both effects separately and derived analytical formulations for either effect.

2.1.4. Airfoil Dynamics

First of all, there is a time lag due to airfoil aerodynamics. As will be seen in the next section, the time lag due to airfoil dynamics can be distinguished from other effects because of the scale. This time lag is on the scale of the airfoil chord c/V_{eff} because the source is on the airfoil level. Two different cases must be extinguished: attached conditions and stall conditions, as both result in unsteady effects on the airfoil scale.

Unsteady effects in attached conditions are caused by the air around the airfoil being accelerated to new conditions. It is often modelled through Theodorsen's model [68]. This is an inviscid model, and this is also what differentiates it from dynamic stall.

In the case of stall, stall delay and flow reattachment radically change the airfoil dynamics. This was shown in experiments performed by Huyer et al. [25]. Lift forces were found to be higher than in the steady case. Furthermore, as stated by Leishman [31], large discrepancies have been found between models when stall is involved. Therefore current models are ill equipped to deal with stall behaviour. In the absence of stall, BEM models fare a lot better though. Björck [7] gave a good overview of dynamic stall models in the EU-Joule project on Dynamic Stall and Three Dimensional Effects. The time delay in c_l corresponding to dynamic stall is often modelled through the following ordinary second order differential equation:

$$\tau \frac{\mathrm{d}c_l}{\mathrm{d}t} + f(\alpha)c_l = g(c_l, \alpha, \frac{\mathrm{d}\alpha}{\mathrm{d}t}, \frac{\mathrm{d}^2\alpha}{\mathrm{d}t^2}) \tag{2.5}$$

Luckily, modern pitch regulated wind turbines usually stay away from stall conditions. So only attached unsteady conditions are usually relevant. Next to this, this work will focus on dynamic inflow effects, and will leave unsteady airfoil dynamics largely alone. This is justified because the time scale in the airfoil unsteady dynamics is different from the dynamic inflow [52].

2.1.5. Dynamic Inflow

The second effect that governs the response lag is called dynamic inflow. Where the time scale of airfoil dynamics is c/V_{eff}, the dynamic inflow effect has a time scale of D/V_0 [59]. This is because the scale of the effect increases with increasing mass of air that needs to be changed: and thus with diameter D of the rotor. And because the time scales of the two effects is different, they can be considered independent [52].

One way to describe it is through the mass of air flowing through the rotor. Because it takes some time before the around the rotor accelerates or decelerates, it takes some time before the flow adjusts to a new equilibrium. And because the 'old' wake behind the turbine has an effect on the rotor, it takes time before the flow and forces reach a new steady state: as a result the induced velocity at the rotor will lag behind. BEM is often modified to include this inertia term (specific applications will be shown in section 2.2). The inertia term depends on the mass of air that is effected by each blade element.

A different way of looking at the time lag is by using vorticity. Any change in loads on the blades requires a new bound circulation. From Helmholtz's theorem it follows that a change in bound circulation results in the shedding of vorticity in the wake. This can be seen in figure 2.4, where two different wake states are pictured with different vorticity strength. The old vorticity still has an effect on the induced velocity upwind of the rotor, and it therefore takes time before this old vorticity is convected downstream and no longer has an effect. [59], [60].

As discussed by Leishman [31], the mass explanation and the vortex explanation are different. The mass surrounding a disc only imply inertia and a static force. The analogy of a wind turbine as a static disc with a mass flowing through is not a very rigid analogy, and therefore it is not a very satisfactory explanation. By using vorticity, it is a more circulatory explanation: with old vorticity delaying the forces in the disc, and new forces creating new vorticity. There is therefore a strong case for including the wake in the calculation of the forces. This approach was used by Hammam [18], who derived analytical solutions for unsteady actuator discs. He states that the apparent mass (inertia) and vorticity (circulatory) explanation are different, and that both require separate formulations. By doing this, each effect can be evaluated and modelled separately. In the case of dynamic wind speed the circulatory explanation is even mandatory, as the convection speed of the wake will be different, and this has an effect on the transient forces in the rotor.

Dynamic inflow has an important effect on blade loads and torque, especially for pitch regulated turbines, as was shown by Snel and Schepers; taking the effects into account is therefore imperative

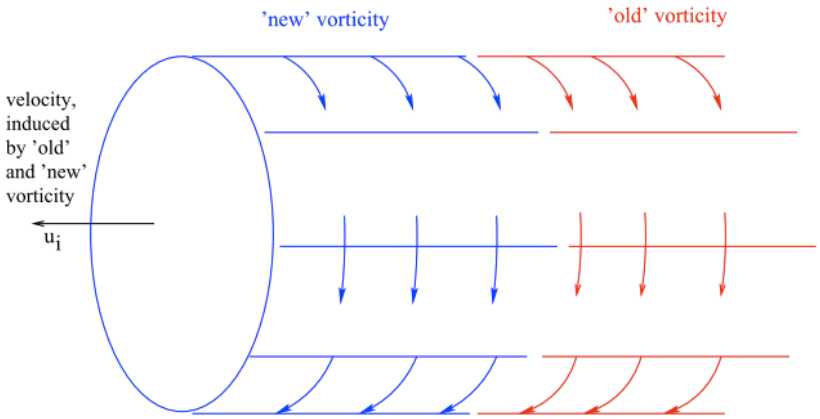

Figure 2.4: Wake with old and new vorticity. From [52].

[58]. However, they also concluded that the effect of dynamic inflow on fatigue loads may be limited, in [59]. The time scale is larger for wind turbines as for helicopters as was shown by Leishman [31]. Where it takes three revolutions to reach steady state for a helicopter, this may take up to 8 revolutions for a wind turbine. The Joule project in 1995 [54] found that the dynamic inflow effect increases with increasing rotor diameters and pitching speed. Since rotor diameters are ever increasing, dynamic inflow is still relevant.

Not only does the scale of the dynamic inflow effect increase, aeroelastic calculations become more important with increasing blade sizes. And properly calculating aeroelastic effects requires a good understanding of unsteady aerodynamics. Hence there is a clear need for good unsteady models. Which was also corroborated by van Engelen and van der Hooft [71] and Odgaaard et al. [40], who showed that incorporating dynamic inflow in the turbine controller is imperative in reducing fatigue loads. Hansen and Madsen [21] give an overview of aeroelastic models and their respective aerodynamic components.

2.2. Engineering Models

To solve the problem of unsteady flow, an actuator disc model can be coupled to a fluid dynamics solver. This is computationally expensive, and in practice there will always be a need for a model such as BEM. As the appeal of BEM is its simplicity [31]. Several engineering models that can be applied to BEM have been developed. Snel and Schepers [58] provide a good overview of engineering models. In the following three sections three engineering models will be discussed. After this they will be compared, and this section finishes with a slightly different engineering approach by Hammam [18].

2.2.1. Øye

Developed by Øye, [42], this model describes the induced velocity response over time by two first-order linear differential equations. It defines the quasi-steady state velocity V_{qs} as the velocity from momentum theory. And $\frac{\mathrm{d}V_{qs}}{\mathrm{d}t}$ as the steady state response to a change, which is immediate in the case of momentum theory. This is then inserted into the following two equations:

$$V_{int} + \tau_1 \frac{\mathrm{d}V_{int}}{\mathrm{d}t} = V_{qs} + \kappa\tau_1 \frac{\mathrm{d}V_{qs}}{\mathrm{d}t} \tag{2.6}$$

$$V + \tau_2 \frac{\mathrm{d}V}{\mathrm{d}t} = V_{int} \tag{2.7}$$

With the quasi-steady state input from BEM, this then results into the actual induced velocity response V. κ, τ_1 and τ_2 were found using Vortex Ring models with a prescribed wake [42].

$$\kappa = 0.6 \tag{2.8}$$

$$\tau_1 = \frac{1.1}{1 - 1.3a}\frac{R}{V_0} \tag{2.9}$$

$$\tau_2 = \left[0.39 - 0.26\left(\frac{r}{R}\right)^2\right]\tau_1 \tag{2.10}$$

The accuracy of Øye's model depends on the values found for the time constants. The original time constants were found with a prescribed wake vortex method and through correlations with experimental data. But the question rises whether such a prescribed wake model is capable of capturing the transient wake response, and whether the experiments can be generalised towards all turbines.

2.2.2. Pitt-Peters

Helicopter research precedes wind turbine research, and it should come to no surprise that in the case of dynamic inflow lessons can be learned from helicopters. Helicopters need to account for dynamic inflow even more than wind turbines, as a helicopter and rotor inflow is very dynamic. However, a helicopter disc is subject to different operating conditions than a wind turbine (different range of loading and induction).

Carpenter and Fridovich [11] did experimental research into unsteady loading. They developed the notion that the transient behaviour observed in unsteady conditions is due to the mass of air that requires time to settle to a new equilibrium. Pitt and Peters [46] developed the following system of linear equations to account for this mass time dependence:

$$(\tau)\begin{pmatrix}\dot{V}_0\\ \dot{V}_s\\ \dot{V}_c\end{pmatrix} + \begin{pmatrix}V_0\\ V_s\\ V_c\end{pmatrix} = (L)\begin{pmatrix}C_T\\ C_{M,y}\\ C_{M,t}\end{pmatrix} \tag{2.11}$$

With τ being the time constant matrix, which is a result of the mass matrix and the static coupling. The Pitt-Peters model has been validated extensively for helicopters, and is convenient because it produces consistent results both in hover as in forward flight (axisymmetric and yawed flow).

In the axisymmetric case and translated to wind turbines it can be applied to BEM through, (see Snel et al. [60]):

$$T_k = \frac{8}{3\pi}\rho A_k r\frac{\mathrm{d}V_{i,k}}{\mathrm{d}t} + 2\rho A_k V_{i,k}\left(V_0 + V_{i,k}\right) \tag{2.12}$$

For every annular ring in k with area A_k, and at every time step i. T_k is the thrust in the annular ring, and $V_{i,k}$ is the induced velocity at time step i in annular ring k. The model by Pitt and Peters is used in most commercial software for BEM, such as GH Bladed. It must be noted that the notation of equation 2.12 is slightly different from the original equations by Pitt-Peters. They used the non-dimensional $u_i = V_i/\Omega r$, and in the implementation into BEM the non-dimensional induction factor a is often used. Which is fine when rotational speed and wind velocity are constant. However in the case of dynamic wind the non-dimensional form V_i must be adopted.

Suzuki and Hansen [66] expanded on the model by Pitt-Peters by adding more higher order terms, which they called the generalized dynamic wake model. In comparison with experiments they found that the transient response was too quick, which could be explained by the helicopter basis of the model by Pitt-Peters, since helicopters operate in a different loading state. This can also be seen in the comparison by Qiu et al. [48]. It is likely that the response of the generalized dynamic wake model is comparable to the Pitt-Peters model.

As mentioned before, there is a distinction between the mass of air explanation and circulatory vortex explanation. The model by Pitt-Peters only considers the apparent mass, and does not take the wake into account. Furthermore, Hammam [18] notes that the basis of the Pitt-Peters model can be considered physically similar to the acceleration potential method. The acceleration potential method was developed for helicopter applications by Van Holten [72] and adapted to wind turbines by [70].

2.2.3. ECN Dynamic Inflow model

Snel and Schepers [60] also outline an additional dynamic inflow model, based on integral relations of a stream tube model (see [20] or [52] for an overview of a stream tube model). The basis of this stream tube follows from potential flow theory applied to a vortex tube, which results in the following equation for induced velocity in axial direction at the disc:

$$V_i(0,r) = \frac{1}{4\pi}\int_0^{\infty}\int_0^{2\pi} \frac{\gamma_t(z)\,(R - r\cos\phi_r)}{(z^2 + R^2 + r^2 - 2rR\cos\phi_r)^{1.5}} R\mathrm{d}\phi_r\mathrm{d}z \tag{2.13}$$

Which can be rewritten into a time dependent form, see [60]:

$$\frac{\delta V_i}{\delta t} = \frac{1}{4\pi}\int_0^{2\pi}\left[\frac{(R - r\cos\phi_r)\,R}{P^3}\cdot\left[\frac{C_t V_0^2}{2} - \frac{3}{2}P^3\int_t^{-\infty}\frac{C_t\,(\tau)\,V_0^2\,(\tau)\,(t-\tau)\,V_{tr}^2\mathrm{d}\tau}{\left([t-\tau]^2\,V_{tr}^2 + P^2\right)^{2.5}}\right]\right] \tag{2.14}$$

This can be reduced to a relatively simple form, by integrating the $\mathrm{d}\phi_r$ integral around $r = 0$:

$$4Rf_a\frac{\mathrm{d}}{\mathrm{d}t}(V_i) + 4V_i\,(V_0 - V_i) = \sigma V_{eff}^2 c_n \tag{2.15}$$

With $P^2 = R^2 + r^2 + 2rR\cos\phi_r$. Equation 2.15 is a differential equation for the induced velocity V_i at each annulus in BEM. In the case of a constant incoming wind V_w (and unsteady thrust) this equation can be rewritten to:

$$\frac{R}{V_0}f_a\frac{\mathrm{d}a}{\mathrm{d}t} + 4a\,(1-a) = C_t \tag{2.16}$$

In this equation the time constant τ is the $\frac{R}{V_0}f_a$ portion. Finally, the dependency on r/R, which was lost in equation 2.15, is reintroduced through f_a as:

$$f_a = 2\pi/\int_0^{2\pi}\frac{[1 - (r/R)\cos\phi_r]}{\left[1 + (r/R)^2 - 2\,(r/R)\cos\phi_r\right]^{3/2}}\mathrm{d}\phi_r \tag{2.17}$$

A similar equation was derived to be applied to the angular momentum balance of BEM:

$$4Rf_t\frac{\mathrm{d}\omega r}{\mathrm{d}t} + 4a'\,(1-a)\,V_\infty\Omega r = C_m \tag{2.18}$$

With C_m being the moment coefficient. f_t is similarly to equation 2.17 a function of r/R and derived from vorticity equations.

2.2.4. Differences Between Engineering Models

All three models share a similarity in the usage of differential equations. But even though the engineering models share some similarity in their physical background and their application to BEM there are two physical differences.

First of all, the models have a different approach with regards to the radial dependency. They all scale the dynamic inflow effect to rotor size obviously, as that is what defines dynamic inflow, but locally their approaches are slightly different. Pitt-Peters uses an inverse relationship with radius. ECN uses a radial dependency based on the vortex wake model (equation 2.17, which results in the physical representation of the tip-vortex dominance (as noted by Snel et al. [60]). Øye only applies the radial dependency to the second timescale.

Secondly, the model by Øye is the only one that uses two time-scales. One rapid response after a change, and the second which is the slower settling to the new equilibrium. This behaviour is more realistic, as it can be observed in both experiments and vortex models [60].

2.3. Dynamic Thrust versus Dynamic Wind Speed

An important note that needs to be made is the distinction between dynamic thrust and dynamic (wind) velocity. Dynamic Inflow (perhaps despite its name) is often regarded as dynamic thrust: a constant

wind and a change in thrust at the disc. This corresponds to the case of a blade pitch change. Most engineering models and experiments use this approach. On the other hand, there is the case of changing wind velocity (or rotor velocity) and a constant disc thrust or constant pitch. Both dynamic thrust and dynamic wind will result in thrust coefficient and induced velocity change at the rotor disc. However, an unsteady inflow velocity will also be felt in the unsteady convection of the wake which influences the transient response. So it can be expected that dynamic wind results in different dynamic inflow effects, as stated by Hammam [18].

Schepers [52] comments on the distinction, and points out that a change in velocity does not lead to a large dynamic inflow effect because the magnitude of the induced velocity does not change as much (though induction factor does change). A change in wind speed was also included in the experiments performed in the Joule 1 project [60]. In the Joule 1 project both wind tunnel experiments with a change in wind speed were done, as well as a comparison on the Tjaereborg turbine between a wind speed change and pitch change (though no field test data were used in this comparison). This comparison is shown in figure 2.5a to 2.5f. The models shown in these figures are two models based on vorticity (ECN,i.w., UBM), an acceleration potential method (DUT, see section 2.4), and three engineering models (ECN,d.e, GH, TUDk). GH is based on Pitt-Peters and TUDk is based on Øye, see section 2.2 for a description of these engineering methods.

Three conclusions could be drawn from these figures:

1. The engineering models do not differ in their responses to induced velocity when comparing wind speed change to pitch change. The ECN,d.e., GH and DUTk all have roughly the same response in figure 2.5a as in figure 2.5b.

2. The vortex models and acceleration potential method (ECN,i.w., DUT, UBM) do differ in their responses to induced velocity when comparing wind speed change to pitch change. This is clearly seen when looking at the response of the DUT model in figure 2.5a and figure 2.5b. A pitch change sees a time delay in induced velocity, while a wind speed change does not see a time-delay. However, the ECN,i.w. has a rather strange response: it does not only predict a time lag in induction, but even a negative response.

3. The responses to the flat-moment and rotorshaft torque are consistent with the induced velocity response for the more sophisticated models: no dynamic inflow effects can be seen both in the induced velocity as the forces. Contrary to this, the engineering models are a bit inconsistent in that regard. While they predict a time delay for the induced velocity, this time delay does not result in a delayed response to flat-moment or rotorshaft torque. However, this is suddenly consistent with the results from the more sophisticated methods.

To conclude, the vortex methods and acceleration potential methods do not predict a dynamic inflow effect of unsteady wind speed. This is best seen in figure 2.5a, as dynamic inflow is best defined as a time-delay in induced velocity. Their actual response to wind speed change on induced velocity is not very clear though, as especially the wake model by ECN has quite an interesting response. In addition to this, the engineering models are inconsistent in their responses when comparing induced velocity to forces. This can only be explained in the same way as Schepers does in [52]: although the absolute induced velocity changes, the induction factor does not. But even then, the time delay in figure 2.5a suggests a gradual change in induction factor.

In the Joule 1 wind tunnel experiment the change in velocity was relatively slow as compared to usual dynamic inflow change rates. Therefore it is difficult to draw conclusions from that experiment. Nonetheless, from those experiments it could be concluded that although models vary a lot in the calculated absolute values of induced velocity, the overall characteristics of power and axial force are pretty spot on compared to each other and to the experimental results.

Hammam [18] recently investigated the dynamic wind case, and used the wind tunnel experiments of Joule 1 as validation for his analytical solutions. He developed an unsteady model which separates the three different effects that are relevant in the dynamic wind case: apparent mass (inertia), wake convection (circulatory) and unsteady airfoil dynamics. By comparing these effects to the Joule 1 wind tunnel experiment he found that the vortex formulation including the circulatory effect predicts the dynamic inflow effects well, as shown in figure 2.6a. The differences that were observed could be attributed to assumptions on the lift and drag polars, see figure 2.6b. Although the models in figure 2.6b do not use circulatory terms, improving airfoil data gives a much better fit. Hammam concluded that including

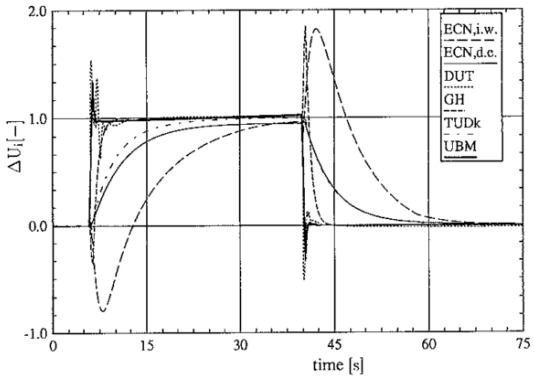

(a) Induced velocity at blade root, wind speed change.

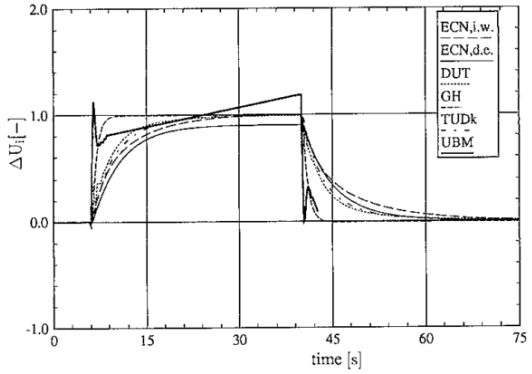

Figure B.14 *Tjæreborg; Non-dimensional induced velocity at blade root; V = 10 m/s; θ = 0° to 2° ; (CASE 1.2)*

(b) Induced velocity at blade root, pitch change.

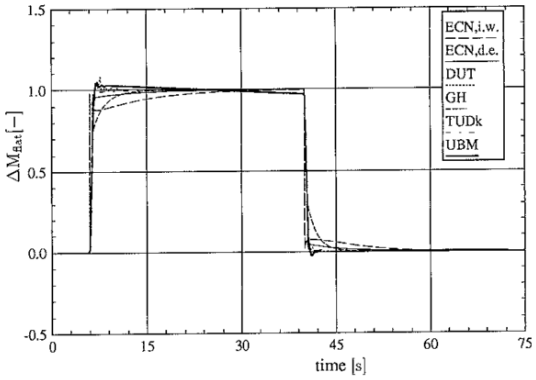

(c) Flat-moment at blade root, wind speed change.

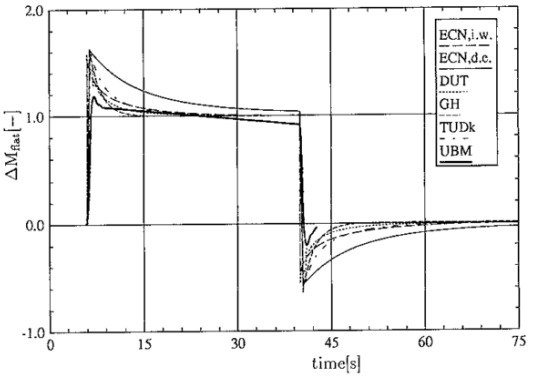

(d) Flat-moment at blade root, pitch change.

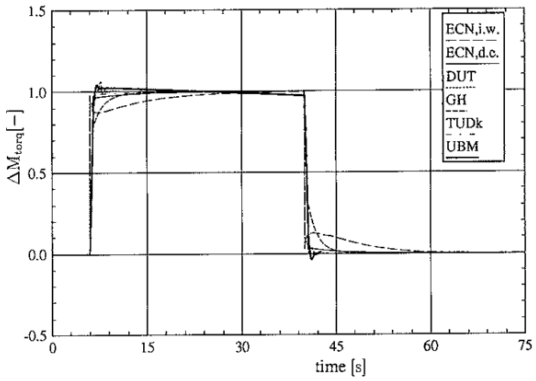

(e) Rotorshaft torque, wind speed change.

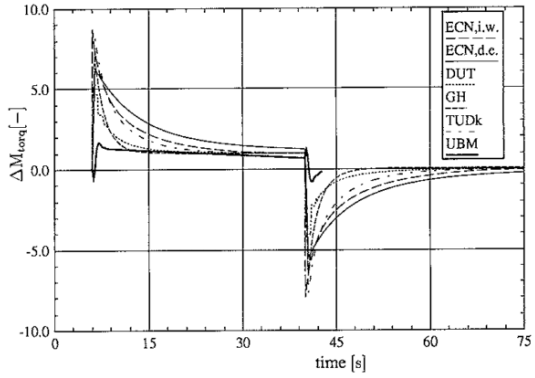

(f) Rotorshaft torque, pitch change.

Figure 2.5: Results from the Joule 1 project by Snel et al. [60]. Left figures: change in wind speed $V = 10$m/s to 13m/s. Right figures: pitch change $\theta = 0°$ to $2°$. All values are non-dimensionalized.

only the apparent mass formulation (such as most engineering models) will still give good results, with a simpler calculation. Including unsteady airfoil effects will smooth the responses on a smaller time scale. The solutions proposed by Hammam appear to be promising and may be used to model the dynamic wind speed case. As the conditions of the test case of Joule 1 were relatively slow, it remains to be seen whether a larger dynamic inflow effect can be observed at faster wind speed changes.

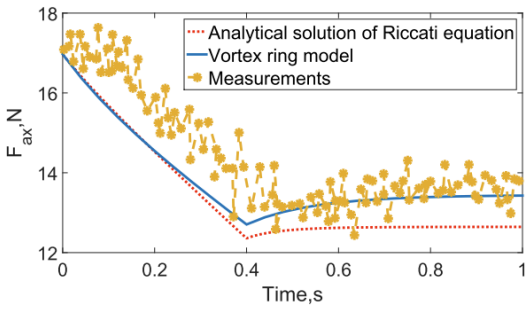

(a) Vortex model (circular), Ricatti equation (apparent mass only) versus Joule 1 Measurements [60], figure from [18].

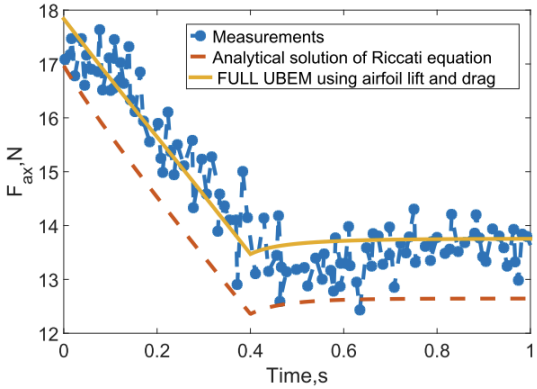

(b) Ricatti (with linear lift assumption) and full unsteady BEM (with detailed airfoil data) versus Joule 1 Measurements [60], figure from [18].

It must be concluded that the effects of dynamic wind speed in the framework of dynamic inflow have not been researched often. While it appears from the Joule 1 project that the effects of dynamic wind speed on dynamic inflow can be neglected, it is not a very convincing conclusion. And even if that can be concluded, the engineering models are inconsistent in their responses. Therefore the main goal of this research will be to look into dynamic wind speed, and the effects it has on dynamic inflow.

2.3.1. Apparent Mass Force versus Circulatory Force

The first and perhaps simplest way to describe dynamic inflow effects is through the inertia of air. Because the air around a rotor has mass, it is inert to changes and therefore a transient response is expected. There is a certain time delay before the air is accelerated to a new equilibrium. Dynamic inflow effects are almost always modelled as a steady solution plus a differential part, with the differential part including a time constant:

$$C_t = 4a(1-a) + \tau_1 \frac{\mathrm{d}a}{\mathrm{d}t} \tag{2.19}$$

And often this time constant is defined as a function of the mass of air. However, various definitions can be given for the time constant, as shown by Snel et al. [60]. The dynamic inflow model by Pitt and Peters [46] uses apparent mass as a basis, where they found that:

$$\mathrm{dm} = \frac{2}{\pi}\rho Vol_{\text{sphere}} = \frac{8}{3}\rho R^3 \tag{2.20}$$

Or, the time constant τ_1 is a function of the apparent mass around the rotor dm, which is equal to $2/\pi = 0.637$ the volume of mass of a sphere of equal radius. The time constant is non dimensionalised such that:

$$\tau_1 = \frac{\mathrm{dm}}{\frac{1}{2}\rho A U_0^2} \tag{2.21}$$

Note that Pitt and Peters are the only ones to actually define it through inertia, or mass of air. Other definitions use the same form but are not necessarily based on air mass. However, this time constant times the differential term will be called the apparent mass effect throughout this work.

Other definitions of the 'apparent mass' for each blade element are given by Hartin [23]:

$$\mathrm{dm}(r) = 8\rho\,(rR)\sqrt{1-(r/R)^2}\,\mathrm{d}r \tag{2.22}$$

And by Snel et al. [60]:

$$\mathrm{d}m(r) = \rho \frac{8}{3\pi} \left(R_2^3 - R_1^3\right) \tag{2.23}$$

As good as this differential part can be as a model for dynamic inflow effects, it misses an important element: the wake behind the rotor.

Because in addition to the apparent mass, there is another driver of unsteady effects, which is sometimes called the circulatory part. It is driven by the wake and can be regarded as the history of the velocity field. As the rotor sheds new vorticity in the wake, the old vorticity still has an effect on the rotor and therefore delays the new equilibrium. It is circulatory because the rotor has an effect on the wake, and the wake has an effect on the rotor. Hence it is fundamentally different from the inertia effect. And while this circulatory explanation can also be used to explain dynamic inflow effects, Hammam [18] makes a case of treating the circulatory force and the inertia force differently. The inertia force is a differential effect; the rate of change of velocity, i.e. mass times acceleration, drives the transient response. Contrary to this, the circulatory effect is an integral relation as the sum of the entire wake has an effect on the rotor. This is shown in the following equation by Hammam [18]:

$$\mathrm{d}F_{ax}(r,t) = \underbrace{\rho A u_{ind,\infty}(t)\left(U_0(t) - 0.5u_{ind,\infty}(t)\right)}_{\text{Far Wake}} + \underbrace{0.5\rho A \int_t^{\infty} \gamma(r,t') \frac{\mathrm{d}U_{vr}(t')}{\mathrm{d}t'} I_\phi(z')\mathrm{d}t'}_{\text{Circulatory Vortex Wake}} + \underbrace{\mathrm{d}m(r)\frac{\partial u_{ind}(t)}{\partial t}}_{\text{Apparant Mass}} \tag{2.24}$$

This equation describes the thrust of annular element at time t as a function of three different terms:

Initial Conditions The first term in equation 2.24 describes the far wake. In the case of a steady solution this term alone equals the axial force, following from momentum theory. $u_{ind,\infty}$ is thus defined as the induced velocity in the far wake.

Circulatory Vortex Wake The second term is the effect due to a change in the cylindrical wake strength. γ' is the strength of the vortex sheet, and U_{vr} is the convection speed of the wake. I_ϕ is a function describing the strength of the effect due to the shape of the wake. I_ϕ can be expressed in terms of the complete and incomplete elliptic integrals of the first and second kind. This expression results from the relations derived by Conway [12], who related cylindrical wake vorticity to induced velocity.

Apparent Mass The last term is again the so-called apparent mass effect. This term can also be expressed in a different way, exemplifying the apparent mass effect through the change in bound circulation Γ_b:

$$\mathrm{d}m(r)\frac{\partial u_{ind}(t)}{\partial t} = \frac{\partial \Gamma_b}{\partial t} \tag{2.25}$$

$\mathrm{d}m$ is also named apparent mass. However, it can also explicitly be derived as the relation between bound circulation and induced velocity, again by Conway [12].

The third term is therefore analogous to the apparent mass terms in equations 2.19 to 2.23. Expressing it in the change of bound circulation also neatly distinguishes it from the circulatory part: the apparent mass is bound to the change at the rotor, while the circulatory is the effect of the wake.

The dynamic inflow engineering models by Øye [42] and ECN [60] already take this circulatory effect into account as they included a vortex wake model in determining the time constants.

The difference between the circulatory and apparent mass effect is important, as it may present itself in the comparison of dynamic wind versus dynamic thrust. Contrary to dynamic thrust, an already accelerated incoming wind speed will not result in an apparent mass force at the rotor. A change in force at the rotor requires the mass of air to accelerate, but that is not necessary for dynamic wind. Additionally, in this study dynamic wind will be defined as constant axial thrust, and therefore constant bound circulation. This constant bound circulation will therefore not result in a change in induced velocity.

However, the wake will need to adjust, and therefore the circulatory part of a transient response is still present. This is further corroborated by Hammam, who found that a change in wind speed does not result in an inertia force. It would thus be interesting to see the results in the light of the differences between inertia and circulatory effects.

It must be kept in mind though that use will be made of a vortex ring model, which inherently models the circulatory effects of the convected wake, and it does not explicitly model the apparent mass term.

2.3.2. Shed Vorticity Strength

Furthermore, from a vorticity strength point a key expected difference could already be noted. Behind the disc the shed vorticity forms a sheet from the edge of the disc to infinity. The strength of the sheet is defined by the strength of the bound vorticity and the 'density' of the shed vorticity, which is defined by the velocity:

$$\gamma = \frac{\Gamma}{\mathrm{d}z} \tag{2.26}$$

In the case of dynamic wind, the bound vorticity strength does not change, while the 'density' does change:

$$\gamma_{wind} = f(\mathrm{d}z) \quad \Gamma = \text{constant} \tag{2.27}$$

In the case of dynamic thrust both the bound vorticity strength and the 'density' change:

$$\gamma_{thrust} = f(\Gamma, \mathrm{d}z) \quad \Gamma \neq \text{constant} \tag{2.28}$$

This fundamental difference between dynamic wind and thrust is expected to result in a different transient response. This is further explained in section 3.2.4, which discusses the exact way a change in wind speed is incorporated in the used model.

2.4. Acceleration Potential Methods

An approach that is a bit similar to vortex methods is the Acceleration Potential Method, which is also based on potential theory. It was first developed for helicopter theory by Van Holten [72] and adapted for usage in wind turbines by Van Bussel [70]. It solves the pressure perturbations as described by the Laplace equation:

$$\nabla^2 p = \frac{\partial^2 p}{\partial x^2} + \frac{\partial^2 p}{\partial y^2} + \frac{\partial^2 p}{\partial z^2} \tag{2.29}$$

As derived by Van Bussel, this equation is solved by using asymptotic expansion techniques, giving the following solution:

$$\begin{aligned} \frac{p}{\frac{1}{2}\rho w^2} = &-\frac{1}{\pi}\frac{l(z_b}{\frac{1}{2}\rho W^2 c(z_b)}\frac{\sin\phi}{\cosh\eta + \cos\phi} \\ &+ \frac{1}{2\pi}\frac{l(z_b)}{\frac{1}{2}\rho W^2 c(z_b)}\frac{c(z_b)}{r_b}\sin\chi \\ &+ \frac{1}{\pi}\sum_{n=1}^{\infty} A_n P_n^1(\cos\theta)\, Q_n^1(\cosh\nu)\sin\chi \end{aligned} \tag{2.30}$$

In this equation $l(z_b)$ is the spanwise lift distribution, and $c(z_b)$ the chord distribution. The first, second and third term on the right hand side are written in local elliptical coordinates, circular cylinder coordinates and prolate spheroidal coordinates respectively. P_n^1 and Q_n^1 denote Legendre functions of the first and second kind. A_n are coefficients that are solved in an iterative way.

This method gives a fairly quick and elegant solution to potential flow theory as it circumvents the problem of solving for the vortex wake. Physically it uses roughly the same assumptions as the free wake vortex method. However it will result in the same solutions as the apparent mass solutions by Carpenter and Fridovich [11] if the same rotor pressure distribution is used.

An example of the usage for turbulent flow and yawed inflow can be seen in [38]. The acceleration potential method was also included in the comparison of the Joule1 project. It performed well and gave good results in the dynamic inflow cases. The drawback of the model is that it is not as flexible as vortex methods.

2.5. CFD

The models that contain the highest fidelity are Compuational Fluid Dynamics models. They are a step up from vortex models in terms of accuracy, because they solve the (incompressible) Navier-Stokes equations in a more direct manner. Sanderse et al. [51], but also Mikkelsen [37] and Vermeer et al. [75], give a good overview of the usage of CFD in wind turbine aerodynamics. More recently, Bai and Wang [2], Kalvig et al. [27], O'Brien et al. [39] and Wang et al. [76] have made overviews of studies that conduct CFD modelling of wind turbines. Since Vermeer listed the state of the art in 2003, a lot of numerical and experimental research has been done, and this is summarized in O'Brien's overview.

The difficulty with solving the Navier-Stokes equations is turbulence. In turbulent flows the range of length and time scales depend on the Reynold's number, and for large Reynold's numbers this results in a wide range of different scales that need to be resolved. Solving the NS-equations through CFD efficiently therefore depends on the way turbulence is modelled. Reynolds-averaged-Navier-Stokes (RANS) and Large-Eddy-Simulation (LES) are two approaches, which will be treated in the following sections 2.5.1 and 2.5.2. After this the different ways of modelling the forces of the rotor is discussed in section 2.5.3.

2.5.1. RANS

Reynolds-averaged-Navier-Stokes (RANS) splits the flow velocity into a mean flow velocity $\bar{\mathrm{u}}$ and a turbulent part u':

$$\mathrm{u}(x,t) = \bar{\mathrm{u}}(x) + \mathrm{u}'(x,t) \tag{2.31}$$

Inserting this velocity description into the Navier-Stokes equations and subsequently averaging these equations results in the RANS equations:

$$\frac{\partial \bar{\mathrm{u}}}{\partial t} + (\bar{\mathrm{u}} \cdot \nabla)\,\bar{\mathrm{u}} = -\frac{1}{\rho}\nabla\bar{p} + \nu\nabla^2\bar{\mathrm{u}} - \nabla \cdot \overline{(\mathrm{u}'\mathrm{u}')} \tag{2.32}$$

The last term in this RANS equation is the Reynolds stress tensor and represents the momentum transfer due to turbulence. The Reynolds stress tensor can be regarded as turbulent viscosity. By using a viscosity term ν_T the Reynolds stress tensor is connected back to mean flow properties:

$$\overline{(\mathrm{u}'\mathrm{u}')} = \nu_T\left(\nabla\bar{\mathrm{u}} + (\nabla\bar{\mathrm{u}})^T\right) \tag{2.33}$$

Effectively the turbulence has been modelled as a function of mean flow properties. This term is lumped together with the diffusion term $\nu\nabla^2\bar{\mathrm{u}}$. Several turbulence models exist that find a solution for ν_T, most notably zero equation (mixing length), one-equation and two-equation models ($\kappa-\omega$ or $\kappa-\epsilon$ models). The $\kappa-\omega$ is used in the vicinity of the rotor, while the $\kappa-\epsilon$ is often used to model the wake of the turbine. However, Krogstad et al. [29] concluded that there is no obvious winner in turbulence models (ϵ or ω) when compared to experimental results. Sanderse [51] and Bai and Wang [2] provide an overview of the turbulence methods used in wind turbine wake computations.

The result of this Reynolds stress simplification is that the computational expense is greatly reduced and that computation time is not as dependent on the Reynolds number. However, it is physically not a very sound assumption, as the turbulent viscosity is just not the same as the molecular viscosity. The link between mean flow properties and turbulent viscosity in equation 2.33 is actually not present, [77]. As a result RANS is not very capable in flows with large strain rates (shear layers), three-dimensional flows and anisotropic flows [77].

2.5.2. LES

Large-Eddy-Simulations (LES) solve the problem of the wide range of length and time scales in a different way. Large eddies are modelled directly, and smaller eddies are solved on a smaller scale grid. The two scales are therefore separated. These two scales are coupled mathematically but no longer physically.

LES is capable of solving anisotropic flows and turbulent mixing in flows governed by larger eddies. This makes it an attractive solution for wind turbines and their wakes. However, this comes at the cost of much larger computational efforts as compared to RANS.

A hybrid solution is often created through RANS and LES, called Detached Eddy Simulation (DES): RANS is used in attached conditions close to blade surfaces as RANS can have a finer mesh with less computational effort, and LES is used where the flow is detached and the power of LES is required.

2.5.3. Blade Models

The final question in CFD modelling is how to model the forces of the rotor in the flow solvers. Four different approaches are distinguished in literature, see figure 2.7. One of these approaches is meshing the blade surface and take a direct approach. This is a rather computational expensive approach as it involves solving the boundary layers around blade surfaces. The other three circumvent this complication by simplifying the blade forces in the rotor (in a very similar manner as BEM or vortex models) to a disc, a line or surface. Instead of generating forces on the blade through CFD, lift and drag are computed through airfoil data. Although this approach is less computational expensive than directly modelling the blade surface, it still relies on momentum equations or airfoil data. And while the CFD part produces valuable information in the wake, this reliance on airfoil data means that the blade or turbine loads are just as accurate as BEM [76].

An overview of the different models can be found again in [2], [27], [37], [39], [51], [75], and [76].

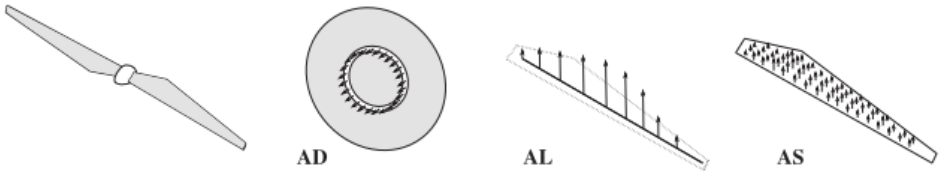

Figure 2.7: Different representations of the forces in a rotor: actuator disc, actuator line, actuator surface. From Sanderse [51].

AD The simplest approach is, just like BEM and vortex methods, the actuator disc. If the disc is uniformly loaded the pressure forces are easily linked to the thrust coefficient of the disc. If the forces vary over radius, they are still easily linked to rotor properties through airfoil sectional lift and drag coefficients. These airfoil polars will have to take into account 3D effects though. This approach was already used by Sørensen and Myken [62], Sørensen and Kock [61] and Sørensen et al. [64]. Furthermore, Madsen used this approach to validate BEM [33]. A comparison between AD models and experiments can be found in the blind test results of Krogstad et al. [30]. The effect of wake rotation was studied by Porté-Agel et al. [47] with an actuator disc approach. Finally, actuator disc models are commonly used in wind farm modelling as it is often enough to model a rotor as a disc, see for example the wind farm simulations done by Meyers and Meneveau [36]. Although AD models are often too coarse to generate meaningful information in the near wake apart from general rotor data (C_p, C_t), they are computationally efficient for usage in the far wake [27].

AL An actuator line is an extension to the non-uniform actuator disc, first described by Sørensen and Shen [63]. Instead of the representation of the forces on a disc, they are projected on a line. The forces in the disc are now a function of time (and are therefore rotating). Again 3-dimensional corrections to 2D airfoil data are required. The advantage over the disc approach is that an actuator line gives more information along the radius and is better to predict the near wake. The study by Sørensen and Shen also showed that an actuator line model is capable of modelling tip and root vortices. Troldborg et al. [69] used the actuator line approach to study the wake and concluded that wake properties could be predicted successfully. This was also found by Martínez-Tossas et al. [34], who also compared the AD and AL approaches. AL fares better in the near wake, but in the far wake the velocity profiles were found to be similar.

A rotating line of forces requires some tweaking to implement it into the mesh in which the flow is solved. The discretisation of forces on the line requires a Gaussian parameter for stability [27], and this parameter unfortunately has an influence on the accuracy of the results. And, just like BEM and vortex models, the accuracy of the actuator line approach depends again on the airfoil data used. This was also concluded by Shen et al., who used the Mexico project to validate the AL model of Sørensen and Shen [63]. In this validation they found that 3D-corrected airfoil data were better than 2D polars. But overall the general consensus is that the actuator line approach provides better results than the actuator disc approach, and that it is a good middle ground for usage in CFD.

AS Instead of airfoil polars, the forces on the surface could also be described by the pressure and skin friction distribution. This requires even more detailed information on airfoils. Often tools such as XFOIL provide accurate enough information to insert this into the flow field. The AS method has some improved accuracy in 3D effects such as the tip, and also close to the blade surface the accuracy is improved as compared to the actuator line method [51].

Direct modelling Finally, the most accurate method to calculate the loads on the blade is simply directly modelling it through CFD by creating a surface mesh. This obviously greatly complicates the computations, but it is the most accurate method. That is, if the separation and re-attachment of the flow around the airfoil is predicted correctly. Kalvig et al. [27] state that predicting this incorrectly will result in large deviations. The selection of the turbulence model is therefore of great importance.

Bechmann et al. [4] created a fully meshed 3D rotor in a RANS solver and compared it to the experiments of the Mexico project [53]. They found very good agreement between the CFD results and experiments. Differences that were found could again be contributed to turbulence differences between the simulations and experiments.

2.6. Experiments

Experimental research into rotor aerodynamics is as old as helicopter research. But while some helicopter research is useful, a wind turbine operates in vastly different operating conditions. So extrapolating quantitative data from helicopter research is usually not possible. Nevertheless, since the 70's there have been quite a lot of studies. While the research in the early years mostly focused on overall wind turbine properties such as C_P, later research uses better measurement techniques, and is capable of capturing more details of the flow such as tip vorticity. Vermeer et al. [75] give a great overview of all experiments and computational methods in wind energy from the 70's up till 2003. A list of experiments from 2003 onwards can be found in the review by O'Brien et al. [39], and to a lesser extent in the review by Bai and Wang [2].

Five experiments or projects require a little more attention though, because of the scale of the experiments and the work done:

Joule 1 and Joule 2 Joule 1 [60] and Joule 2 [54] were collaborations between several research institutes in Europe. The goal was to investigate dynamic inflow and yawed flow. Using both field tests of the 2MW Tjaereborg turbine as wind tunnel tests in the OJF at TU Delft current engineering models, as well as vortex models, could be validated and benchmarked. The conclusions were that dynamic inflow and vortex models are in good agreement.

NREL Benchmark NREL invited a wide range of research institutes to test their models against a large scale wind tunnel experiment [57]. The results showed large differences between different models. It also showed that BEM had several deficiencies, which were mostly attributed to uncertainties in airfoil polars.

IEA Annex XVIII Project In the IEA Annex XVIII by Schepers et al. [55] a large collaboration was set up again. Seven organisations and institutions collaborated in the gathering of detailed full scale field test data. The aim was to measure local aerodynamic parameters at several blade locations. This detailed data across the span of the blade was stored in a database and can be used as validation tool.

MEXICO Project The MEXICO project [53] is just like the Joule projects a European collaboration. A large set of data has been collected at the rotor location and in the wake using PIV. Pressure data at the blade surface has also been collected. The data collected in this project has been used and will be used in a large number of studies validating CFD models.

Blind Test Norwitech and Norcowe, Bergen Just like the NREL benchmark project, a blind test was organized to compare different models against wind tunnel tests. These models varied from BEM to CFD. The first Blind Test 1 [29] was a single model wind turbine of which performance and wake data was collected. The later two tests Blind Test 2 [45] and Blind Test 3 [30] investigated a turbine in the wake of another. Wake data was again collected.

2.7. Comparisons of BEM/CFD/Vortex Models

General Performance of BEM In general, there is still quite some uncertainty between models. This was shown by the experiments in the NASA-AMES windtunnel by Fingersh et al. [15] and Simms et al. [57]. According to Leishman [31], some of these discrepancies between models can be attributed to input parameters, most notably airfoil polars. This was also found by Tangler [67], who considered it the main source of errors in BEM. From the experiments and the benchmark performed by Krogstad et al. [29] it even followed that the spread between different CFD results was surprisingly large, and that it may even be concluded that CFD does not necessarily produce better results than BEM. This was especially true for off-design conditions. Predicting the blade forces is also for CFD the critical issue.

AD vs Bladed Models The actuator disc assumption may also seem like a drastic assumption. However, experiments show that it is actually a pretty reasonable assumption. Madsen [33] compared BEM with AD simulations in CFD, and concluded that BEM gives good results, at least if a tip correction is applied. Schepers [52] suggested that AD models could only be used after 5 diameters behind the disc. But Lignarolo et al. [32] compared an AD and a bladed model in a wind tunnel, and found that the wakes are very much comparable. Turbulence and mixing in the wake are intrinsically different though, and this needs to be accounted for in AD models. If the turbulence is properly included, AD models can be used even in the near wake. Medici and Alfredsson [35] also compared an AD and a bladed model in a wind tunnel, and found that above a certain tip speed ratio a bladed model can be regarded as a disc. Aubrun et al. [1] found that after 3 diameters both wakes are very comparable, and that an AD model performed better than expected in a wind tunnel.

Dynamic Inflow Models More specifically in the case of dynamic inflow models, Snel and Schepers [58] have tested the dynamic inflow models of Øye, Pitt Peters and ECN against experiments [60]. They found good agreement between the engineering models itself, and only time constants may require adjustment to get good results [58]. VTM and engineering models are also generally in good agreement [9]. Which makes sense, as the model by Øye and Pitt-Peters rely on tuned constants from VTM. A special note must be made about the Pitt-Peters model, as it repeatedly shows the smallest response time, which may be caused by its derivation from helicopter dynamics [66], [48].

On the other hand, it was noted by Yu et al. [81] that CFD and experiments show a slower decay rate than the engineering models. This also becomes clear when vortex tube models (VTM) are compared to CFD or experiments. VTM and engineering models both show the same faster decay than CFD or experiments. This is corroborated by the findings by Hong [24], who concluded that turbulence intensity is a dominant driver behind decay rates. This implies that turbulence intensity should be included in engineering models.

Interestingly, a faster decay rate may perhaps be more representative of reality. A bladed turbine with varying radial load may have additional shedding of vorticity, resulting in a faster 'recovery' [24].

Another interesting effect that was shown by Hong, was that CFD, FWVR and experiments show a non-symmetric response for an increase or decrease, whereas engineering models predict the same response for either an increase or decrease in loading. The asymmetry can be explained by different convection speeds for an increase or decrease, and therefore a different delay as wake vorticity is transported downstream. This asymmetry was also discussed by Sørensen and Madsen [65]. They remark that the time constants used in the engineering models are usually non-dimensionalised using the free-stream velocity. However, this approach neglects the influence of rotor loading on the induction in the wake. Therefore they propose to scale the time constant with the velocity in the wake instead of the free-stream velocity. Their findings were compared to a vortex model, CFD and the NASA-AMES experiments, which supported their findings. This importance of unsteady loading was also discussed by Hammam [18] and Hartin [23], who state that the time lag in dynamic inflow is sensitive to the loading. There is therefore a strong case for using the loading or induction in the wake instead of the free stream velocity.

The need for better dynamic inflow models was further stressed by Yu et al. [83]. In this study engineering models were compared against vortex models and it was concluded that an improvement on the engineering models is required because the models do not handle radial variations well. This was not yet found in 1995 by Schepers et al. [54], who found that in the case of partial pitch the radial independence assumption is valid. From this study it was also found that the dynamic inflow effects of

gusts is quite limited.

In conclusion, the current engineering models have a few flaws, and therefore Yu created a new model. The thesis will validate this new dynamic inflow model.

2.8. Review Summary

Dynamic inflow is a result of unsteady effects: it is the time delay for a new equilibrium to settle around a rotor. The results of dynamic inflow can be observed at the rotor disc [43], [54], [60], [83] but also in the wake [24], [28]. It is also in the wake where the cause of the time delay can be found [52]. Blade Element Momentum theory does not account for this time delay though. Because it is important to understand and model unsteady effects, dynamic Inflow has been researched extensively. As a result different engineering models that deal with the effect have been developed [43], [46], [58]. Vortex methods such as Vortex Tube Methods and Free Wake Vortex Ring methods are also very capable of predicting dynamic inflow effects [9], [83].

However, it has become apparent that current engineering models are not as capable as once thought. The Joule projects in 1995 [60], [54] concluded that engineering models are in good agreement, but Hong [24] and Yu et al. [83] have shown recently that current engineering models do have flaws. This is mainly because the models of Pitt-Peters and Øye use a vortex tube model to tweak the transient response, and it can be concluded that the VTM is not very capable of predicting the wake response as was noted by Yu et al. [81]. The quick response by the model of Pitt-Peters may be explained by its basis in helicopter applications [66], which is an inherently different loading regime.

In addition to this, almost all research has focused on the dynamic loading case in dynamic inflow. The case of dynamic wind has been neglected in general, with the exception of the Joule project [60]. Schepers [52] states that dynamic wind is not very relevant, and this was shown in [60]. However, the question remains whether these experiments could actually capture dynamic inflow effects. It has not been shown with absolute certainty that dynamic wind does not produce the same dynamic inflow effects as dynamic loading. This was shown by Hammam [18], who showed the presence of dynamic inflow effects on rotor loading which was not fully captured by current engineering models. The model by Hammam may prove valuable in investigating the dynamic wind effect, to see to which extent dynamic wind differs from dynamic loading.

2.9. Conclusions

In this literature review the modelling of unsteady loads and unsteady wind has been investigated. Modelling the unsteady effects correctly is important to calculate fatigue loads and aeroelastic effects well. The transient response in the flow around the rotor to unsteady loads or wind is called dynamic inflow. Dynamic inflow is caused by the wake and the time it takes for a mass of air to settle to a new equilibrium.

In rotor aerodynamics, modelling the loads and the flow is commonly done in Blade-Element-Momentum method (BEM). However, BEM is only able to capture unsteady conditions with the use of engineering models. The applicability of these engineering models was the main subject of the review. Vortex methods, CFD and experiments are capable of providing more accurate solutions or data to evaluate the engineering models. Therefore these more sophisticated methods have also been reviewed, together with their limitations and advantages.

It was found that although BEM performs well in general, the engineering models have a few areas where they could be improved. When comparing the models with more sophisticated methods, it was found that the response to change was often too quick. Furthermore, the engineering methods do not capture non-uniform loads in radial direction well. It was also found that research into the dynamic wind case is scarce, although Hammam [18] recently developed an analytical solution to be applied to dynamic wind. This approach seems promising and could be used in the further investigation into dynamic wind: an investigation to rule out any differences between dynamic wind and dynamic loading, and to see whether the conclusion by Snel et al. [60] that dynamic wind does not produce dynamic inflow effects is correct.

In general the trend in rotor aerodynamics is towards more sophisticated methods such as vortex models and CFD. Both methods have seen more and more applications in wind energy as computing power improves. And in the case of unsteady conditions, vortex methods and CFD were found to be more than adequate to capture the unsteady responses. In the case of vortex methods, the more elaborate free wake method is required though. Vortex tube models with a prescribed wake are not capable of

modelling the transient response due to unsteadiness in the wake. Unfortunately, most engineering models currently rely on the results from prescribed wake vortex tube models.

To correctly model the rotor aerodynamics in CFD, the choice of turbulence model is of utmost importance otherwise the improved accuracy of CFD is quickly lost. Because CFD requires more computational effort than vortex methods, a free wake vortex simulation is probably the best way to model the unsteady response. This simulation could then be used to further verify and improve the engineering models. Experimental research could aid in this aspect, as a lot of data on wind turbines has been gathered.

To conclude, engineering models require improvements or further investigation in two aspects: first of all in the dynamic wind case, and secondly to remedy the identified flaws in the dynamic loading case. These improvements could very well be found with the use of vortex methods and the available experimental data.

3

Vortex Model and Test Cases

The previous chapter discussed a lot of different methods, but one method was reserved for this chapter: the free wake vortex ring model. It is the main model used to investigate the effects of dynamic wind and is therefore discussed separately. The assumptions behind using this model in this research are discussed in the following section 3.1. The model itself, the equations, are shown in section 3.2. Afterwards the test cases that have been investigated in this thesis are shown in section 3.3. Finally the verification and comparison against other FWVR results is shown in section 3.4.

3.1. Assumptions

It can be tempting to look at dynamic inflow effects at the blade level. Load changes and changing inflow velocities may seem like a very local effect. In the case of dynamic inflow this is not necessarily true (though Yu et al. [83] showed that there is some radial dependence). But because dynamic inflow is per definition an effect on the scale of the rotor diameter, the rotor will be represented as a uniformly loaded disc in this investigation.

In addition to this, it is assumed that unsteady thrust and unsteady wind can be regarded independent. This is not so much a problem in the case of dynamic thrust, as the forces on the rotor can easily be changed with constant incoming velocity, by pitching the blade. In the case of unsteady wind this is slightly more difficult, as unsteady wind should result in a change of rotor forces. Here it is assumed that the forces on the rotor (F_{ax}) remain constant in the dynamic wind case. Thus the difference between dynamic thrust and dynamic wind lies in the way the thrust coefficient C_t changes, as a function of F_{ax}, or as a function of U_0.

Finally, by representing the rotor as a disc two other effects or inputs are neglected. The first one is unsteady airfoil dynamics, which is not the effect we are interested in and on a different time scale. The second input that is neglected is the rotor controller. In a realistic scenario the rotor controller may be able to negate some of the dynamic wind effects by controlling the rotor speed or pitch angle. If the rotor controller is able to react fast enough, it may be the case that from a rotor perspective not much changes. Fundamentally, it is still important to investigate the difference between unsteady wind and unsteady thrust though.

3.1.1. Induction Factor

One of the things that must be kept in mind when comparing dynamic wind to dynamic thrust, is that the induction factor is not a very convenient measure. As the induction factor itself is a function of the incoming flow, it does not compare well with the instantaneous induction factor in the dynamic thrust case. On the other hand, because thrust coefficients will be kept the same in both cases, and because the thrust coefficient can be defined in terms of induction factor, any difference in induction factor between the two effects could tell something about the underlying differences. Nevertheless, using the induction factor is a bit artificial in the case of unsteady wind conditions.

3.1.2. Governing Parameters

The main governing parameters are obviously the thrust coefficient C_t and the incoming wind velocity U_0. Together these define the system around the actuator disc. Hence it can be expected that ΔC_t and ΔU_0 play a large role. Dynamic inflow is an effect on the scale of D/U_0, therefore the diameter and velocity are also important on the time scales. Hence the time scale used here is non-dimensionalised as: $\tau = tU_0/R$. The same counts for the frequency: $k = \omega R/U_0$ and the slope of change $\delta t^* = \delta t U_0/D$. In the latter case D is chosen instead of R to easily conform with experimental data of V. Hong [24].

As mentioned before, in the actuator disc assumption a couple of important parameters are neglected, such as the tip speed ratio λ, rotor solidity σ and $\mathrm{d}C_l/\mathrm{d}\alpha$.

3.2. Free Wake Vortex Ring Model

In this work the focus lies on an actuator disc without distinct lifting bodies. And if no wake rotation is also assumed, then all vorticity is concentrated in rings that are continually being shed by the actuator disc, and thus form a sheet behind the disc. This is the simplest description available, and already posed by Joukowsky, see Okulov et al. [41]. Yoon and Heister [78] have derived analytical solutions for an infinitely thin vortex ring.

Because investigating dynamic inflow effects requires a dynamically changing wake, a prescribed wake vortex ring model will not suffice. A free wake vortex ring (FWVR) model is better at capturing the velocity response in the dynamic inflow case than a prescribed wake model because it allows the wake to have a transient response to a change. This can be seen in the study conducted by Yu et al. [81]. Van Kuik and Lignarolo [73] showed that the model is very useful to validate certain assumptions of BEM, and that its results can give good insight in the physics of rotor aerodynamics.

The FWVR that will be discussed in this section is based on the model outlined by Baldacchino and van Bussel [3]. The same approach is also used by Van Kuik and Lignarolo [73], Øye [42] and Yu et al. [83]. It consists of a free wake part, and a part where the wake is fully expanded which is regarded as a semi-infinite tube.

3.2.1. Free Wake Part (near wake)

As mentioned before, in the case of a vortex ring method, all vorticity is concentrated in vortex rings that are continually being shed from the actuator disc at radial locations where $\frac{\mathrm{d}p}{\mathrm{d}r} \neq 0$, most notable at the edge of the disc. This vorticity forms a sheet. A free wake model applies the condition that there is no pressure difference across the sheet. Van Kuik and Lignarolo [73] showed that the strength of the shed vorticity ring in axial axi-symmetric flow is:

$$\frac{\Gamma}{\Delta t} = \frac{\Delta p}{\rho} \tag{3.1}$$

With Γ being the strength of the circulation of the ring. Circulation is linked to the thrust coefficient C_t through:

$$\Gamma = \frac{\Delta p}{\rho}\Delta t = \frac{C_t \rho U_0^2}{2}\frac{\Delta t}{\rho} = \frac{C_t U_0^2 \Delta t}{\rho} \tag{3.2}$$

Hence, circulation in a vorticity ring can be equated to thrust and inflow velocity. The next step is linking the induced velocity by the vortex ring to the strength of the vorticity. Yoon and Heister [78] derived an analytical solution for an infinitely thin vortex ring:

$$u_z^{ind} = \frac{\Gamma_i}{2\pi\sqrt{\left(z_p - z_i\right)^2 + \left(r_p + R_i\right)^2 + \delta}}\left[K(m^2) + \frac{R_i^2 - r_p^2 - \left(z_p - z_i\right)^2}{\left(z_p - z_i\right)^2 + \left(r_p - R_i\right)^2 + \delta}E(m^2)\right] \tag{3.3}$$

$$u_r^{ind} = -\frac{\left(z_p - z_i\right)\Gamma_i}{2\pi r_p\sqrt{\left(z_p - z_i\right)^2 + \left(r_p + R_i\right)^2 + \delta}}\left[K(m^2) - \frac{R_i^2 + r_p^2 + \left(z_p - z_i\right)^2}{\left(z_p - z_i\right)^2 + \left(r_p - R_i\right)^2 + \delta}E(m^2)\right] \tag{3.4}$$

Γ_i, z_i, R_i denote the strength, the z-coordinate and radius of the i^{th} vortex ring. z_p and r_p are the coordinates of the point where the induced velocity is required, see figure 3.1. K and E are the complete

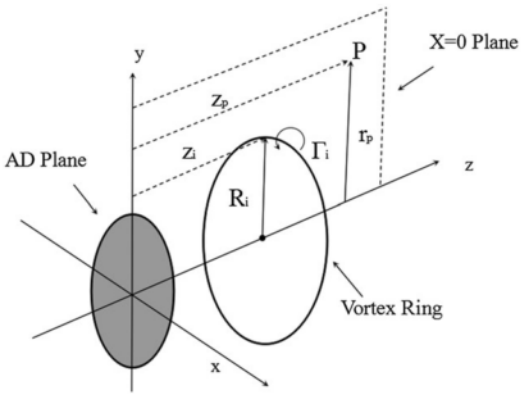

Figure 3.1: Vortex ring model and coordinate system, from Yu et al. [83].

elliptic integrals of the first and second kind respectively. With:

$$m^2 = \frac{4r_p R_i}{\left(z_p - z_i\right)^2 + \left(r_p + R_i\right)^2 + \delta} \tag{3.5}$$

δ in equations 3.3 to 3.5 is used to avoid the singularity when the position P gets close to the vortex ring. By using δ in this way it is effectively a cut-off radius in which the strength of the vortex decreases to zero, to avoid velocities going to infinity. Yu et al. [83] show different cut-off radii and their effects on the solution.

This singularity also means that the induced velocity by the vortex ring on itself cannot be calculated using equations 3.3 and 3.4. As stated by Baldacchino and Van Bussel [3], in that case the induced velocity at the center of the vortex ring can be used to calculate the self-induced velocity:

$$u_z^s = \frac{\Gamma_i}{2R_i} \tag{3.6}$$

$$u_r^s = 0 \tag{3.7}$$

Which is only valid if the vortex core of the vortex ring is small compared to the radius of the ring. Usually infinitely thin vortex rings are assumed, and then the above relations can be used. While this is true for an infinitely small disc, it must be kept in mind that this way a radial velocity component is neglected, as was shown by Van Kuik et al. [74]. This radial component will have an influence on the development of the wake.

3.2.2. Fixed Wake Part (far wake)

In the fixed wake part the rings are replaced with a tube with constant vorticity strength γ, as already stated in equation 2.26”

$$\gamma = \frac{\Gamma}{\mathrm{d}z}$$

The induced axial velocity then follows from the vorticity strength and the size and position of the tube [73]:

$$u_z^{ind} = \frac{\gamma}{4\pi}\Omega(z_0) \tag{3.8}$$

Where Ω is the solid angle between the calculation point and the opening of the tube, which can be calculated using the derivation by Paxton [44]. Fully written out the equation for axial induced velocity by a vortex tube reads:

$$u_z^{ind} = \frac{\gamma}{4\pi}\left[\left(\frac{R_{tube} - r_p}{\left|R_{tube} - r_p\right|} + 1\right)\pi + m\frac{z_p - z_{tube}}{\sqrt{r_p R_{tube}}}\left(K\left(m^2\right) - \frac{r_p - R_{tube}}{r_p + R_{tube}}\Pi\left(\alpha, m^2\right)\right)\right] \tag{3.9}$$

With m^2 is given analogous to equation 3.5, with the radius and z location of the tube opening. α is defined as:

$$\alpha = \frac{4r_p R_{tube}}{r_p + R_{tube}} \tag{3.10}$$

Branlard and Gaunaa [8] derived the same equations, though in a different way. They also derived the equation for induced radial velocity:

$$u_r^{ind} = -\frac{\gamma}{2\pi}\sqrt{\frac{R_{tube}}{r_p}}\left(\left(\frac{2}{m} - m\right)K\left(m^2\right) - \frac{2}{m}E\left(m^2\right)\right) \tag{3.11}$$

$K(m^2)$ and $E(m^2)$ are again the complete elliptic integrals of the first and second kind, and $\Pi(m^2)$ is the complete elliptic integral of the third kind.

3.2.3. Limiting Parameters

In this FWVR model there are three parameters that govern the accuracy and speed: the time step Δt, the cut-off radius δ and the point at which the free wake ends and the tube starts. Yu et al. [83] and Van Kuik and Lignarolo [73] all found convergence values for these parameters. This FWVR model has been validated against experiments by Yu et al. [83], and was cross-verified by Van Kuik and Lignarolo [73]. The model parameters that have been used here are shown in table 3.1. The same model parameters

Table 3.1: Limiting parameters used in the FWVR model.

Parameter	Value	From Yu et al. [83]
Vortex cut-off δ	10^{-5}	10^{-5}
Time Step $\Delta\tau$	0.02	0.02
Extension of vortex rings	11R	11R

have been chosen as the FWVR model by Yu et al., who estimated the modelling error with these parameters. It was shown that by using these values the influence of the time step, cut-off radius and number of vortex rings is very small.

Depending on the thrust coefficient, the number of vortex rings that are included in the calculation varies. For $C_t = 7/9$ and with a far wake start of $11R$, roughly 750 vortex rings are evaluated at each time step.

3.2.4. Dynamic Wind Implementation

Imposing a wind speed change on a vortex model should not provide too much difficulties as being able to add any velocity field on top of the vorticity model is one of the advantages of potential flow theory. However, how this wind change is implemented will determine how a change is perceived at the rotor and wake. Three options exist:

Wave-front: $U_{wind} = f(z, a)$ The first option is to change the wind in the domain in a wave-like way. The wind speed is not constant at every z but a function of z. If the wave speed is the absolute wind speed: $U(1-a)$ the 'gust' convects at the same speed as the vortex rings, the wave front coincides with a vortex ring. The wind speed at $t = i$ can then be implemented as an inherent property of the i-th vortex ring.

Wave-front: $U_{wind} = f(z)$ The second option is again a wave, but now the wave-front speed is constant and the same as the wind speed: the 'gust' convects faster or slower than the vortex rings.

Uniform change: $U_{wind} = f(t)$ The third and final option is a uniform change across the spatial domain. The wind changes everywhere at the same time. This is the least 'physical' description of a wind gust.

In the dynamic wind cases the incoming wind velocity U_0 at the rotor ($z = 0$) at time τ is established such that the C_t is matched to the varying C_t in the load varying case. Instead of $C_t = f(F_{ax})$, the thrust

coefficient is a function of $C_t = f(1/U^2)$. Therefore:

$$\frac{C_t(\tau)}{C_t(0)} = \frac{U_0^2(0)}{U_0^2(\tau)}$$
$$\Rightarrow$$
$$U_0^2(\tau)C_t(\tau) = U_0^2(0)C_t(0) \tag{3.12}$$

As a result from this, the circulation strength of the vortex rings does not change in the dynamic wind case, as the circulation is defined as $\Gamma = C_t U_0^2 \Delta t/\rho$. In the dynamic load case the circulation Γ does change. However, because the convection speed of the vortex rings changes, the vortex sheet strength γ does change, as $\gamma = \Gamma/\mathrm{d}z$.

3.3. Test Cases

Table 3.2: Dynamic Inflow Experiments and Selected Cases.

Rotor/disc	Step		Harmonic	Gust	
	Loading	Rotor speed	Loading	IEC gust	Extreme rise
FWVR Dyn. Inflow [83]	A		C	x	x
Experiments Hong [24]	B			x	x
Experiments Kaur [28]			D		
Tjaereborg	x				
Oldenburg	x				
NASA AMES	x				
Mexico rotor		x			

The goal is to model different rotors and conditions at the same conditions as available experimental measurements or available model computations of dynamic thrust. This way dynamic thrust can be compared in different test cases to dynamic wind. Seven rotors or discs could be used in the comparison as shown in table 3.2. However, the Tjaereborg, Oldenburg, NASA AMES and Mexico rotors are all bladed models. Therefore only an actuator disc will be analysed and only the results from the FWVR computations by Yu et al. [83] will be used in the comparison. The cases used in the experiments by Hong [24] and Kaur [28] will be evaluated in the FWVR, however the results are not presented as it was relatively difficult to compare the findings in the experiments against the FWVR results. They are however used in the verification of the FWVR model. The IEC gust / extreme rise gust cases are also left aside. No experimental data exists with respect to dynamic inflow effects anyway for realistic gusts. Nonetheless these cases could be interesting to show the effects of a real physical example of dynamic wind.

To conclude, only 4 cases are selected: A & B for a step change, and C & D for a harmonic change. The step change cases are described in section 3.3.1 and the harmonic cases are described in section 3.3.2.

The only input in all cases is the thrust coefficient C_t and the way it changes, harmonically or with a step change. In the load case the thrust coefficient is solely a function of the axial force at the rotor:

$$C_t(\tau) = f(F_{ax}) = \frac{F_{ax}(\tau)}{\frac{1}{2}\rho A U_0^2} \tag{3.13}$$

In the dynamic wind case the thrust coefficient is a function of the incoming wind speed:

$$C_t(\tau) = f(U_0) = \frac{F_{ax}}{\frac{1}{2}\rho A U_0^2(\tau)} \tag{3.14}$$

3.3.1. Case A & B: Step Wind Change

The step cases are relatively straight forward. A change in C_t is imposed at $\tau = 1$. The simulation runs till $\tau = 40$. The change is instant for cases A1-A8, and has a ramp up time for cases B1-B14. The ramp

up time is non-dimensionalised as:

$$\delta t^* = \delta t \frac{U_0}{D} \tag{3.15}$$

Where δt is the time it takes to change the thrust coefficient. Because τ is non-dimensionalised as $\tau = t\frac{U_0}{R}$, the ramp time should manifest itself as $2\delta\tau$ on the plotted timescale. The thrust coefficients and change in C_t are shown in tables 3.3 and 3.4.

Wind Speed Convection Three special cases are added to the step changes. A1-A3 and B1-B3 have different implementations of the wind speed convection U_{wind} as discussed in section 3.2.4. This is to give an idea of the effect of the way the 'gust' is modelled as the implementation could have quite an impact on the results.

Table 3.3: Step cases which are compared against results from Yu et al. [83].

	Case							
	Wind					Load		
C_t	7/9	7/9	7/9	7/9	6/9	7/9	7/9	6/9
dC_t	1/9	1/9	1/9	-1/9	1/9	1/9	-1/9	1/9
δt^*	0	0	0	0	0	0	0	0
$U_{wind} = f(z,a)$	x			x	x	x	x	x
$U_{wind} = f(z,t)$		x						
$U_{wind} = f(t)$			x					
$No.$	A1	A2	A3	A4	A5	A6	A7	A8

Table 3.4: Step cases which can be compared against results from Hong [24].

	Case													
	Wind								Load					
C_t	0.77	0.77	0.77	0.93	0.77	0.93	0.77	0.93	0.77	0.93	0.77	0.93	0.77	0.93
dC_t	0.17	0.17	0.17	-0.17	0.17	-0.17	0.17	-0.17	0.17	-0.17	0.17	-0.17	0.17	-0.17
δt^*	0.2	0.2	0.2	0.2	0.4	0.4	0.8	0.8	0.2	0.2	0.4	0.4	0.8	0.8
$U_{wind} = f(z,a)$	x			x	x	x	x	x	x	x	x	x	x	x
$U_{wind} = f(z,t)$		x												
$U_{wind} = f(t)$			x											
$No.$	B1	B2	B3	B4	B5	B6	B7	B8	B9	B10	B11	B12	B13	B14

3.3.2. Case C & D: Harmonic Change

In addition to a step change, a harmonic change has also been simulated. A harmonic change is ideal because it gives a good idea of the phase difference between the instantaneous thrust coefficient and the induction in the wake. A phase difference between wind and thrust would indicate a difference in the way the wake 'deals' with a change. It could also indicate that there is a different time delay associated with a wind change as compared to a thrust change. The harmonic cases are shown in tables 3.5a and 3.5b. The main parameter here is the reduced frequency k, which is defined as:

$$k = \frac{\omega R}{U_0} \tag{3.16}$$

And the thrust behaves like a sine wave:

$$C_t = C_{t,steady} + dC_t \sin(2\pi k t)$$

These cases can be verified and compared against simulations and experiments by Yu et al. [83] and Kaur [28] for respectively the C and D cases.

Table 3.5: Harmonic Cases

(a) Harmonic cases which can be compared against results from Yu et al. [83].

	Case					
	Wind			Load		
C_t	7/9	7/9	7/9	7/9	7/9	7/9
dC_t	1/9	1/9	1/9	1/9	1/9	1/9
k	1	0.5	0.2	1	0.5	0.2
$U_{wind} = f(z, a)$	x	x	x	x	x	x
$U_{wind} = f(z, t)$						
$U_{wind} = f(t)$						
$No.$	C1	C2	C3	C4	C5	C6

(b) Harmonic cases which can be compared against results from Kaur [28].

	Case					
	Wind			Load		
C_t	0.68	0.68	0.68	0.68	0.68	0.68
dC_t	0.13	0.13	0.13	0.13	0.13	0.13
k	1.57	0.94	0.47	1.57	0.94	0.47
$U_{wind} = f(z, a)$	x	x	x	x	x	x
$U_{wind} = f(z, t)$						
$U_{wind} = f(t)$						
$No.$	D1	D2	D3	D4	D5	D6

3.4. Verification of FWVR Model

In this section a few results will be presented to verify whether the model produces sensible results. Steady results, step change results and harmonic results will be compared to theoretical values and against results from computations by the FWVR from Yu et al. [83].

Steady Solution Table 3.6 shows the predicted induction factors at several thrust coefficients and these are compared against theoretical values from momentum theory. The induction factors are within 0-1% of theoretical values. In general it can be concluded that the model converges well to the supposed values. Any differences may be attributed to small modelling estimations (e.g. the cut-off radius δ), or because the model is still reaching convergence at $\tau = 40$.

Table 3.6: Steady solutions induction factors compared to momentum theory.

	Initial				Final			
Case	C_t	FWVR a [-]	Momentum a [-]	Δ %	C_t	FWVR a [-]	Momentum a [-]	Δ [%]
A6	7/9	0.265	0.264	0.3%	8/9	0.333	0.333	0.0%
A7	7/9	0.265	0.264	0.3%	6/9	0.210	0.211	-0.5%
A8	6/9	0.211	0.211	-0.0%	7/9	0.264	0.264	-0.2%
B9	0.767	0.259	0.259	0.3%	0.933	0.368	0.371	-0.6%
B10	0.933	0.374	0.371	0.9%	0.767	0.257	0.259	-0.5%
D4	0.68	0.217	0.217	-0.2%	-	-	-	

Step Change The step change case A6 is used to verify the model against a FWVR model by Yu et al. [83]. Figure 3.2a shows the comparison of case A6 against results from Yu et al. It can be seen that both models produce the same response after a step change. The only difference is a bit of a wiggle as compared to the smooth result in the FWVR of Yu et al. This can be attributed to the way the far wake is modelled: its properties are a function of the near wake, and the way this is implemented may differ.

In figure 3.3 the results from case A6 are compared against the experimental results by Hong [24] (as presented by Yu et al. [82]). Because the steady C_t and change in C_t differ, the velocity is non-dimensionalised. The initial response is very different, but the overall time delay appears to be consistent: the time scale of the dynamic inflow effect is captured well by the FWVR. The reason for the initial difference may be twofold: firstly, a semi-porous disc is used during the experiments, which may result in a different response than the uniform porosity assumed in the vortex model, secondly it must be noted that the experimental results shown here are measured behind the rotor at location $z/R = 1$.

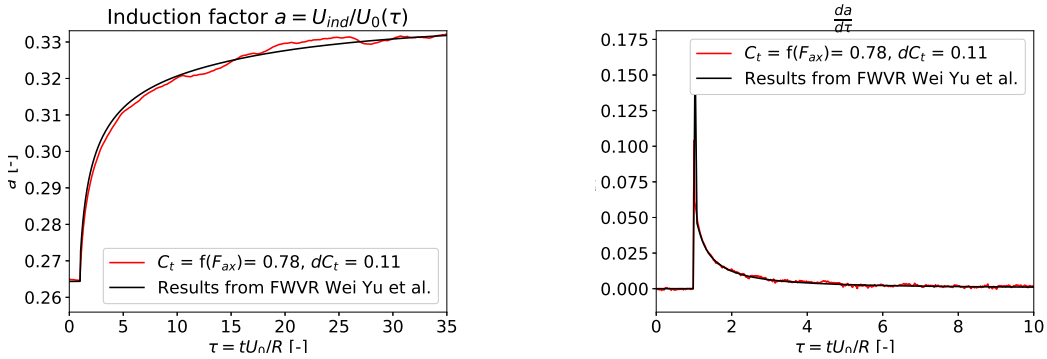

(a) Induction factor

(b) Rate of change of induced velocity at the rotor.

Figure 3.2: Comparison of the FWVR results against results from Yu et al. [83] after a load step change, case A6.

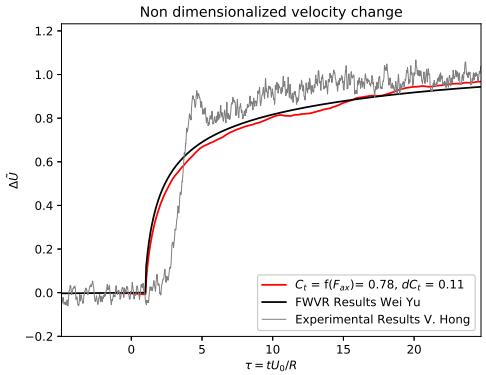

Figure 3.3: Non-dimensionalised velocity change, case A6, against experimental results by V. Hong [24] and Yu et al. [83].

Harmonic The harmonic case is verified against results from the FWVR by Yu et al. [83] (again). The comparison is shown in figures 3.4a and 3.4b. The models vary in their initial steady solution, but apart from that they are very similar in the harmonic case. Both in an absolute sense (figure 3.4a) and in the way they predict the phase difference between the induction and C_t (figure 3.4b similar results are produced.

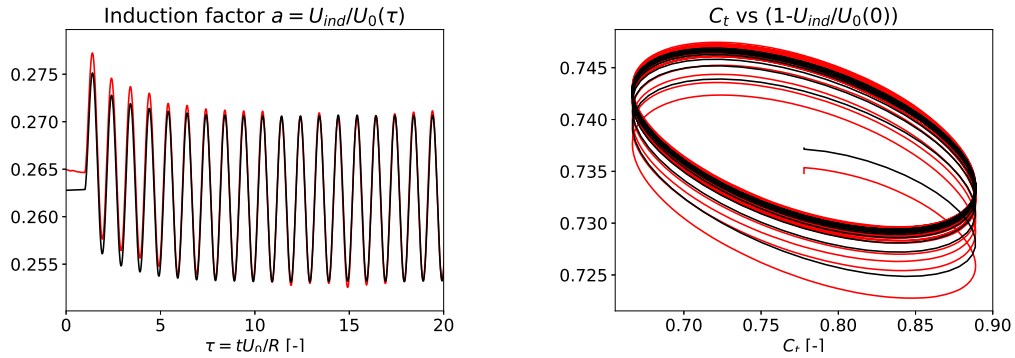

(a) Induction factor vs τ.

(b) U_z vs C_t.

Figure 3.4: Comparison of the FWVR against results by Yu et al. [83] at $k = 1$.

4

Performance Engineering Models

In the first part of this thesis, Part I it was found that dynamic wind results in a different response at the rotor. It also discussed the way current engineering models handle dynamic wind. This chapter will go into a bit more detail regarding the new model by Yu and two alternative models.

This chapter will show the different models in sections 4.1 and 4.2. The performance of these models is discussed in section 4.3. The performance of all models together is summarised in the conclusions in section 4.4.

4.1. Engineering Models and Alternatives

The three most commonly used engineering models will be evaluated here, to see how they perform in dynamic inflow as compared to the FWVR model. Both the dynamic thrust cases as dynamic wind cases will be used in the evaluation.

The three models that will first be compared against the results from the FWVR model are:

Øye's Model Developed by Øye [42].

Pitt-Peter's Model by Pitt and Peters [46].

ECN Model by Snel and Schepers [60].

See section 2.2 for a detailed description of the models. After the evaluation of the performance of these models the following alternatives will be proposed:

Vortex Tube Model As proposed by Branlard and Gaunaa [8]. The model by ECN is based on the same principle.

Hammam's model As described by Hammam [18]. An integro-differential equation describing dynamic wind and dynamic thrust in separate terms.

Duhamel's integral by Yu [79]. Analogous to the approach commonly used in the prediciton of unsteady airfoil aerodynamics. An exponential indicial function is inserted into Duhamel's integral to find the induced velocity response at the rotor.

These models are described further in section 4.2.

4.2. Alternative Models

It has been established that current engineering models underestimate the effect of dynamic inflow due to dynamic thrust, and that they do not distinguish between dynamic thrust and dynamic wind. Therefore three alternative models will be tested against the FWVR as well. The first model is analogous to ECN's model, and discussed in section 4.2.1. The second model is Hammam's model 4.2.2 and the third model is Yu's model 4.2.3. After this their performance as compared to the FWVR model is shown in section 4.3.

4.2.1. Vortex Tube Model

The first alternative is a simplified model as compared to the free wake vortex ring model as discussed in chapter 3. This simplification is because contrary to the FWVR model, a vortex tube model simplifies the convection velocity in the wake. Instead of calculating the self-induced velocity in the wake by all vortex elements, a fixed velocity is used. Transportation of the vortex elements is therefore easily calculated. The induced velocity at the rotor can then be calculated in the same way as outlined in section 3.2.2 for every vortex tube element.

The equation used to calculate the induced velocity from a vortex tube element was previously discussed in section 3.2.2, see equation 3.9. It is repeated here for convenience.

$$\begin{aligned} u_z^{ind} &= \frac{\gamma}{4\pi}\Omega(z_p, r_p) \\ &= \frac{\gamma}{4\pi}\left[\left(\frac{R_{tube}-r_p}{|R_{tube}-r_p|}+1\right)\pi + m\frac{z_p - z_{tube}}{\sqrt{r_p R_{tube}}}\left(K\left(m^2\right) - \frac{r_p - R_{tube}}{r_p + R_{tube}}\Pi\left(\alpha, m^2\right)\right)\right] \end{aligned}$$

With m^2 defined in equation 3.5, and α is defined in equation 3.10. If $z_p = 0$, the induced velocity at the rotor is calculated. The induced velocity at time step i is then simply the starting vorticity strength with $z_{tube} = 0$ and the summation of the differences with respect to the previous vortex tube:

$$u_z^{ind}(r_p, i) = \frac{\gamma(0)}{4\pi}\Omega(r_p, 0) + \sum_{i=1}^{\infty}\frac{\Delta\gamma_i}{4\pi}\Omega(r_p, z_{tube,i}) \tag{4.1}$$

The vorticity strength of each element γ has been discussed before, but it can be defined as:

$$\gamma = \frac{\Gamma}{\mathrm{d}z} = \frac{C_t U_0^2/2\mathrm{d}t}{\mathrm{d}z} = \frac{C_t U_0^2}{2\left(U_0 - u_z^{ind}\right)} \tag{4.2}$$

And finally, $\Delta\gamma_i$ is the difference in vorticity strength between two time steps:

$$\Delta\gamma_i = \gamma_i - \gamma_{i-1} \tag{4.3}$$

The remaining variable to play with is the location z_{tube} and transport velocity of the vortex tubes. The most straightforward application is simply using the velocity at the rotor, and let all vortex tubes move downstream with the same velocity at each time step.

4.2.2. Model by Hammam

Hammam [18] proposes a different approach to a time constant application in BEM. In his thesis he defines the three effects that cover unsteady rotor aerodynamics, being airfoil aerodynamics, inertia terms (apparent mass) and circulatory (wake) terms. The inertia terms resemble the way the other way engineering models represent dynamic inflow.

His equation was already briefly mentioned chapter 2 in equation 2.24. This approach could aid in the definition of dynamic wind because of the distinction made between the circulation (apparent mass) at the rotor, and the vorticity in the wake.

$$\mathrm{d}F_{ax}(r,t) = \rho A u_{ind,\infty}(t)\left(U_0(t) - 0.5u_{ind,\infty}(t)\right) + 0.5\rho A\int_t^{\infty}\gamma(r,t')\frac{\mathrm{d}U_{vr}(t')}{\mathrm{d}t'}I_\phi(z')\mathrm{d}t' + \mathrm{dm}(r)\frac{\partial u_{ind}(t)}{\partial t}$$

The second term on the right side shows the effect of the wake through the wake vorticity strength γ, the wake convection speed U_{vr} and the relation between the vorticity and velocity I_ϕ. The function I_ϕ follows from Conway's relation between a vortex ring at location x' and induced velocity at the disc [12]. Therefore:

$$I_\phi(r, x') = \frac{(-x')\,K\,(k_1)}{\pi\sqrt{rR}} + \Lambda_0 \tag{4.4}$$

In which K is the complete elliptic integral of the first kind, and Λ is a function of the complete and incomplete elliptic integrals of the first and second kind. See Hammam [18] for their complete definitions.

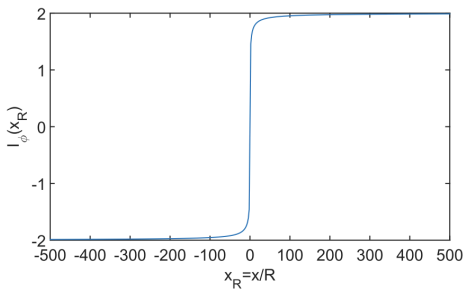

Figure 4.1: Response function at the rotor disc versus distance from the disc, from Hammam [18].

k_1^2 is equal to m^2 as defined in equation 3.5. Equation 4.4 is very similar to equation 3.9. The response of I_ϕ at the rotor tip is shown in figure 4.1.

The second term should replace the first term over time, as the unsteady wake defines the induced velocity response and the far wake is transported downstream with a diminishing effect on the disc. This is done through the following equation:

$$u_\infty(\tau) = 2u_{ind}\left[\frac{1}{2} + \frac{1}{4}I_\phi\left(\zeta - \zeta'\right)\right] \tag{4.5}$$

Which describes the induced velocity in the far wake u_∞ as a function of the far wake location ζ, for which Hammam uses $30R$. ζ' is the location of the steady wake, which convects downstream. At $\tau = 0$, $\zeta - \zeta' = 30R$ and $I_\phi \approx 2$, at $\tau = \infty$, $\zeta - \zeta' = -\infty$ and $I_\phi = -2$, therefore the first term goes to zero as time moves on. The second term has replaced the steady wake.

The final term on the right hand side shows the effect of the change in induced velocity at the rotor in a similar expression as the engineering models.

4.2.3. Duhamel's Integral

Yu [79] proposes a different approach by using the general solution to the second order damping equation, which can often be found to be of the form of one or more exponentials. Yu uses a free wake vortex ring model to fit the damping coefficients and frequencies. This exponential function can then be inserted in Duhamel's integral to calculate the response.

The following form of the indicial response function was defined, which describes the induced velocity response due to a change in vorticity:

$$\Phi_d(r,t) = 1 - \beta e^{\omega^1 t} - (1-\beta)\, e^{\omega^2 t} \tag{4.6}$$

In this equation β, ω^1 and ω^2 are the coefficients used to make the fit. These coefficients are a function of radius and base thrust coefficient, and the radial dependency was created through a third order polynomial:

$$\beta(r) = a_3 r^3 + a_2 r^2 + a_1 r^1 + a_0 r^0 \tag{4.7}$$

$$\omega^1(r) = a_3 r^3 + a_2 r^2 + a_1 r^1 + a_0 r^0 \tag{4.8}$$

$$\omega^2(r) = \frac{1}{a_3 r^3 + a_2 r^2 + a_1 r^1 + a_0 r^0} \tag{4.9}$$

These polynomial parameters were then fitted to the response calculated through a free wake vortex ring method, and they are shown in table 4.1. The accuracy of the fit through these parameters is shown by Yu in [79]. The Duhamel's integral describes the response x to an arbitrary excitation $F(\tau)$, and the response function $h(t-\tau)$ to that excitation at time τ:

$$x(t) = \int_0^t F(\tau)\, h(t-\tau)\, \mathrm{d}\tau \tag{4.10}$$

Table 4.1: Polynomial parameters of the exponential coefficients β, ω^1 and ω^2, based on a free wake vortex ring method.

	β	ω^1	ω^2
a_3	$0.98C_t - 1.09$	$3.45C_t^2 - 5.19C_t + 2.01$	$0.05C_t - 0.60$
a_2	$-2.01C_t + 1.99$	$-4.60C_t^2 + 7.01 - 2.81$	$-0.38C_t + 1.6$
a_1	$0.57C_t - 0.34$	$0.06C_t - 0.09$	$0.32C_t - 0.23$
a_0	$0.62C_t - 0.03$	$-0.07C_t - 0.12$	$-0.19C_t - 0.79$

The induced velocity response is then written in terms of the Duhamel's integral as:

$$u_{ind}(r,t) = \gamma(0)\Phi_d(r,t) + \int_0^t \frac{\mathrm{d}\gamma}{\mathrm{d}\sigma}\Phi_d(r,t-\sigma)\mathrm{d}\sigma \tag{4.11}$$

Combining equations 4.6 and 4.11, and differentiating the Duhamel's integral, Yu finds the following expression for the induced velocity response at time step j in the form of a time marching scheme:

$$u_{ind}(r,t) = 0.5\left(\gamma(t) - c_j^1(t) - c_j^2(t)\right) \tag{4.12}$$

With c_j^1 and c_j^2 being intermediate differential functions:

$$\frac{\mathrm{d}c_j^1(t)}{\mathrm{d}t} - \omega_j^1 c_j^1(t) = \beta_j \frac{\mathrm{d}\gamma(t)}{\mathrm{d}t} \tag{4.13}$$

$$\frac{\mathrm{d}c_j^2(t)}{\mathrm{d}t} - \omega_j^2 c_j^2(t) = \left(1-\beta_j\right)\frac{\mathrm{d}\gamma(t)}{\mathrm{d}t} \tag{4.14}$$

With ω^1, ω^2 and β_j the coefficients as shown in table 4.1. Equation 4.12 can then be implemented into BEM.

4.3. Performance Alternative Models

The alternative models have been compared against the current engineering models and the FWVR model. Both the dynamic wind case and dynamic thrust case have been tested here. Figures 4.2 and 4.3 show the response to a step change in $\Delta C_t = 1/9$ at $C_t = 7/9$.

4.3.1. Vortex Tube Model

The vortex tube model is interesting, because the difference between the free wake vortex model and the fixed wake model is the way the wake convects. In addition to this, ECN's model and Øye's model are based on this vortex representation of the wake. And this can be seen in the results as shown in figures 4.2 and 4.3. Both in the dynamic wind and dynamic thrust cases the vortex tube model is comparable to ECN's model. Small differences between the VTM and ECN's model may be attributed to the way the convection speed and vorticity strength are calculated.

Although the VTM performs better than the engineering models in dynamic thrust (albeit only slightly), it does not perform well in the dynamic wind case. It shows the same quick response as modelled by the engineering models. This is attributed to the way the wake is modelled in the VTM. A change in wind speed changes the convection of the entire wake immediately, and does not result in a gradual change in vorticity strength throughout the wake, as was seen in the dynamic wind case. In order to model this, a free wake model is therefore necessary. This effect was also seen in part 1 in the evaluation of different implementation of wind speed: when changing the wind speed in the entire wake instantly, the same sudden change was observed in the FWVR model.

The question that follows from this result is whether the vortex tube model can be changed to accommodate this convection in the wake. Four different methods have been added or changed in the vortex tube method, and the results are shown in figures 4.4a to 4.4c. The different approaches are:

Method 1: basic Vortex Tube Model This is the model outlined in section 4.2.1. The vorticity strength $\gamma(t)$ changes gradually as a function of the induced velocity as shown in equation 4.2. All wake elements move at the same prescribed velocity downstream at each time step.

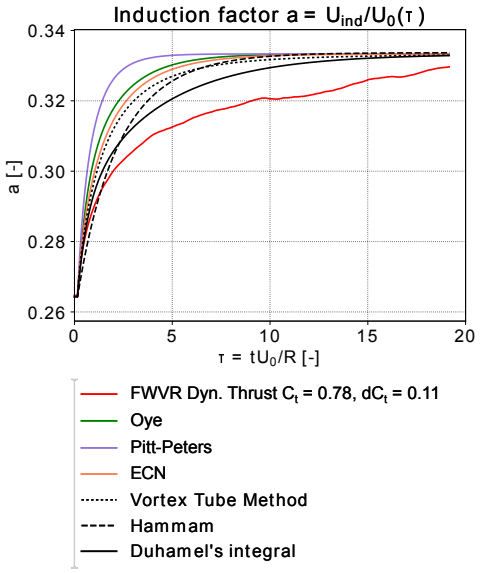

(a) Induction factor vs time.

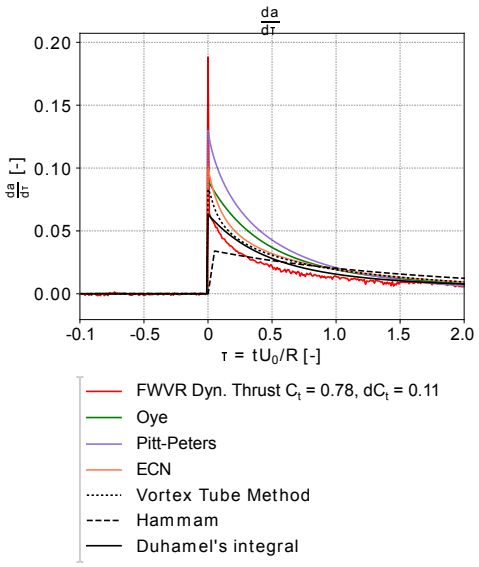

(b) Induction factor change per unit of time.

Figure 4.2: Alternative models vs FWVR and engineering models $C_t = 7/9$, $\Delta C_t = 1/9$, dynamic thrust case.

Method 2: $\gamma(t) = f(C_t, U_0)$ In this case $\gamma(t)$ is no longer a function of the induced velocity of the rotor, but only a function of the thrust coefficient and wind speed. It is the same as the circulation at the rotor, and therefore changes instantly at a step change. The effect of this change will be further discussed in section 4.3.3. As can be seen from figure 4.4, this results in a faster response, as can be expected.

Method 3: Induced velocity at $r = 0$ Here the induced velocity at the rotor centre is used to calculate the convection velocity, instead of the averaged value of the rotor. The resulting response is slightly slower, but the differences are small.

Method 4: Non-fixed wake velocity This is only shown in figures 4.4c and 4.4b. Instead of a constant wake velocity throughout at the wake at every time step, in this case the vortex elements retain their wake velocity at the time they were shed. This means that the entire wake convects downstream at different velocities. The effect is surprisingly small, and not close to the free wake model. Meaning that the effect of dynamic wind is really an effect of the self induced velocity in the wake.

Two calculations can be drawn from these changes. Firstly, using the instantaneous $\gamma(t)$ as a function of C_t and U_0 only shows that it is important to model $\gamma(t)$ in a different way then the circulation $\Gamma(t)$. Therefore in $\gamma(t) = \Gamma/\mathrm{d}z$ the way the circulation is distributed through $\mathrm{d}z$ is of importance.

Secondly, changing the convection velocity in the vortex tube model does not improve the performance. It still shows a quick response, which is not reflective of the results shown by the FWVR model.

4.3.2. Hammam

The results of Hammam's model as outlined in [18] are not as good as expected. Equation 2.24 by Hammam was promising, but when put to the test a couple of problems appear. The results shown in figures 4.2 and 4.3 are not bad, but that is because the following problems are masked. These problems are shown in figures 4.5a to 4.5d.

For clarity Hammam's equation is repeated here, as the three terms on the right hand will be discussed separately.

$$\mathrm{d}F_{ax}(r,t) = \underbrace{\rho A u_{ind,\infty}(t)\left(U_0(t) - 0.5u_{ind,\infty}(t)\right)}_{\text{Far Wake}} + \underbrace{0.5\rho A \int_t^{\infty} \gamma(r,t')\frac{\mathrm{d}U_{vr}(t')}{\mathrm{d}t'} I_\phi(z')\mathrm{d}t'}_{\text{Circulatory Vortex Wake}} + \underbrace{\mathrm{dm}(r)\frac{\partial u_{ind}(t)}{\partial t}}_{\text{Apparant Mass}} \tag{4.15}$$

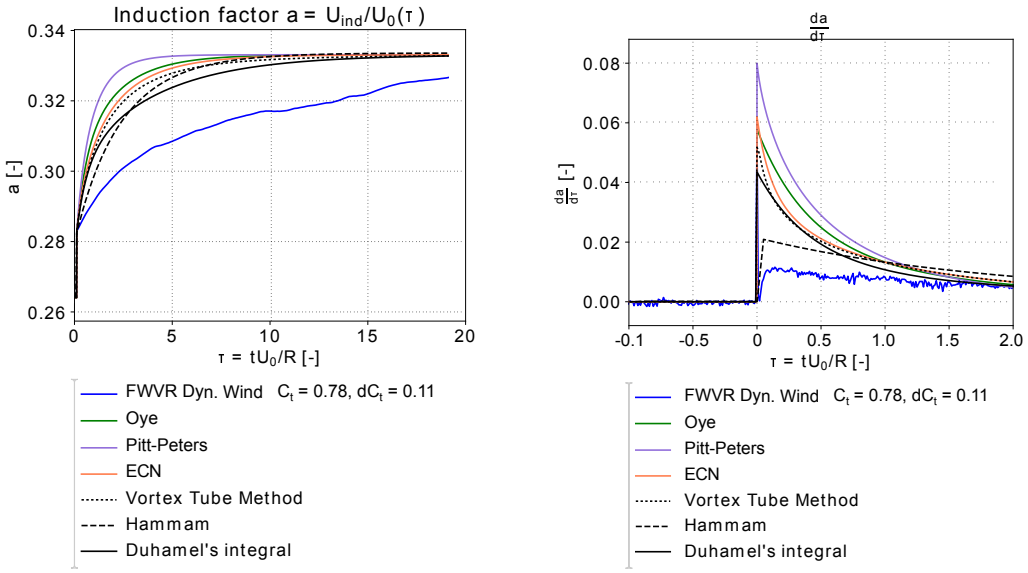

(a) Induction factor vs time.

(b) Induction factor change per unit of time.

Figure 4.3: Alternative models vs FWVR and engineering models $C_t = 7/9$, $\Delta C_t = 1/9$, dynamic wind case.

Circulatory Term In the form proposed by Hammam, this integral is very small, and has a negligible contribution. The change in convection speed $\frac{\mathrm{d}U_{vr}}{\mathrm{d}\tau}$ is small, and Hammam actually defines $\gamma = 2\frac{\mathrm{d}u_{ind}}{\mathrm{d}\tau}$, making the integral even smaller. If Hammam's definition for γ is used, his equation basically reduces to a similar expression as the engineering models. See figure 4.5b, the second term has barely any effect. However, Hammam describes the second term to be the replacement of the far wake steady term over time. In that case γ should be equal to $\gamma = 2u_{ind}$, see figure 4.5c. But, in that case the steady state solution is not reached.

Far wake steady term Thus, if the circulatory term is given a more prominent role as replacement of the steady solution, another problem arises. The integral adds to the steady state solution of the first term, and therefore the steady term should be coupled to the circulatory term. The function I_ϕ describes the strength of the vortex elements, and Hammam also uses I_ϕ in the steady solution, see equation 4.5. Therefore the circulatory term and the far wake are in a sense coupled through I_ϕ.

But, the model also fails in that regard. In the case of no change in wind speed or thrust, $\frac{\mathrm{d}U_{vr}}{\mathrm{d}\tau} = 0$, as there is no change in convection speed. The second and third term remain zero, but the first term also goes to zero, because of its dependency on I_ϕ through equation 4.5.

This is fixed by removing this I_ϕ from the response due to the initial steady state, but then the model does not reach momentum steady state because it is no longer coupled to the far wake term.

Using I_ϕ in the far wake is in itself problematic, as Hammam predefines the far wake location as $\zeta = 30R$. When the initial steady state vortex cylinder reaches the far wake location $\zeta - \zeta' = 0$ and therefore $\frac{\mathrm{d}I_\phi}{\mathrm{d}x}$ is large. This means that after a certain amount of time the far wake term has a huge influence on the solution. This is shown in figure 4.5a and 4.5d, where it is shown that with a far wake location of $\zeta = 10R$ the first term disappears and no solution is reached.

Apparent Mass Term The final term in equation 4.15 is the standard differential term, as also seen in other engineering models. Hammam's derivation for this term follows directly from Conway's [12] relation between vorticity and induced velocity. It shows a slower response as compared to the other engineering models, see figure 4.2a, but the rate of change is very different from all other models.

In the end, the second term in equation 4.15 does not work in its proposed form by Hammam. It is too small to have an effect, and even if amended does not add up to the replacement of the steady state.

As a result, the solution provided by Hammam's model is very different from the other models. Even though Hammam's model may appear to perform better, the results are questionable. This is both true for dynamic thrust as for dynamic wind.

4.3.3. Duhamel's Integral

Yu's model in the form of the Duhamel's integral performs better than all the other models in the case of dynamic thrust, and shows a comparable response as the FWVR model. This is expected, as Yu's model is fitted to the FWVR model.

This can be seen in the response to dynamic thrust as shown in figure 4.2. The Duhamel's integral approach shows a slower initial response and a longer overall duration to reach the new equilibrium. This is comparable to the findings from the FWVR model: two different time scales for the effect of bound circulation change and wake vorticity change.

Nevertheless, in the dynamic wind case, the Duhamel's integral behaves the same as the other engineering models. This is due to the usage of γ as a function of the instantaneous thrust coefficient:

$$\gamma(t) = U_0(t)\left(\sqrt{1 - C_t\,(t)} - 1\right) \tag{4.16}$$

As a result, $\gamma(t)$ has an instant quick response, instead of the slower adjustment of the wake. $\gamma(t)$ may in that regard replaced by the circulation at the rotor $\Gamma(t)$, which is only a function of the instantaneous thrust coefficient and wind speed.

This becomes more clear if one looks at $\frac{\mathrm{d}\gamma(t)}{\mathrm{d}t}$. The derivative of $\gamma(t)$ is zero everywhere in the case of a step change, except at $t = \tau$, when the step change happens. In the case of a step change, the Duhamel's integral is simply the response to a single excitation. And this is the same for both a change in wind speed as a change in load. Therefore the model by Yu does not distinguish between dynamic thrust and dynamic wind in its input.

A different approach could therefore be to use the velocity at the rotor at time t in the calculation of $\gamma(t)$:

$$\gamma(t) = \frac{C_t U_0^2}{2U_1} = \frac{C_t U_0^2}{2\,(U_0 - u_{ind})} \tag{4.17}$$

See figure 4.6 for the differences in response in vorticity between equation 4.16 and 4.17.

The response at the rotor then becomes a summation of excitations at the rotor due to $\mathrm{d}\gamma/\mathrm{d}t$ being non zero for a longer period of time, which is more reflective of the adjustment of the wake and its response at the rotor. The adjusting convection speed in the wake is taken into account in that regard.

However, the indicial response function as shown in equation 4.6 and its coefficients are fitted to the response due to an instantaneous change in $\Gamma(t)$. Altering the definition of the excitation force to $\Gamma(t)$ changes the indicial response function. In addition to this, the output does show two time scales: the effect of the wake is fitted to a change in bound circulation. Therefore, to model both effects a fit to a change in bound circulation and a fit to a change in wind speed may be better than a single fit to bound circulation to capture both effects.

To conclude, in order to distinguish between $\Gamma(t)$ and $\gamma(t)$ a new fit or amendment to Yu's model is necessary.

4.4. Conclusions

In this chapter three engineering models have been tested against the FWVR model in the case of a changing rotor thrust (dynamic thrust) and a changing wind speed (dynamic wind speed). The first question posed in this chapter was whether current models capture the effect of dynamic wind, or the second order effect that is present due to a changing wake.

The answer to that question is that the engineering models do not distinguish between dynamic thrust and dynamic wind, and only Øye's model attempts to model two different time scales and therefore differentiates between the response to bound circulation change and the response due to an adjusting wake. However, all engineering models lack the input parameters to model dynamic wind. On top of that, all engineering models underestimate the dynamic inflow effect in general.

The second question that was posed at the start of this chapter, is whether alternative models could produce better results. Three alternatives were proposed and again tested against dynamic thrust and dynamic wind. The vortex tube model could not produce better results in the case of dynamic wind, and was similar to ECN's engineering model. Hammam's model could not produce consistent results in either case. Yu's model was better than all other models in the case of dynamic thrust. It also produced the two time scales that are present in dynamic inflow. However it lacked the input parameters to model dynamic wind properly.

So, to conclude, only two models use two time scales in dynamic inflow. No model is able to model the effects of dynamic wind. This is caused by the fact that no model distinguishes between a change in bound circulation and change in wake vorticity strength, and if they do, the two input parameters are not linked to the two output effects.

The performance of all models is summarised in table 4.2. The input parameters Γ and γ reflect the two ways dynamic inflow could be inserted. $\Delta\Gamma$ denotes a change in bound circulation, and is commonly regarded as the cause of dynamic inflow. $\Delta\gamma$ denotes the second input that could be used. In the case of dynamic wind $\Delta\gamma$ would cause the effect, with $\Delta\Gamma$ being zero. The output of the models should reflect the two time scales of dynamic inflow: a fast response due to the bound circulation change, and a slower second order effect due to a change in wake.

Table 4.2: Input parameters defining the model and output results.

		Model Input		Model Output		
		$\frac{d\Gamma}{dt}$	$\frac{d\gamma}{dt}$	1st order	2nd order	Dynamic wind
Eng. models	BEM MT	-	-	-	-	-
	Pitt-Peters	+	-	+	-	-
	Øye	+	-	+	+/-	-
	ECN	+	-	+	-	-
Alt. models	VTM	+	+/-	+	-	-
	Hammam	+	+	+/-	-	-
	Duhamel's integral	+	-	+	+	-

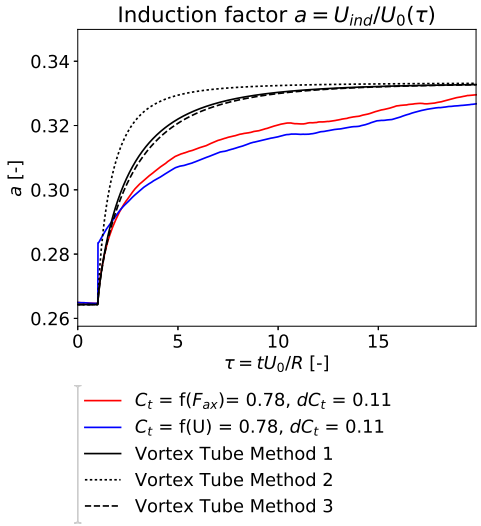

(a) Induction factor vs time, dynamic thrust case.

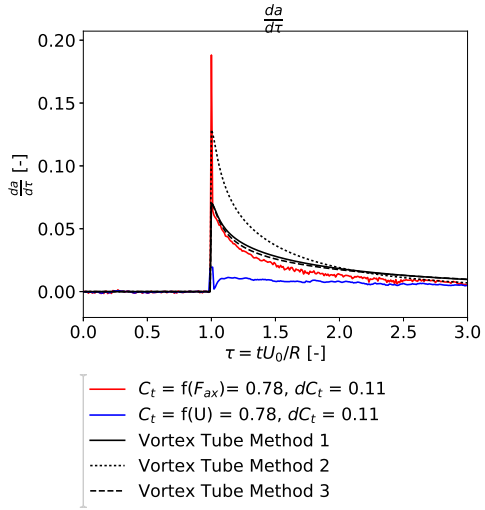

(b) Induction factor change per unit of time, dynamic thrust case.

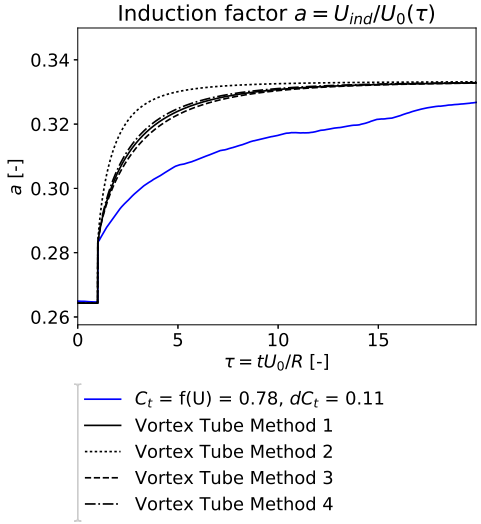

(c) Induction factor vs time, dynamic wind case.

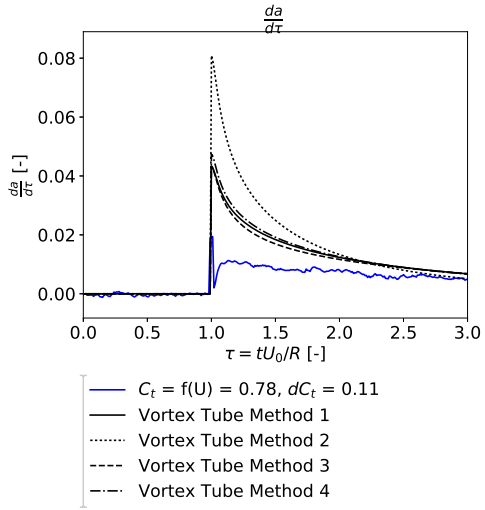

(d) Induction factor change per unit of time, dynamic wind case.

Figure 4.4: Different methods to model the wake convection speed in the VTM, dynamic thrust and dynamic wind case. $C_t = 7/9$, $\Delta C_t = 1/9$.

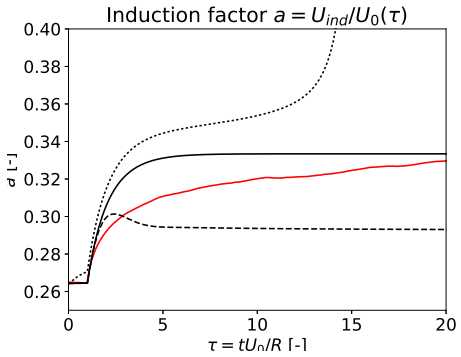

(a) Induction factor a vs τ for different implementations of Hammam's model.

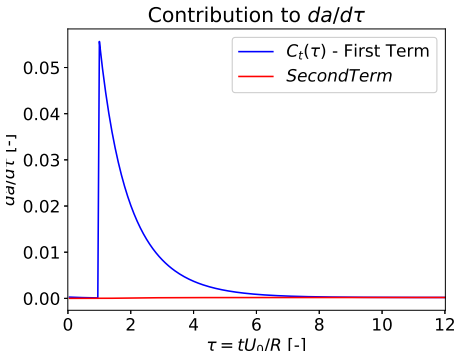

(b) Contributions of the first and second term to the rate of change of induced velocity, Hammam's model $\gamma = 2\Delta u_{ind}$.

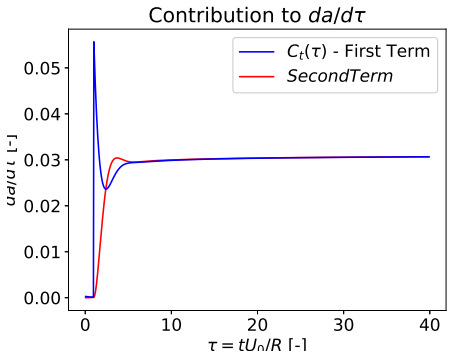

(c) Contributions of the first and second term to the rate of change of induced velocity, Hammam's model $\gamma = 2u_{ind}$.

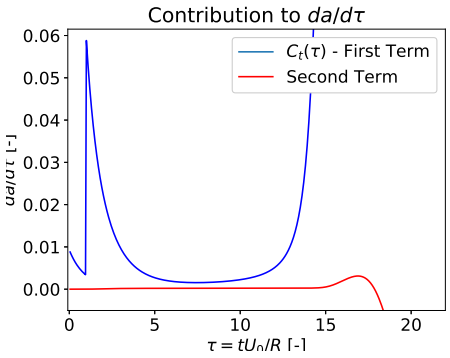

(d) Contributions of the first and second term to the rate of change of induced velocity, Hammam's model with far wake location $\zeta = 10R$.

Figure 4.5: Comparison of different implementations of Hammam's model. $C_t = 7/9$, $\Delta C_t = 1/9$.

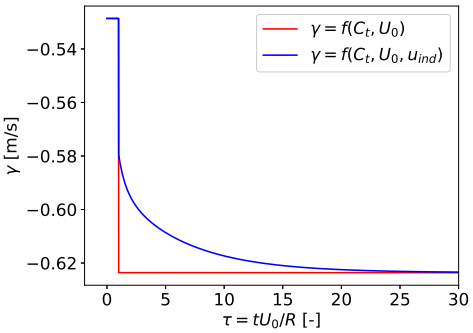

Figure 4.6: Different expressions of the vorticity distribution $\gamma(t)$ at the rotor in the dynamic wind case for $C_t = 7/9$ and $\Delta C_t = 1/9$.

5

Duhamel's Integral Extension

In the previous chapter it was established that the engineering models are unable to model the response to dynamic wind. On top of that, the models generally underestimate the effect of dynamic inflow, and Yu's model is an improvement over the other models. Therefore it will be attempted to extend Yu's model such that it also incorporates a varying wind speed. First three different options will be discussed, after this one method will be investigated further.

5.1. Extension Options

Wei Yu's model could be extended or amended in three ways. The first two options could in theory represent the effects of changing Γ and γ better, while the third option is the most straightforward and pragmatic approach:

1. Split Duhamel's Integral The first way would perhaps be the most straightforward. In this case the induced velocity response is defined as a response to two indicial response functions:

$$u_{ind}(r,t) = \gamma(0)\Phi_d(r,t) + \int_0^t \frac{1}{U_0}\frac{\mathrm{d}\Gamma}{\mathrm{d}\sigma}\Phi_{d,1}(r,t-\sigma)\mathrm{d}\sigma + \int_0^t \frac{\mathrm{d}\gamma}{\mathrm{d}\sigma}\Phi_{d,2}(r,t-\sigma)\mathrm{d}\sigma \tag{5.1}$$

And the response function $\Phi_d(r,t)$ is split into two as well:

$$\Phi_{d,1}(r,t) = 1 - e^{\omega_1 t} \tag{5.2}$$

$$\Phi_{d,1}(r,t) = 1 - e^{\omega_2 t} \tag{5.3}$$

The first integral is the response due to a change in thrust, and thus a change in shed vorticity strength. The second integral is the response due to a change in vorticity density. This could either be the second order effect due to thrust change or the sole effect due to a wind speed change. The advantage here is that it can easily be fitted to a dynamic wind response, and the remainder can be fitted to dynamic thrust. Also, it does not require the coefficient β determining which part is dominant.

The caveat here is the requirement that dynamic thrust is indeed a summation of the first and second order effect, and that the two responses can be modelled independently. If that is the case, this method links the two frequencies ω_1 and ω_2 to the physical effects. Furthermore, all coefficients need to be refitted, though β may possibly be discarded.

It could also be expected that the second frequency ω_2, as fitted by Wei Yu, is already a fit to the second order effect. This is not the case however. Which casts doubt on the notion that the two frequencies can model the two effects separately, or that dynamic thrust may be regarded as a summation of the two effects.

2. Change γ The second method would be to simply change the definition of γ into:

$$\gamma(t) = \frac{C_t U_0^2}{2U_1 \Delta t} = \frac{C_t U_0^2}{2\left(U_0 - u_{ind}\right)\Delta t} \tag{5.4}$$

That way the second order effect of the changing vorticity density due to the changing thrust coefficient is instantly implied. The resulting change in γ over time can be seen in figure 4.6. It was also found that this gives a rather good fit to the dynamic wind case already with the same coefficients as in the dynamic thrust case by Wei Yu. The induced velocity response is a summation of smaller changes in γ instead.

However, the fit with dynamic thrust is lost in this case, which means that describing the general case of a thrust and wind change may be impossible. Moreover, dynamic wind may require more tweaking of the coefficients and finding a good fit could prove to be difficult as the relation between u_{ind} and γ is now a differential relation. This makes it hard to extract the forcing function from the FWVR response.

3. Add additional frequencies ω_3, ω_4 The third method could be to extend the response function Φ_d to include a third and fourth coefficient for the dynamic wind case:

$$\Phi_d(r,t) = \left(1 - \beta_1 e^{\omega^1 t} - (1-\beta_1)\, e^{\omega^2 t}\right) f(\Delta F_{ax}) + \left(1 - \beta_2 e^{\omega^3 t} - (1-\beta_2)\, e^{\omega^4 t}\right) f(\Delta U_0) \tag{5.5}$$

This could also be seen as two different Duhamel's integral responses:

$$u_{ind}(r,t) = 0.5\gamma(0) + (1-\kappa) \underbrace{\int_0^t \frac{\mathrm{d}\gamma}{\mathrm{d}\sigma} \Phi_{d,1}(r, t-\sigma)\mathrm{d}\sigma}_{\text{Fit to dynamic thrust}} + \kappa \underbrace{\int_0^t \frac{\mathrm{d}\gamma}{\mathrm{d}\sigma} \Phi_{d,2}(r, t-\sigma)\mathrm{d}\sigma}_{\text{Fit do dynamic wind}} \tag{5.6}$$

And κ would define which fit is the most relevant one:

$$\kappa = \frac{C_t}{\Delta C_t}\left(\left(\frac{U_0}{U_0 + \Delta U_0}\right)^2 - 1\right) \tag{5.7}$$

Which becomes 0 if $\Delta U_0 = 0$.

The advantage is that only a fit to the two additional frequencies is required, and that the dynamic thrust case does not require a refit. The question is how this would perform in the combination case of dynamic wind and dynamic thrust.

This third method is selected for the extension. In the next section a fit will be made to β_2, ω_3 and ω_4.

5.2. Fit to Exponential Coefficients

Analogous to the fit made by Yu, the following response function is defined which can be fitted to the FWVR response to dynamic wind:

$$\Phi_{d,2}(r,t) = \left(1 - \beta_2 e^{\omega^3 t} - (1-\beta_2)\, e^{\omega^4 t}\right) \tag{5.8}$$

A range of thrust coefficients is used to make the fit: $C_t = 0.1, 0.2 \ldots 0.8$, both for a load increase (LI) as a load decrease (LD): $\Delta C_t = \pm 0.1$. The results of the fit at different radial locations for $C_t = 0.4$ are shown in figure 5.1.

As can be seen in figure 5.1, a decrease or increase makes a difference, and the response is different for different radial positions. Therefore the exponential coefficients β, ω^3 and ω^4 are made dependent on r/R through the following third order polynomial fits:

$$\beta_2(r) = \frac{1}{a_3 r^3 + a_2 r^2 + a_1 r^1 + a_0 r^0} \tag{5.9}$$

$$\omega^3(r) = a_3 r^3 + a_2 r^2 + a_1 r^1 + a_0 r^0 \tag{5.10}$$

$$\omega^4(r) = \frac{1}{a_3 r^3 + a_2 r^2 + a_1 r^1 + a_0 r^0} \tag{5.11}$$

The polynomial fits to the 3 coefficients are shown in figure 5.2. In general the radial dependency can be fitted well through the polynomial. However, there are two areas where the fit is off. The first note is the bad fit at the tip. After $r/R > 0.95$ the frequencies tend to go to zero or to infinity. This was also observed in the dynamic thrust case in the fit made by Yu. The tip experiences different timescales and

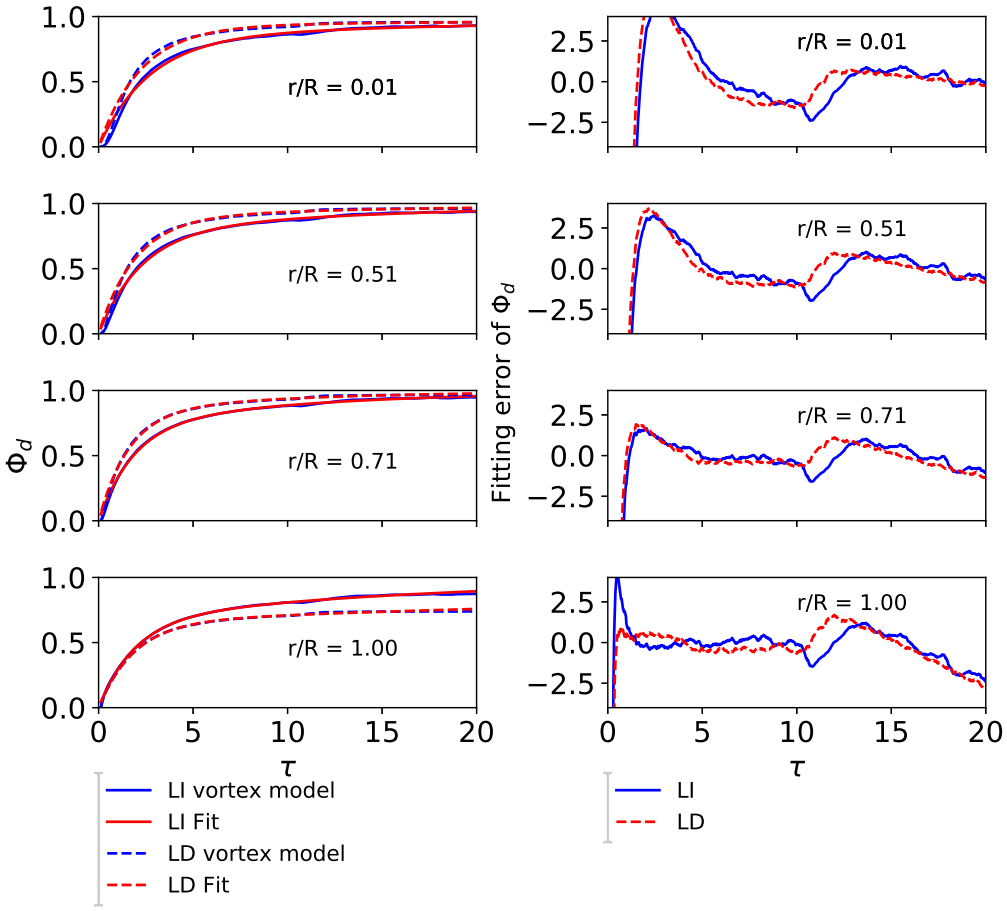

Figure 5.1: Response function from the FWVR and the fitted response for different radial positions. $C_t = 0.4$. Load increase (LI): $\Delta C_t = 0.1$. Load decrease (LD): $\Delta C_t = -0.1$.

different lagging effects as compared to the rest of the blade. The second note is that at lower thrust coefficients ω^3 is not easily captured in the polynomial. The fit may slightly be off in that area, although the effect is likely small.

In addition to this, an interesting observation could be made on the differences in β_2 in the load increase and load decrease cases. A load decrease is surprisingly different from a load increase, especially at larger thrust coefficients. An explanation may be in the way the new and the old wake interact. In a load decrease the new wake catches up to the old wake, while in a load increase the old wake travels faster than the new wake. This may result in different 'damping' effects on the rotor, and therefore different timescales. This difference is less profound in the dynamic thrust case, and it therefore tells us something about the wake. However, this also means that in general the fit may be less good for large thrust coefficients, since the coefficients are averaged across load increase and load decrease.

The next step is to link the polynomial coefficients a_3 to a_0 to the steady thrust coefficient, such that the response is a function of both radius and thrust coefficient. Luckily, the coefficients a_{0-3} can quite easily be fitted as a function of thrust coefficient, as shown in figure 5.3. Especially the fits for β_2 and ω^3 are good, while ω^4 has a slightly less linear relation with C_t.

The functions for the polynomial coefficients are summarised in table 5.1. β_2 is a quadratic function of C_t, while ω^3 and ω^4 are linearly approximated. With these functions the response to a change in C_t due to a changing wind speed are now fitted and defined in a similar way as the Duhamel's integral model to dynamic thrust. The next chapter will show the performance of this fit and verify the accuracy of the response.

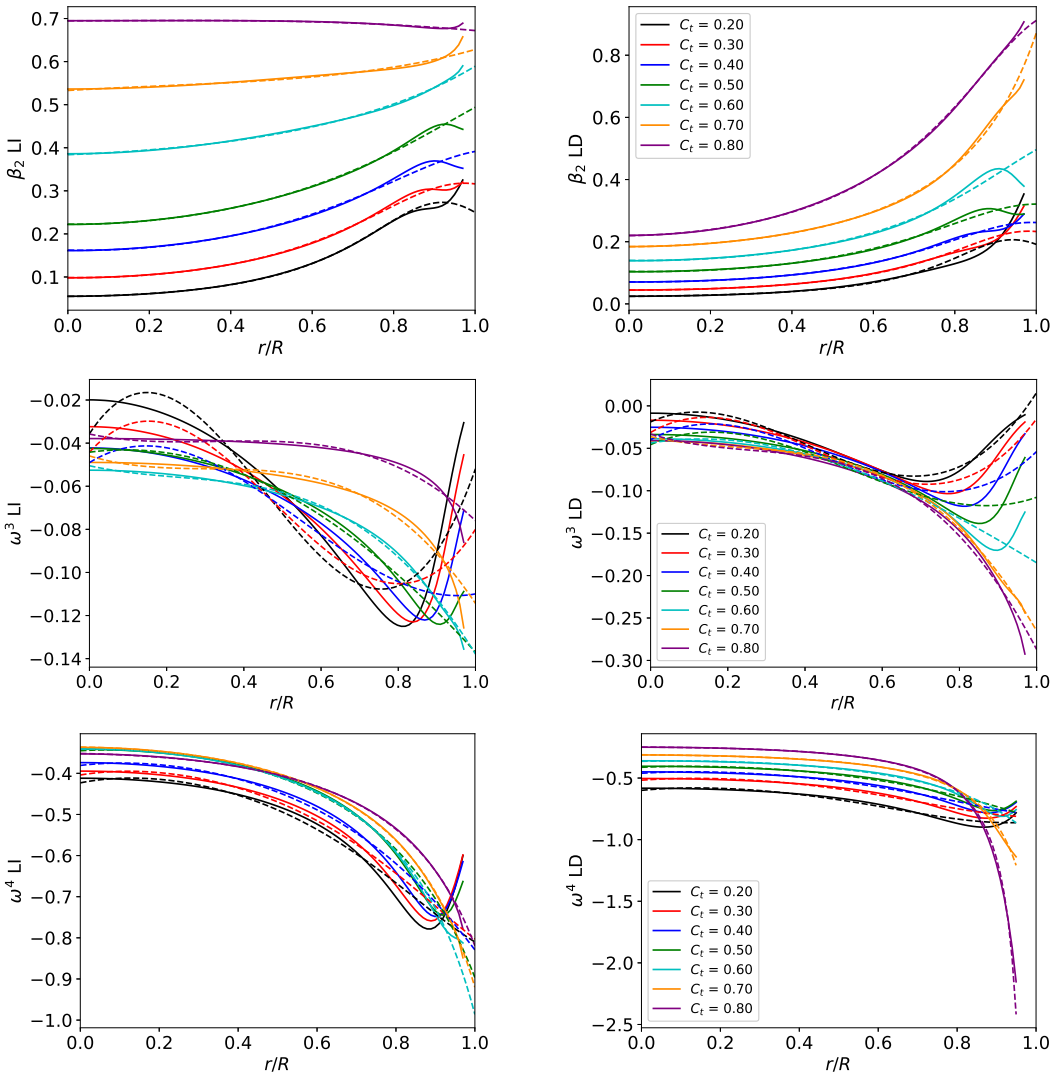

Figure 5.2: Exponential coefficients β_2, ω^3 and ω^4 (solid line) and the polynomial fit (dashed line) as function of r/R for different levels of C_t, load increase (LI) and load decrease (LD).

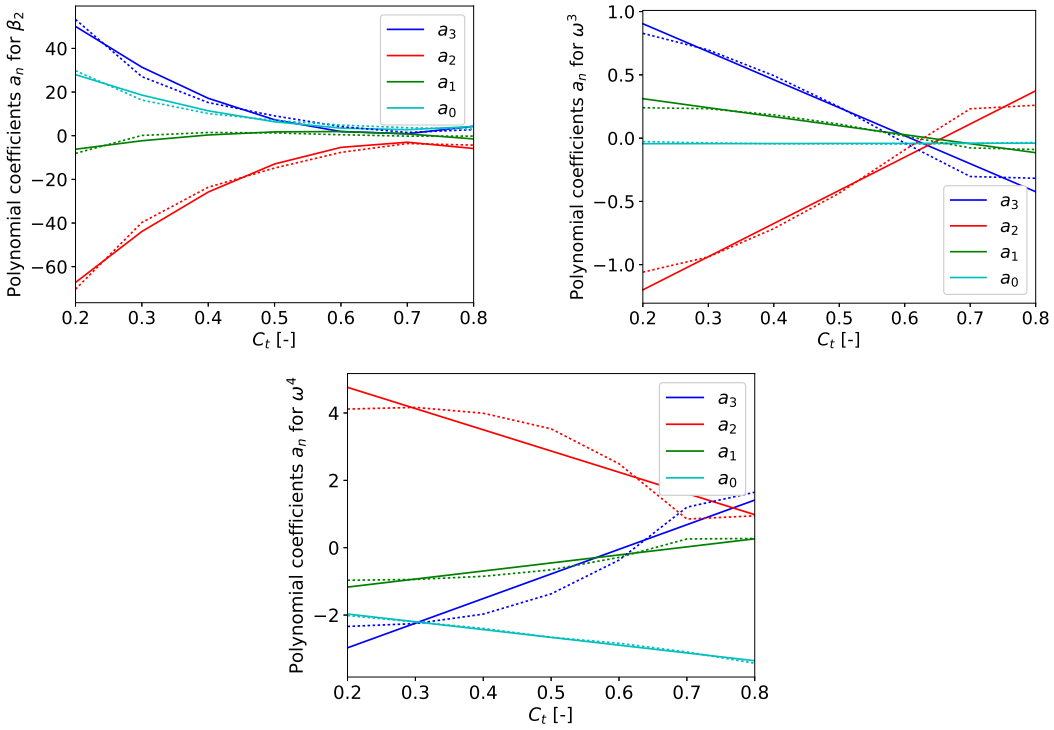

Figure 5.3: Polynomial coefficients a_3 to a_0 (dashed line) and the fit as function of C_t (solid line) versus C_t.

Table 5.1: Polynomial parameters of the exponential coefficients β_2, ω^3 and ω^4 for the dynamic wind case, based on a free wake vortex ring method.

	β_2	ω^3	ω^4
a_3	$221C_t^2 - 297C_t - 101$	$-2.21C_t + 1.35$	$7.31C_t - 4.43$
a_2	$-262C_t^2 + 364C_t - 130$	$2.62C_t - 1.72$	$-6.30C_t + 6.02$
a_1	$-62.1C_t^2 + 70.0C_t - 17.7$	$-0.71C_t + 0.45$	$2.39C_t - 1.65$
a_0	$108C_t^2 - 147.7C_t + 53.2$	$0.01C_t - 0.05$	$-2.31C_t - 1.51$

6

Verification

The new coefficients to the Duhamel's integral model will be tested in the dynamic wind case in section 6.1 and against a combination of dynamic wind and dynamic thrust in section 6.2. Both a step changes and harmonic changes will be shown, to see whether the new coefficients predict a correct response to change, and whether the phase difference and amplitude are correct.

6.1. Dynamic Wind Case

Two step changes are shown in figures 6.1 and 6.2 for a baseline thrust coefficient of $C_t = 0.2$ and $C_t = 0.8$ respectively. Both the induced velocity and the rate of change of induction factor are shown. From these figures it can be concluded that the new coefficients used in the Duhamel's integral model are an improvement over the old coefficients. The slow response of dynamic wind is now correctly modelled. In the previous chapter the fitted coefficients were shown, and it appeared that the fit was not as good at lower thrust coefficients. From these figures the opposite appears to be true, since at $C_t = 0.8$ the response is underestimated slightly, although the initial rate of change is correct.

In addition to this a harmonic variation of $k = 1$ at $C_t = 4/9$ and $\Delta C_t = 1/9$ is shown in figures 6.3 and 6.4. Here it is shown that the amplitude and rate of change of the induced velocity is correctly modelled. And because of this a correct phase difference between $C_t(\tau)$ and induced velocity is shown in figure 6.4. Overall it can be concluded that the new coefficients are an improvement over the old Duhamel's integral model coefficients in the case of dynamic wind.

Note in this case that the Duhamel's integral does not correctly predict the mean induced velocity value in the harmonic variation. This can be explained by the fact that γ is only a function of C_t and U_0. In case of a variation these values are (relatively) symmetrical (U_0 slightly less so though). However, the actual average γ in the wake is also a function of U_{ind}, and this non-linearity is the cause of the slight upward translation of the Duhamel's integral models in figure 6.3.

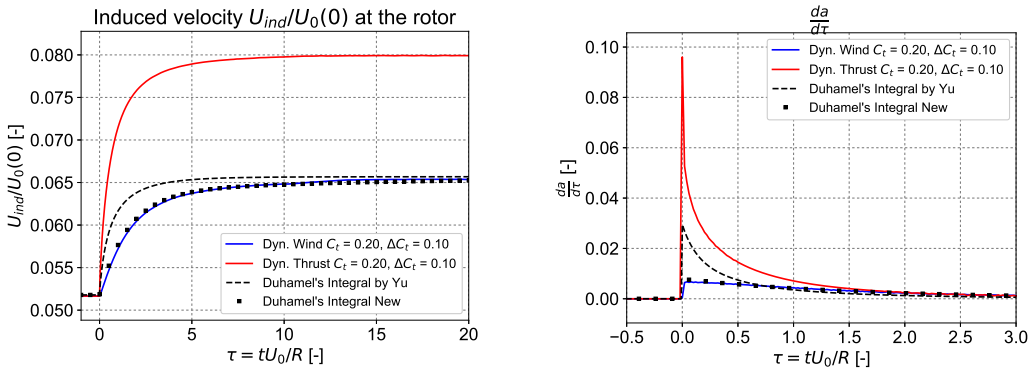

(a) Induced velocity U_{ind} vs τ.

(b) Change in induction factor per unit of time.

Figure 6.1: Results of FWVR versus Duhamel's integral models, with different coefficients. $C_t = 0.2$, $\Delta C_t = 0.1$.

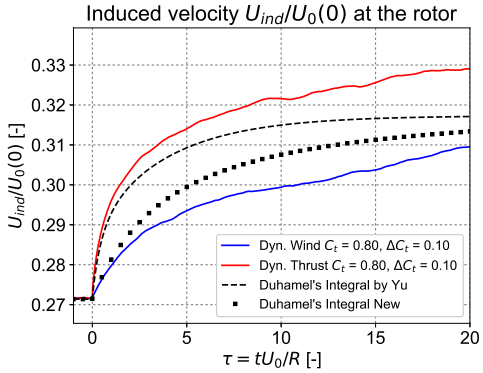

(a) Induced velocity U_{ind} vs τ.

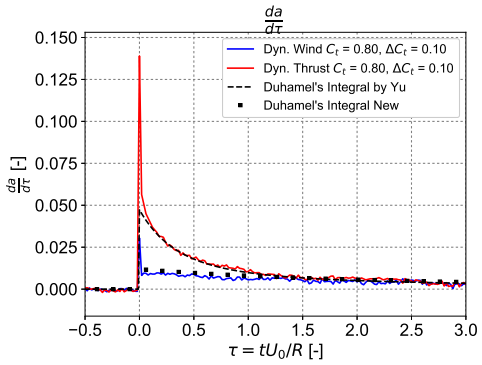

(b) Change in induction factor per unit of time.

Figure 6.2: Results of FWVR versus Duhamel's integral models, with different coefficients. $C_t = 0.8$, $\Delta C_t = 0.1$.

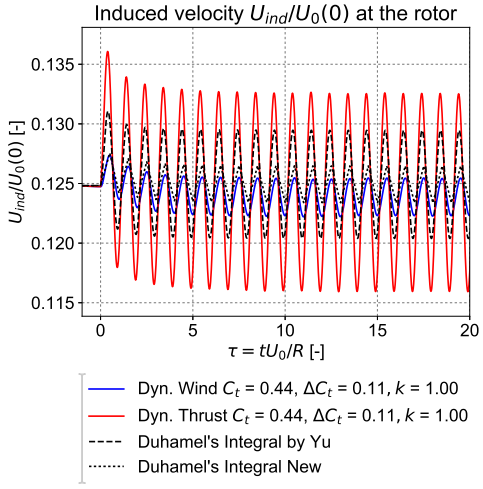

(a) Induced velocity U_{ind} vs τ.

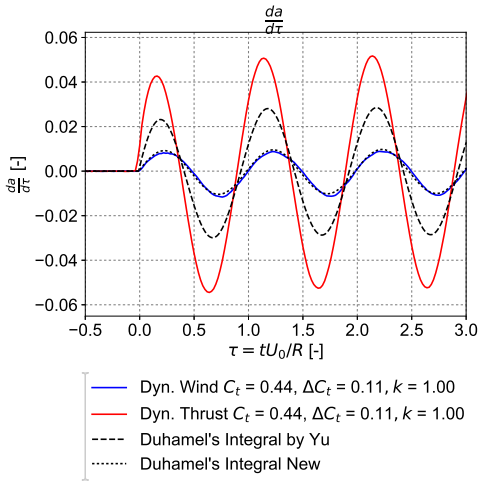

(b) Change in induction factor per unit of time.

Figure 6.3: Results of FWVR versus Duhamel's integral models, with different coefficients. $C_t = 4/9$, $\Delta C_t = 1/9$, $k = 1$.

6.2. Combination Dynamic Wind and Thrust

Next to a single dynamic wind change it is also interesting to see the performance of a combined dynamic wind and dynamic thrust excitation. In that case both the exponential coefficients by Yu and the new coefficients are used in tandem.

Dynamic wind and thrust are combined such that the change in wind speed is responsible for a portion of ΔC_t, and the other portion is due to a change in thrust. The response to this combined excitation is modelled in the FWVR model, and through the Duhamel's integral model. Both the response function $\Phi_{d,1}$ to thrust, and the response function $\Phi_{d,2}$ to wind both cover the relevant portion of the response. This was estimated in the previous chapter through κ in equation 5.6.

The results are shown in figures 6.5, 6.6 for $C_t = 0.2$ and $C_t = 0.8$ respectively where the combination of the two effects is 50/50. Figures 6.7 and 6.8 show a combination of the two effects where the change in thrust coefficient is 80% the result of a change in wind speed for $C_t = 0.2$ and $C_t = 0.8$. Two things can be noted from these figures. First of all it can be concluded that the combination of the two coefficients works well, and can be used to predict the response to a mixed input. Second of all, it becomes clear that in the case of a mixed input, the dynamic thrust effect is dominant. Even if only 20% of the response is due to a change in thrust coefficient, the exponentially decaying quick response is still present and very similar to the dynamic thrust case. Hence in the combined case Yu's model with a single response function may already give good results, and an additional response function is not really necessary.

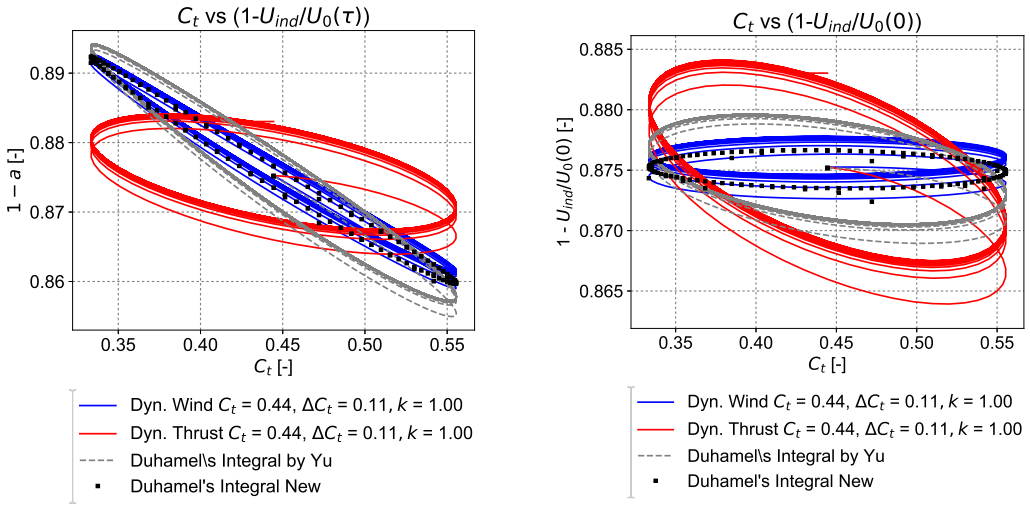

(a) C_t vs $u_z/U_{0,t}$

(b) C_t vs $u_z/U_{0,0}$

Figure 6.4: Results of FWVR versus Duhamel's integral models, with different coefficients. $C_t = 4/9$, $\Delta C_t = 1/9$, $k = 1$.

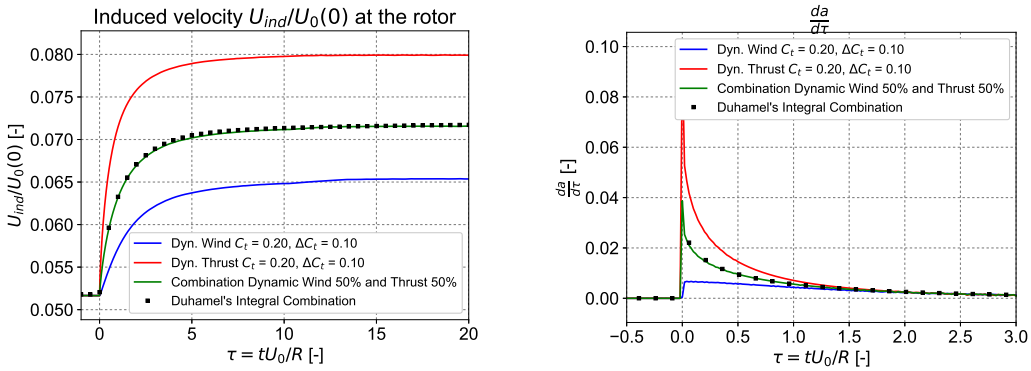

(a) Induced velocity U_{ind} vs τ.

(b) Change in induction factor per unit of time.

Figure 6.5: Results of FWVR versus Duhamel's integral models, with different coefficients. $C_t = 0.2$, $\Delta C_t = 0.1$.

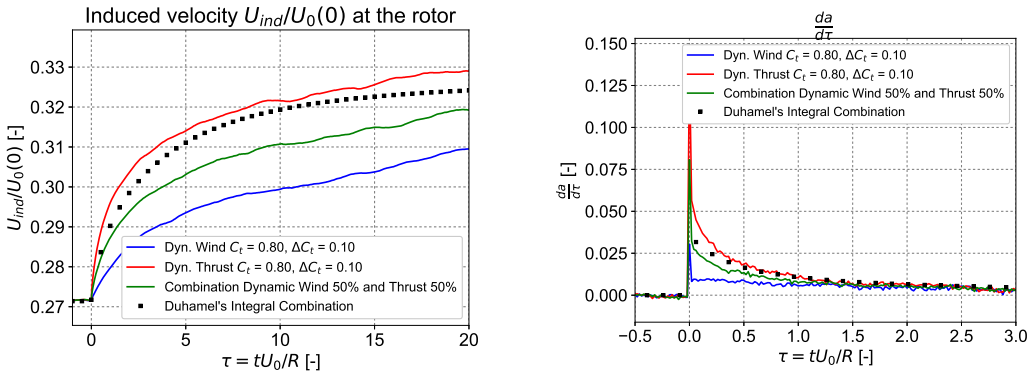

(a) Induced velocity U_{ind} vs τ.

(b) Change in induction factor per unit of time.

Figure 6.6: Results of FWVR versus Duhamel's integral models, combination of two models. $C_t = 0.8$, $\Delta C_t = f(0.5F_{ax}, 0.5U_0) = 0.1$.

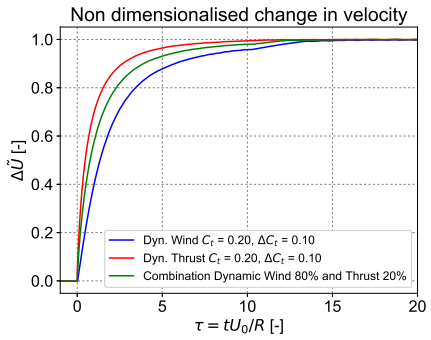

(a) Non dimensionalised change in induced velocity U_{ind} vs τ.

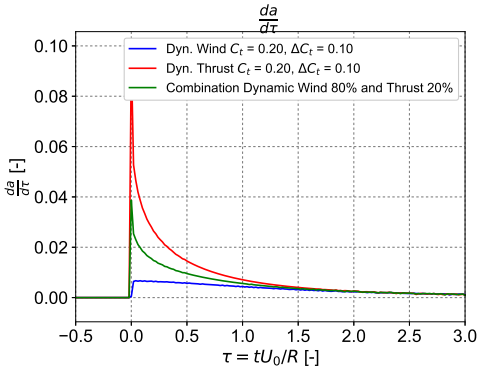

(b) Change in induction factor per unit of time.

Figure 6.7: Results of FWVR versus Duhamel's integral models, with different coefficients. $C_t = 0.2$, $\Delta C_t = 0.1$. Green line and Duhamel's Integral express a combination of dynamic wind (80%) and dynamic thrust (20%).

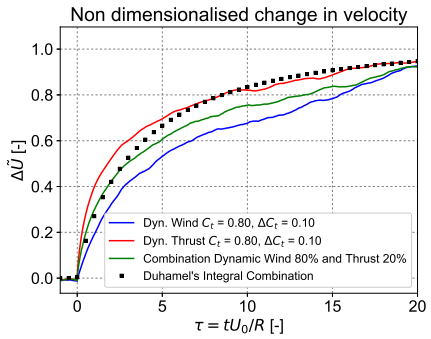

(a) Non dimensionalised change in induced velocity U_{ind} vs τ.

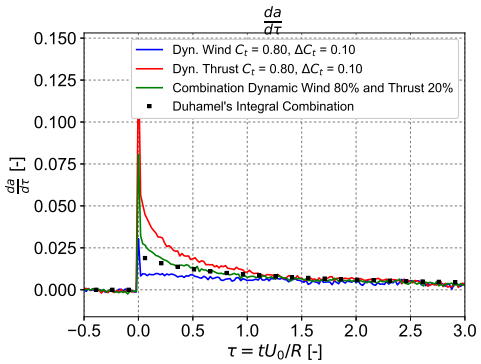

(b) Change in induction factor per unit of time.

Figure 6.8: Results of FWVR versus Duhamel's integral models, with different coefficients. $C_t = 0.8$, $\Delta C_t = 0.1$. Green line and Duhamel's Integral express a combination of dynamic wind (80%) and dynamic thrust (20%).

6.3. Amplitude and Phase Delay Evaluation

In this section the performance of the Duhamel's integral models will be shown through the induced velocity amplitude and phase delay response to a harmonically varying wind and/or thrust. Ten cases have been established, which are shown in tables 6.1 and 6.2. The cases considered are two different thrust coefficients: $C_t = 4/9, 7/9$, two different reduced frequencies: $k = 0.2, 1$, and 4 different levels of dynamic wind versus thrust. The response to a combination of dynamically changing wind and thrust is shown for 80% and 50% dynamic wind.

The phase delay is compared to the momentum theory, and the amplitude is normalised with respect to the difference in momentum theory. Figure 6.9 shows the definition of the velocity amplitude A. C is defined as the amplitude when C_t is the steady value (zero crossing height). The figures in 6.4 show this loop for the dynamic wind case $C_t = 4/9$ and $k = 1$. The phase delay is defined as follows:

$$\Delta\theta = -\left(180\,\mathrm{deg} - \arcsin\left(C/A\right)\right) + 180\,\mathrm{deg} \tag{6.1}$$

$180\,\mathrm{deg}$ is added because that is the momentum theory value. $\Delta\theta$ is thus the difference between momentum theory and the dynamic response.

From the phase delay values shown in table 6.1 it is not immediately clear that the Duhamel's integral models are an improvement over the old engineering models. This can be explained by the large effect the initial few seconds have on the phase delay. These initial seconds are dominant in the phase delay, but it is also where the largest fitting error is, as shown in figures 5.1. However, as shown by Yu in [79], the Duhamel's integral method does behave correctly as a function of radius, contrary to the engineering models. The fact that the old engineering models sometimes provide a good phase delay prediction is not necessarily because they are better at modelling the response.

This can also be seen by the (normalised) amplitude, as shown in table 6.2. In this case the Duhamel's integral methods are a clear improvement over the other engineering models. Here it is also immediately clear that the new coefficients are better at predicting the dynamic wind case, and that all the other models (PP / Øye / ECN / Yu's coefficients) are unable to distinguish between dynamic wind and dynamic thrust.

Table 6.1: Comparison of phase delay in degrees [deg] for different models for different frequencies and thrust coefficient. Dynamic Wind, Dynamic Thrust and a combination of both is shown. In bold the best performing model for each case as compared to the FWVR.

Case			FWVR	PP	Øye	ECN	DI Yu	DI New
Dynamic Wind or Thrust Case	C_t [-]	k [-]						
Wind: ΔU_0	$7/9$	0.2	68.1	33.6	37.5	40.7	42.3	**70.4**
Thrust: ΔF_{ax}	$7/9$	0.2	41.9	33.9	37.9	**41.6**	42.5	-
Wind: ΔU_0	$7/9$	1	59.9	47.3	48.0	42.6	**61.1**	72.6
Combination: 80% ΔU_0 / 20% ΔF_{ax}	$7/9$	1	49.7	47.7	**48.3**	43.2	67.8	69.7
Combination: 50% ΔU_0 / 50% ΔF_{ax}	$7/9$	1	47.7	**48.5**	48.9	44.3	67.9	67.7
Thrust: ΔF_{ax}	$7/9$	1	53.4	50.2	**50.7**	46.9	61.3	-
Wind: ΔU_0	$4/9$	1	77.2	46.3	45.3	41.9	64.2	**82.0**
Combination: 80% ΔU_0 / 20% ΔF_{ax}	$4/9$	1	67.8	46.7	45.8	42.5	64.2	**73.4**
Combination: 50% ΔU_0 / 50% ΔF_{ax}	$4/9$	1	58.5	47.5	47.1	43.7	**64.2**	67.6
Thrust: ΔF_{ax}	$4/9$	1	53.5	49.1	**50.0**	46.5	64.2	-

6.4. Conclusions

In this chapter the new coefficients for the Duhamel's integral models have been tested against the dynamic wind cases. It was shown that the dynamic wind case is correctly modelled by the extension to the model. In addition to this, the combination of the fit to dynamic thrust by Yu and the new fit to dynamic wind is tested against a combined variation of dynamic wind and dynamic thrust. Although the improvement in this combined case is not as large, it was shown that a combination works just as well as either Duhamel's integral individually.

Table 6.2: Comparison of normalised velocity amplitude for different models. Dynamic Wind, Dynamic Thrust and a combination of both is shown. In bold the best performing model for each case as compared to the FWVR.

Case			FWVR	PP	Øye	ECN	DI Yu	DI New
Dynamic Wind or Thrust Case	$C_t[-]$	$k[-]$						
Wind: ΔU_0	$7/9$	0.2	0.21	0.78	0.62	0.58	0.41	**0.20**
Thrust: ΔF_{ax}	$7/9$	0.2	0.39	0.78	0.62	0.58	**0.41**	-
Wind: ΔU_0	$7/9$	1	0.06	0.34	0.26	0.24	0.15	**0.04**
Combination: 80% ΔU_0 / 20% ΔF_{ax}	$7/9$	1	0.08	0.33	0.26	0.24	0.15	**0.07**
Combination: 50% ΔU_0 / 50% ΔF_{ax}	$7/9$	1	0.12	0.34	0.26	0.24	0.15	**0.10**
Thrust: ΔF_{ax}	$7/9$	1	0.15	0.33	0.25	0.23	**0.15**	-
Wind: ΔU_0	$4/9$	1	0.08	0.48	0.33	0.34	0.21	**0.07**
Combination: 80% ΔU_0 / 20% ΔF_{ax}	$4/9$	1	0.12	0.48	0.33	0.34	0.21	**0.10**
Combination: 50% ΔU_0 / 50% ΔF_{ax}	$4/9$	1	0.17	0.47	0.32	0.33	0.21	**0.14**
Thrust: ΔF_{ax}	$4/9$	1	0.22	0.46	0.31	0.32	**0.21**	-

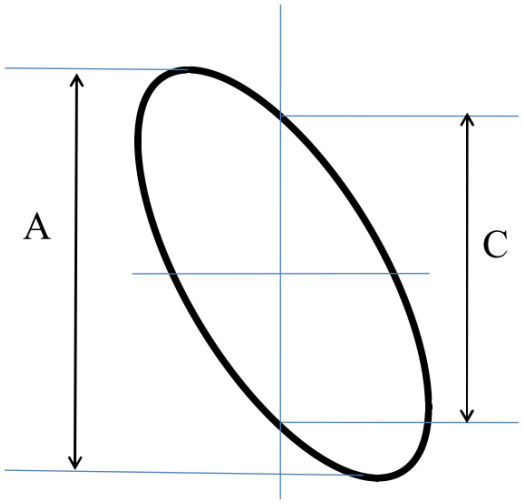

Figure 6.9: Lissajous hysteresis loop.

7

Conclusions

In the previous chapters the two main drivers of unsteady effects on the rotor level have been investigated. These unsteady effects are called dynamic inflow, and its two drivers are dynamic thrust and dynamic wind speed. The aim in this thesis was to distinguish between these two drivers, and by doing this find out how the transient induced velocity response should be modelled in blade element-momentum theory in general.

Three objectives were identified at the start of this work:

1. Investigate the effect of dynamic wind as compared to dynamic loading by modelling it in a FWVR model, and by comparing it to dynamic thrust.

2. Verify and evaluate current and alternative engineering models in the dynamic wind case by comparing it against the FWVR model.

3. Include dynamic wind in an engineering model by extending the Duhamel's integral model by Yu.

The conclusions are also summarised along these three objectives, and will be discussed in the following three sections.

7.1. Hypothesis

The first of these objectives was the investigation into dynamic wind and its effects. This also corresponded to the main hypothesis:

> *The effect of dynamic wind speed on the actuator disc and the wake is different from the effect of dynamic thrust, and it therefore needs to be included in current engineering models.*

That dynamic wind results in dynamic inflow effects is contrary to what has generally been assumed in literature. However, the hypothesis was found to be true. Dynamic wind does result in a transient response and the effect of dynamic wind is different from dynamic thrust. The response to dynamic wind is slower and a more gradual change, as compared to an exponential decay of dynamic thrust. And this slower change also means a larger phase difference between C_t and induced velocity, and a different amplitude of the induced velocity response.

The comparison between dynamic wind and dynamic thrust furthermore showed that dynamic inflow in general may be regarded as a summation of two effects. This is because both cases converged to the same asymptote in the rate of change. Therefore, dynamic thrust can be regarded as a first order quick response due to the downwind convection of changing shed vorticity, and the effect of the wake itself on the induced velocity, (the 'circulatory' effect). The wake adapts to the shedding of new vorticity, which causes a second order slow effect. By only adjusting the convection speed in the wake this second order effect could be distilled from the dynamic inflow general case.

7.2. Performance Engineering Models

And because a changing wind speed was found to result in a different transient response, the second objective was to find out to what extent current engineering models were able to capture the difference between the two effects. And if alternative models existed that could model this difference.

The current engineering models by Øye, Pitt-Peters and ECN were investigated and compared against the FWVR results, and it was found that neither could model the slow change of the wake in the dynamic wind case. All engineering models translated the known quick response of dynamic thrust to the dynamic wind case, resulting in an underestimation of the dynamic inflow effects. Furthermore, only Øye's model correctly modelled the general dynamic inflow effects as having two different timescales, although the values for the time constants were off. So it can be concluded that current engineering models were unable to model the effects of dynamic wind.

Moreover, these current engineering models also underestimated the dynamic inflow effects in the dynamic thrust case. The three models predicted a faster response than the FWVR model, which was also found in literature. To improve the prediction in the dynamic thrust case, Yu recently proposed a different model based on the Duhamel's integral. Here it was found that the model gave good results in the dynamic thrust cases.

Nevertheless, this proposed model by Yu was fitted to the dynamic thrust response, hence it was also unable to predict the dynamic wind response. Two other engineering models were also investigated, a fixed wake vortex model (vortex tube model), and an integro-differential model by Hammam. The vortex tube model offered little improvement (and in fact already exists in ECN's model. Hammam's model was unable to provide consistent results.

So although Yu's model improved the modelling of dynamic thrust, none of the engineering models was able to capture the transient response to dynamic wind as seen in the FWVR model. The performance of all models is summarised in table 7.1. The ideal model distinguishes between a thrust change (through circulation Γ) and a wake convection change (through vorticity γ) and has two timescales as output.

Table 7.1: Input parameters defining the model and output results.

		Model Input		Model Output		
		$\frac{d\Gamma}{dt}$	$\frac{d\gamma}{dt}$	1st order	2nd order	Dynamic wind
Eng. models	BEM MT	-	-	-	-	-
	Pitt-Peters	+	-	+	-	-
	Øye	+	-	+	+/-	-
	ECN	+	-	+	-	-
Alt. models	VTM	+	+/-	+	-	-
	Hammam	+	+	+/-	-	-
	Duhamel's integral	+	-	+	+	-

7.3. Extension to Yu's Model

The final and third objective in this thesis was therefore to extend Yu's model to incorporate the dynamic wind case. This was done in an analogous way as the dynamic thrust model. Dynamic wind speed could be fitted to be function of radius and thrust coefficient. The total general model would then be a combination of Yu's model and additionally a similar model with different coefficients. The predicted response to dynamic wind speed was found to be good, and found to be an improvement over Yu's model in the dynamic wind case. The new fitted coefficients were also tested in a combination of dynamic thrust and wind, and the modelled response would also be a combination of the two models. The predicted response to a mixed input was good, although the question could be to what extent dynamic wind plays a role if it is combined to dynamic thrust.

An interesting note about the effects of dynamic wind speed also came up when the fitted coefficients

were found. An increase or decrease in C_t matters in the case of dynamic wind. The response is slightly different, which may be explained by the influence of wake convection speed of the new wake.

To summarise the conclusions: dynamic wind speed is fundamentally different from dynamic thrust and current engineering models are unable to capture that difference. The model by Yu was extended such that this difference could be modelled.

7.4. Recommendations

In the free wake vortex ring model a clear difference between dynamic thrust and dynamic wind speed could be observed. Three notes for furter research can be made here:

- In the dynamic wind case it is assumed that the thrust remains constant. In reality the thrust will change with changing wind speed as well, and they can not be viewed independently. As a result it may be expected that a changing wind speed will also result in a thrust change, and may therefore result in a similar response as simply changing the thrust force directly. So the remaining question here is whether the effect can also be observed independently in reality. And following from this, whether the same scale of the effect is present in reality.
- Dynamic wind speed has been modelled as a wave-front moving through the wake. Although a sudden uniform change throughout the domain does not resemble reality, the conclusions posed here rely on the wave-front assumption. A different representation of a wind speed change will have pro-found effects on the way the wake behaves. This gust wave-front therefore requires further verification.
- The results in the FWVR model on dynamic wind suggest that dynamic inflow in general could be modelled as a function of circulation change and vorticity change. This means that a simplified model could be made on this basis, or adapted into the Duhamel's integral approach. This approach could be more general and more elegant than the current extension, which is the resultant fit of 6 coefficients.

Bibliography

[1] S. Aubrun, S. Loyer, P.E. Hancock, and P. Hayden. Wind turbine wake properties: Comparison between a non-rotating simplified wind turbine model and a rotating model. *Journal of Wind Engineering and Industrial Aerodynamics*, 120:1–8, 2013. ISSN 01676105. doi: 10.1016/j.jweia.2013.06.007. URL http://ac.els-cdn.com/S0167610513001220/1-s2.0-S0167610513001220-main.pdf?{_}tid=3b45581c-96db-11e7-9834-00000aacb361{&}acdnat=1505125581{_}f5f2da8fd3d11e5b5fa706d919d9d727.

[2] C.J. Bai and W.C. Wang. Review of computational and experimental approaches to analysis of aerodynamic performance in horizontal-axis wind turbines (HAWTs). *Renewable and Sustainable Energy Reviews*, 63:506–519, 2016. ISSN 18790690. doi: 10.1016/j.rser.2016.05.078. URL https://ac.els-cdn.com/S1364032116301903/1-s2.0-S1364032116301903-main.pdf?{_}tid=142e36c2-a298-11e7-92c8-00000aab0f27{&}acdnat=1506416153{_}2fcd7bf64033a7df262712ed9a575b1d.

[3] D. Baldacchino and G.J.W. van Bussel. Wind turbine wake stability investigations using a vortex ring modelling approach. *Journal of Physics: Conference Series*, 555: 012111, dec 2014. ISSN 1742-6588. doi: 10.1088/1742-6596/555/1/012111. URL http://stacks.iop.org/1742-6596/555/i=1/a=012111?key=crossref.50e47c89e158595612bdaac665081407.

[4] A. Bechmann, N.N. Sørensen, and F. Zahle. CFD simulations of the MEXICO rotor. *Wind Energy*, 14 (5):677–689, jul 2011. ISSN 10954244. doi: 10.1002/we.450. URL http://onlinelibrary.wiley.com/doi/10.1002/we.1608/fullhttp://doi.wiley.com/10.1002/we.450.

[5] J.C. Berg, M.F. Barone, and N.C. Yoder. SMART Wind Turbine Rotor: Data Analysis and Conclusions. Technical Report January, Sandia National Laboratories, 2014. URL https://www.energy.gov/sites/prod/files/smart{_}wind{_}turbine{_}data.pdfhttp://energy.sandia.gov/wp/wp-content/gallery/uploads/SAND2014-0712.pdf.

[6] W.A.A.M. Bierbooms. *Constrained Stochastic Simulation of Wind Gusts for Wind Turbine Design*. Phd., TUDelft, 2009. URL https://repository.tudelft.nl/islandora/object/uuid:f1d17514-77c0-4ed1-88ff-c46a1006f66d/datastream/OBJ.

[7] A. Björck. Dynamic Stall and Three Dimensional Effect. *Final Report for the EC DGXII Joule II Project JOU2-CT93-0345, FFA TN 1995*, 31, 1995.

[8] E. Branlard and M. Gaunaa. Cylindrical vortex wake model: right cylinder. *Wind Energy*, 18(11):1973–1987, nov 2015. ISSN 10954244. doi: 10.1002/we.1800. URL http://onlinelibrary.wiley.com/doi/10.1002/we.1608/fullhttp://doi.wiley.com/10.1002/we.1800.

[9] E. Branlard and M. Gaunaa. Superposition of vortex cylinders for steady and unsteady simulation of rotors of finite tip-speed ratio. *Wind Energy*, 19(7):1307–1323, jul 2016. ISSN 10991824. doi: 10.1002/we.1899. URL http://doi.wiley.com/10.1002/we.1899.

[10] T. Burton, N. Jenkins, D. Sharpe, and E. Bossanyi. *Wind energy handbook*. 2011. ISBN 0471489972. URL http://books.google.com/books?hl=en{&}lr={&}id=qVjtDxyN-joC{&}oi=fnd{&}pg=PR5{&}dq=Wind+Energy+Handbook{&}ots=Q5tVC8vshE{&}sig=puxGWCuOdoT8wndgPAUvrRHFIBM.

[11] P.J. Carpenter and B. Fridovich. Effect of a Rapid Blade-Pitch Increase on the Thrust and Induced-Velocity Response of a Full-Scale Helicopter Rotor. Technical Report November, NACA, 1953. URL https://ntrs.nasa.gov/archive/nasa/casi.ntrs.nasa.gov/19930083686.pdf.

[12] J.T. Conway. Analytical solutions for the actuator disk with variable radial distribution of load. *Journal of Fluid Mechanics*, 297(-1):327, aug 1995. ISSN 0022-1120. doi: 10.1017/S0022112095003120. URL http://www.journals.cambridge.org/abstract{_}S0022112095003120.

[13] S.K. Drzewiecki. *Des hélices aériennes: théorie générale des propulseurs hélicoïdaux et méthode de calcul des ces propulseurs pour l'air*. Librairie des sciences aéronautiques, 1909.

[14] European Commission. Energy roadmap. Technical report, European Commission, Luxembourg, 2012. URL https://ec.europa.eu/energy/sites/ener/files/documents/2012{_}energy{_}roadmap{_}2050{_}en{_}0.pdf.

[15] L.J. Fingersh, D. Simms, M. Hand, D. Jager, J. Cotrell, M. Robinson, S.J. Schreck, and S. Larwood. Wind Tunnel Testing of NREL's Unsteady Aerodynamics Experiment. In *Proc. of the AIAA 39th Aerospace Sciences Meeting & Exhibit*, 2001. doi: doi:10.2514/6.2001-35. URL https://arc.aiaa.org/doi/pdfplus/10.2514/6.2001-35.

[16] R.E. Froude. On the part played in propulsion by differences of fluid pressure. *Transactions of the Institute of Naval Architects*, 30:390–405, 1889.

[17] H. Glauert. Airplane Propellers. In *Aerodynamic Theory SE - 3*, pages 169–360. Springer Berlin Heidelberg, 1935. ISBN 978-3-642-89630-9. doi: 10.1007/978-3-642-91487-4_3. URL http://dx.doi.org/10.1007/978-3-642-91487-4{_}3.

[18] M. Hammam. *Analytical Unsteady Aerodynamic Models for Horizontal Axis Wind Turbines*. Phd., University of Calgary, 2016. URL http://theses.ucalgary.ca/bitstream/11023/2863/1/ucalgary{_}2016{_}hammam{_}mohamed.pdf?cv=1{&}session-id=77fb13d02c792e5c800101830f7f4319.

[19] M.M. Hand, D. Simms, L.J. Fingersh, D.W. Jager, J.R. Cotrell, S. Schreck, and S.M. Larwood. Unsteady Aerodynamics Experiment Phase VI: Wind Tunnel Test Configurations and Available Data Campaigns. Technical report, 2001. URL https://www.nrel.gov/docs/fy02osti/29955.pdfhttp://www.osti.gov/servlets/purl/15000240-1FhaHo/native/.

[20] M.O.L. Hansen. *Aerodynamics of Wind Turbines*. 2nd edition, 2008. ISBN 1-84407-438-2. URL www.earthscan.co.uk.

[21] M.O.L. Hansen and H.Aa. Madsen. Review Paper on Wind Turbine Aerodynamics. *Journal of Fluids Engineering*, 133(11):114001, nov 2011. ISSN 00982202. doi: 10.1115/1.4005031. URL http://fluidsengineering.asmedigitalcollection.asme.org/article.aspx?articleid=1439572.

[22] M.O.L. Hansen, J.N. Sørensen, S. Voutsinas, N. Sørensen, and H.Aa. Madsen. State of the art in wind turbine aerodynamics and aeroelasticity, 2006. ISSN 03760421. URL http://ac.els-cdn.com/S0376042106000649/1-s2.0-S0376042106000649-main.pdf?{_}tid=f2a3c098-60b2-11e7-a985-00000aab0f6c{&}acdnat=1499170915{_}7543c9a4cc3d4ee81f0b60bf3b384dc0.

[23] J.R. Hartin. *Evaluation of Horizontal Axis Wind Turbine Blade Loads Using Unsteady Aerodynamics*. Phd., Oregon State University, 1990. URL http://ir.library.oregonstate.edu/xmlui/bitstream/handle/1957/38381/HartinJohnR1990.pdf?sequence=1.

[24] V.W. Hong. *Analysis of an actuator disc under unsteady loading*. Msc. thesis, TU Delft, 2015.

[25] S.A. Huyer, D. Simms, and M.C. Robinson. Unsteady aerodynamics associated with a horizontal-axis wind turbine. *AIAA Journal*, 34(7):1410–1419, 1996. ISSN 0001-1452. doi: 10.2514/3.13247. URL https://arc.aiaa.org/doi/pdfplus/10.2514/3.13247http://arc.aiaa.org/doi/10.2514/3.13247.

[26] IEC. Wind Turbine—Part 1: Design Requirements, IEC 61400-1. Technical report, International Electrotechnical Commission, 2005.

[27] S. Kalvig, E. Manger, and B. Hjertager. Comparing different CFD wind turbine modelling approaches with wind tunnel measurements. *Journal of Physics: Conference Series*, 555:012056, 2014. ISSN 1742-6588. doi: 10.1088/1742-6596/555/1/012056. URL http://iopscience.iop.org/article/10.1088/1742-6596/555/1/012056/pdfhttp://stacks.iop.org/1742-6596/555/i=1/a=012056?key=crossref.978511ffd879d65381965a0d9e23a0f9.

[28] K. Kaur. *Experimental Analysis of an Actuator Disk under cyclic unsteady loading*. Msc. thesis, TU Delft, 2017.

[29] P. Krogstad and P.E. Eriksen. "Blind test" calculations of the performance and wake development for a model wind turbine. *Renewable Energy*, 50:325–333, 2013. ISSN 09601481. doi: 10.1016/j.renene.2012.06.044. URL https://ac.els-cdn.com/S0960148112003953/1-s2.0-S0960148112003953-main.pdf?{_}tid=f69ef9f8-a296-11e7-af7f-00000aab0f6b{&}acdnat=1506415673{_}acf78bf46eba904be0faf4b697072bbe.

[30] P. Krogstad, L. Sætran, and M.S. Adaramola. "Blind Test 3" calculations of the performance and wake development behind two in-line and offset model wind turbines. *Journal of Fluids and Structures*, 52:65–80, 2015. ISSN 10958622. doi: 10.1016/j.jfluidstructs.2014.10.002. URL https://ac.els-cdn.com/S0889974614002175/1-s2.0-S0889974614002175-main.pdf?{_}tid=aa0dc50a-a297-11e7-ba18-00000aacb362{&}acdnat=1506415975{_}bec6f9ee471f2b07adec0ce7404f444a.

[31] J.G. Leishman. Challenges in modelling the unsteady aerodynamics of wind turbines. *Wind Energy*, 5(2-3):85–132, apr 2002. ISSN 1095-4244. doi: 10.1002/we.62. URL http://doi.wiley.com/10.1002/we.62.

[32] L.E.M. Lignarolo, D. Ragni, C.J. Simão Ferreira, and G.J.W. van Bussel. Kinetic energy entrainment in wind turbine and actuator disc wakes: an experimental analysis. *Journal of Physics: Conference Series*, 524:012163, 2014. ISSN 1742-6596. doi: 10.1088/1742-6596/524/1/012163. URL http://iopscience.iop.org/1742-6596/524/1/012163http://stacks.iop.org/1742-6596/524/i=1/a=012163?key=crossref.dce65096b892a609e45b441e0a9fae0f.

[33] H.Aa. Madsen. A CFD analysis of the actuator disc flow compared with momentum theory results. In *10th IEA meeting on aerodynamics*, number December, pages 109–124, Edinburgh, 1997. Technical University of Denmark. Department of Fluid Mechanics.

[34] L.A. Martínez-Tossas, M.J. Churchfield, and S. Leonardi. Large eddy simulations of the flow past wind turbines: actuator line and disk modeling. *Wind Energy*, 18(6):1047–1060, jun 2015. ISSN 10954244. doi: 10.1002/we.1747. URL http://onlinelibrary.wiley.com/doi/10.1002/we.1608/fullhttp://doi.wiley.com/10.1002/we.1747.

[35] D. Medici and P.H. Alfredsson. Wind Turbine Near Wakes and Comparisons to the Wake Behind a Disc. In *43rd AIAA Aerospace Sciences Meeting and Exhibit*, Reston, Virigina, jan 2005. American Institute of Aeronautics and Astronautics. ISBN 978-1-62410-064-2. doi: 10.2514/6.2005-595. URL https://arc.aiaa.org/doi/pdfplus/10.2514/6.2005-595http://arc.aiaa.org/doi/10.2514/6.2005-595.

[36] J. Meyers and C. Meneveau. Large Eddy Simulations of Large Wind-Turbine Arrays in the Atmospheric Boundary Layer. In *48th AIAA aerospace sciences meeting including the new horizons forum and aerospace exposition*, number January, pages AIAA 2010–827, Orlando, 2010. American Institute of Aeronautics and Astronautics. ISBN 9781600867392. doi: 10.2514/6.2010-827. URL https://arc.aiaa.org/doi/pdf/10.2514/6.2010-827http://arc.aiaa.org/doi/abs/10.2514/6.2010-827.

[37] R.F. Mikkelsen. *Actuator Disc Methods Applied to Wind Turbines*. PhD thesis, DTU, 2003. URL http://orbit.dtu.dk/files/5452244/Robert.PDF.

[38] J. Murata, Y. Hasegawa, and H. Imamura. Numerical Analysis of Combined Inflow Effects on Fatigue Loads of Horizontal Axis Wind Turbine Rotors. In *Proceedings of International Symposium on EcoTopia Science 2007, ISETS07 (2007)*, pages 290–295, 2007. URL http://www.esi.nagoya-u.ac.jp/h/isets07/Contents/Session03/1199Murata.pdf.

[39] J.M. O'Brien, T.M. Young, D.C. O'Mahoney, and P.C. Griffin. Horizontal axis wind turbine research: A review of commercial CFD, FE codes and experimental practices. *Progress in Aerospace Sciences*, 92:1–24, 2017. ISSN 03760421. doi: 10.1016/j.paerosci.2017.05.001. URL https://ac.els-cdn.com/S0376042116301579/1-s2.0-S0376042116301579-main.pdf?{_}tid=a8f6c30a-a298-11e7-88bf-00000aacb360{&}acdnat=1506416402{_}e330834cc3628185e8fb1d3e4101e179.

[40] P.F. Odgaaard, T. Knudsen, A. Overgaard, H. Steffensen, and M. Jørgensen. Importance of Dynamic Inflow in Model Predictive Control of Wind Turbines. *IFAC-PapersOnLine*, 48(30):90–95, 2015. ISSN 24058963. doi: 10.1016/j.ifacol.2015.12.359. URL www.sciencedirect.comhttp://linkinghub.elsevier.com/retrieve/pii/S2405896315030013.

[41] V.L. Okulov, J.N. Sørensen, and D.H. Wood. The rotor theories by Professor Joukowsky: Vortex theories. *Progress in Aerospace Sciences*, 73:19–46, 2015. ISSN 03760421. doi: 10.1016/j.paerosci.2014.10.002. URL https://ac.els-cdn.com/S0376042114000967/1-s2.0-S0376042114000967-main.pdf?{_}tid=d950f5fc-a4fa-11e7-a4f1-00000aab0f27{&}acdnat=1506678475{_}6e4a2cf79666a3985c6f95672a3f7553.

[42] S. Øye. A simple vortex model. In *Proc. of the third IEA Symposium on the Aerodynamics of Wind Turbines, ETSU, Harwell*, pages 1–4, 1990.

[43] S. Øye. Wind turbine: dynamic flow measurement. Technical report, Department of Fluid Mechanics, Technical University of Denmark, DTU, Copenhagen, 1992.

[44] F. Paxton. Solid angle calculation for a circular disk. *Review of Scientific Instruments*, 30(4):254–258, 1959. ISSN 00346748. doi: 10.1063/1.1716590. URL http://dx.doi.org/10.1063/1.1716590http://aip.scitation.org/toc/rsi/30/4.

[45] F. Pierella, P. Krogstad, and L. Sætran. Blind Test 2 calculations for two in-line model wind turbines where the downstream turbine operates at various rotational speeds. *Renewable Energy*, 70:62–77, 2014. ISSN 09601481. doi: 10.1016/j.renene.2014.03.034. URL https://ac.els-cdn.com/S0960148114001815/1-s2.0-S0960148114001815-main.pdf?{_}tid=666fd95a-a297-11e7-8409-00000aab0f6c{&}acdnat=1506415861{_}f0d7917c205672e034a21182d277658c.

[46] M.P. Pitt and D.A. Peters. Theoretical Prediction of Dynamic-Inflow Derivatives. In *Sixth European Rotorcraft and Powered Lift Aircraft Forum*, number 47, Bristol, England, 1980. URL https://dspace-erf.nlr.nl/xmlui/bitstream/handle/20.500.11881/1796/ERF1980-47.pdf?sequence=1.

[47] F. Porté-Agel, H. Lu, and Y.T. Wu. A large-eddy simulation framework for wind energy applications. In *Fifth International Symposium on Computational Wind Engineering*, page 21, Chapel Hill, 2010. URL https://www.researchgate.net/profile/Yu{_}Ting{_}Wu8/publication/268371344{_}A{_}large-eddy{_}simulation{_}framework{_}for{_}wind{_}energy{_}applicat
links/56c1d98d08ae2f498efcd38e.pdf.

[48] Y.X. Qiu, X.D. Wang, S. Kang, M. Zhao, and J.Y. Liang. Predictions of unsteady HAWT aerodynamics in yawing and pitching using the free vortex method. *Renewable Energy*, 70:93–106, 2014. ISSN 09601481. doi: 10.1016/j.renene.2014.03.071. URL https://ac.els-cdn.com/S0960148114002468/1-s2.0-S0960148114002468-main.pdf?{_}tid=d6cf8552-a381-11e7-908e-00000aab0f6b{&}acdnat=1506516551{_}ba6f5740cbab53d7eae28ccdf7e872e2.

[49] W.J.M. Rankine. On the Mechanical Principles of the Action of Propellers. *Transactions of the Institution of Naval Architects*, 6:13–39, 1865.

[50] B. Sanderse. Aerodynamics of wind turbine wakes: Literature review. Technical report, 2009. URL https://www.ecn.nl/docs/library/report/2009/e09016.pdf.

[51] B. Sanderse, S.P. Van Der Pijl, and B. Koren. Review of computational fluid dynamics for wind turbine wake aerodynamics. *Wind Energy*, 14(7):799–819, oct 2011. ISSN 10954244. doi: 10.1002/we.458. URL http://doi.wiley.com/10.1002/we.458.

[52] J.G. Schepers. *Engineering models in wind energy aerodynamics*. Phd thesis, Delft University of Technology, 2012. URL http://repository.tudelft.nl/assets/uuid:92123c07-cc12-4945-973f-103bd744ec87/PhD{_}Schepers.pdf.

[53] J.G. Schepers and H. Snel. Model Experiments in Controlled Conditions - Final Report. Technical report, 2007. URL ftp://ftp.ecn.nl/pub/www/library/report/2007/e07042.pdf.

[54] J.G. Schepers, H. Snel, G.J.W. van Bussel, L.J. Vermeer, R.J. Rawlinson Smith, S. Voutsinas, S. Huberson, T. van Holten, S. Øye, H. Ganander, B. Montgomerie, R. Bareiß, and K. Braun. Dynamic Inflow: Yawed Conditions and Partial Span Pitch Control. Technical report, ECN, 1995. URL https://www.ecn.nl/publications/PdfFetch.aspx?nr=ECN-C--95-056.

[55] J.G. Schepers, A.J. Brand, A. Bruining, J.M.R. Graham, M.M. Hand, D.G. Infield, H.Aa. Madsen, T. Maeda, J.H. Paynter, R. van Rooij, Y. Shimizu, D. Simms, and N. Stefanatos. Final report of IEA Annex XVIII : 'Enhanced Field Rotor Aerodynamics Database'. Technical Report February, ECN, 2002. URL ftp://ftp.ecn.nl/pub/www/library/report/2002/c02016.pdf.

[56] J.G. Schepers, K. Boorsma, T. Cho, S. Gomez-Iradi, P. Schaffarczyk, A. Jeromin, W.Z. Shen, T. Lutz, K. Meister, B. Stoevesandt, S. Schreck, D. Micallef, R. Pereira, T. Sant, H.Aa. Madsen, and N.N. S{\o}rensen. Final report of IEA Task 29, Mexnext (Phase 1): Analysis of Mexico wind tunnel measurements. Technical Report Phase 1, 2012. URL http://orbit.dtu.dk/files/56752175/ecn{_}e12004.pdf.

[57] D. Simms, S.J. Schreck, M. Hand, and L.J. Fingersh. NREL Unsteady Aerodynamics Experiment in the NASA-Ames Wind Tunnel: A Comparison of Predictions to Measurements. Technical Report June, 2001. URL https://www.nrel.gov/docs/fy01osti/29494.pdfhttp://arc.aiaa.org/doi/abs/10.2514/6.2001-35.

[58] H. Snel and J.G. Schepers. Engineering moles for dynamic inflow phenomena. *Journal of Wind Engineering and Industrial Aerodynamics*, 39(1-3):267–281, 1992. ISSN 01676105. doi: 10.1016/0167-6105(92)90552-L. URL http://ac.els-cdn.com/016761059290552L/1-s2.0-016761059290552L-main.pdf?{_}tid=6e0261ba-7754-11e7-b786-00000aab0f26{&}acdnat=1501659201{_}625c6ee2f809b427400bd83d81ca687f.

[59] H. Snel and J.G. Schepers. Investigation and modelling of dynamic inflow effects. Technical report, 1993. URL ftp://ftp.ecn.nl/pub/www/library/report/1993/rx93029.pdfftp://question.ecn.nl/pub/www/library/report/1993/rx93029.pdf{%}5Cnpapers3://publication/uuid/B431F9AD-74D4-44AE-B87B-F5BD750673FF.

[60] H. Snel and J.G. Schepers. Joint investigation of dynamic inflow effects and implementation of an engineering method. Technical report, 1995.

[61] J.N. Sørensen and C.W. Kock. A model for unsteady rotor aerodynamics. *Journal of Wind Engineering and Industrial Aerodynamics*, 58(3):259–275, 1995. ISSN 01676105. doi: 10.1016/0167-6105(95)00027-5. URL http://ac.els-cdn.com/0167610595000275/1-s2.0-0167610595000275-main.pdf?{_}tid=210f83b8-686f-11e7-acb7-00000aacb35e{&}acdnat=1500021396{_}d5817bfd9541926a462c7f8eb87200c0.

[62] J.N. Sørensen and A. Myken. Unsteady actuator disc model for horizontal axis wind turbines. *Journal of Wind Engineering and Industrial Aerodynamics*, 39(1-3):139–149, 1992. ISSN 01676105. doi: 10.1016/0167-6105(92)90540-Q. URL

http://ac.els-cdn.com/016761059290540Q/1-s2.0-016761059290540Q-main.pdf?{_}tid=06155f4c-686f-11e7-90e7-00000aacb360{&}acdnat=1500021351{_}a8d079f3a6c782784f3688ee2c9c8db4.

[63] J.N. Sørensen and W.Z. Shen. Numerical Modeling of Wind Turbine Wakes. *Journal of Fluids Engineering*, 124(2):393, jun 2002. ISSN 00982202. doi: 10.1115/1.1471361. URL http://fluidsengineering.asmedigitalcollection.asme.org/article.aspx?articleid=1429525.

[64] J.N. Sørensen, W.Z. Shen, and X. Munduate. Analysis of Wake States by a Full-Field Actuator Disc Model. *Wind Energy*, 1(2):73–88, dec 1998. ISSN 10954244. doi: 10.1002/(SICI)1099-1824(199812)1:2<73::AID-WE12>3.0.CO;2-L. URL http://doi.wiley.com/10.1002/{%}28SICI{%}291099-1824{%}28199812{%}291{%}3A2{%}3C73{%}3A{%}3AAID-WE12{%}3E3.0.CO{%}3B2-L.

[65] N.N. Sørensen and H.Aa. Madsen. Modelling of transient wind turbine loads during pitch motion. In *European Wind Energy Association (EWEA)*, 2006. ISBN 9781622764679. URL https://www.researchgate.net/profile/Helge{_}Madsen2/publication/266908214{_}Modelling{_}of{_}transient{_}wind{_}turbine{_}loads{_}during{_}pitch{_}m
links/552e1fcb0cf2e089a3ad9dc9.pdf.

[66] A. Suzuki and A.C. Hansen. Generalized dynamic wake model for YawDyn. In *37th Aerospace Sciences Meeting and Exhibit*, Reston, Virigina, jan 1999. American Institute of Aeronautics and Astronautics. doi: 10.2514/6.1999-41. URL http://arc.aiaa.org/doi/10.2514/6.1999-41.

[67] J.L. Tangler. The Nebulous Art of Using Wind Tunnel Aerofoil Data for Predicting Rotor Performance. *Wind Energy*, 5(2-3):245–257, apr 2002. ISSN 1099-1824. doi: 10.1002/we.71. URL http://doi.wiley.com/10.1002/we.71.

[68] T. Theodorsen. General theory of aerodynamic instability and the mechanism of flutter, 1935. ISSN 1098-6596. URL http://www.tree-o-life.org/ARO202/naca-report-496.pdf.

[69] N. Troldborg, J.N. Sorensen, and R. Mikkelsen. Numerical simulations of wake characteristics of a wind turbine in uniform inflow. *Wind Energy*, 13(1):86–99, jan 2010. ISSN 10954244. doi: 10.1002/we.345. URL http://onlinelibrary.wiley.com/doi/10.1002/we.1608/fullhttp://doi.wiley.com/10.1002/we.345.

[70] G.J.W. van Bussel. The use of the asymptotic accelertion potential method for horizontal axis windturbine rotor aerodynamics. *Journal of Wind Engineering and Industrial Aerodynamics*, 39(1-3):161–172, 1992. ISSN 01676105. doi: 10.1016/0167-6105(92)90542-I. URL http://ac.els-cdn.com/016761059290542I/1-s2.0-016761059290542I-main.pdf?{_}tid=4120393e-9ec7-11e7-a1de-00000aacb35e{&}acdnat=1505996609{_}2c80ac87b2c080f08cbda53be0137639.

[71] T.G. van Engelen and E.L. van der Hooft. Dynamic inflow compensation for pitch controlled wind turbines. In *Proceedings of EWEC*, number November, pages 22–25, London, 2004. URL ftp://ftp.ecn.nl/pub/www/library/report/2004/rx04129.pdf.

[72] T. van Holten. *The computation of aerodynamic loads on helicopter blades in forward flight, using the method of the acceleration potential*. Phd., TU Delft, 1975. URL https://repository.tudelft.nl/islandora/object/uuid:4e96fb1b-693e-443e-be90-97b79a500ad6/datastream/OBJhttp://www.csa.com/partners/viewrecord.php?requester=gs{&}collection=TRD{&}recid=20021211033564MT.

[73] G.A.M. van Kuik and L.E.M. Lignarolo. Potential flow solutions for energy extracting actuator disc flows. *Wind Energy*, 19(8):1391–1406, aug 2016. ISSN 10991824. doi: 10.1002/we.1902. URL http://doi.wiley.com/10.1002/we.1902.

[74] G.A.M. van Kuik, D. Micallef, I. Herraez, A.H. van Zuijlen, and D. Ragni. The role of conservative forces in rotor aerodynamics. *Journal of Fluid Mechanics*, 750:284–315, jul 2014. ISSN 0022-1120. doi: 10.1017/jfm.2014.256. URL http://www.journals.cambridge.org/abstract{_}S0022112014002560.

[75] L.J. Vermeer, J.N. Sørensen, and A. Crespo. Wind turbine wake aerodynamics. *Progress in Aerospace Sciences*, 39(6):467–510, 2003. ISSN 03760421. doi: 10.1016/S0376-0421(03)00078-2. URL http://ac.els-cdn.com/S0376042103000782/1-s2.0-S0376042103000782-main.pdf?{_}tid=24bbd604-609c-11e7-9b73-00000aacb361{&}acdnat=1499161120{_}babc1e31a32a068fa55d40d627948a71.

[76] L. Wang, X. Liu, and A. Kolios. State of the art in the aeroelasticity of wind turbine blades: Aeroelastic modelling, 2016. ISSN 18790690. URL https://ac.els-cdn.com/S1364032116302234/1-s2.0-S1364032116302234-main.pdf?{_}tid=bb445d26-a296-11e7-8efd-00000aacb35e{&}acdnat=1506415573{_}00c289873a3409387aa53d728b60d250.

[77] D.C. Wilcox. *Turbulence Modeling for CFD*. Number v. 1 in Turbulence Modeling for CFD. DCW Industries, 2006. ISBN 9781928729082. URL https://books.google.nl/books?id=q4ypAQAACAAJ.

[78] S.S. Yoon and S.D. Heister. Analytical formulas for the velocity field induced by an infinitely thin vortex ring. *International Journal for Numerical Methods in Fluids*, 44(6):665–672, feb 2004. ISSN 02712091. doi: 10.1002/fld.666. URL http://doi.wiley.com/10.1002/fld.666.

[79] W. Yu. *The wake of an unsteady actuator disc*. Phd., TU Delft, 2018.

[80] W. Yu, C.J. Simão Ferreira, and G.A.M. van Kuik. Is blade element momentum theory (BEM) enough for smart rotor design. In *10th PhD Seminor on Wind Energy in Europe*, number October, pages 3–6, Orléans, France, 2014. EAWE.

[81] W. Yu, V.W. Hong, C.J. Simão Ferreira, and G.A.M. van Kuik. Validation of engineering dynamic inflow models by experimental and numerical approaches. *Journal of Physics: Conference Series*, 753(2):022024, sep 2016. ISSN 1742-6588. doi: 10.1088/1742-6596/753/2/022024. URL http://stacks.iop.org/1742-6596/753/i=2/a=022024?key=crossref.a5021875b25c355fb9838721e1c241a3.

[82] W. Yu, V.W. Hong, C.J. Simão Ferreira, and G.A.M. van Kuik. Experimental analysis on the dynamic wake of an actuator disc undergoing transient loads. *Experiments in Fluids*, 58(10):149, oct 2017. ISSN 07234864. doi: 10.1007/s00348-017-2432-9. URL http://link.springer.com/10.1007/s00348-017-2432-9.

[83] W. Yu, C.J. Simão Ferreira, G.A.M. van Kuik, and D. Baldacchino. Verifying the Blade Element Momentum Method in unsteady, radially varied, axisymmetric loading using a vortex ring model. *Wind Energy*, 20(2):269–288, feb 2017. ISSN 10991824. doi: 10.1002/we.2005. URL http://doi.wiley.com/10.1002/we.2005.